INSTITUTE OF BUILDING DESIGN

Report no. 123

BJARNE CHR. JENSEN

SOME APPLICATIONS OF PLASTIC ANALYSIS TO PLAIN AND REINFORCED CONCRETE

Den polytekniske Læreanstalt, Danmarks tekniske Højskole
Technical University of Denmark, DK-2800 Lyngby 1977

PREFACE TO THE ENGLISH EDITION

This report is an English translation of my licentiate thesis. Only minor alterations have been made in relation to the Danish edition, apart from section 6.2, which has been somewhat condensed.

Publication of the English edition has been made possible through the financial support of the Knud Højgaard Fund. The report has been translated by Mrs. Pauline Katborg, and the Institute of Building Design has taken care of its publication. In particular, Lic. Techn. Egil Borchersen has been most helpful.

I wish to take this opportunity of thanking all those who have assisted me in my work.

Aarup
July 1977

Bjarne Chr. Jensen

PREFACE TO THE DANISH EDITION

This thesis has been written to fulfil part of the requirements for a licentiate degree.

The work on which it is based was carried out at the Institute of Building Design of the Technical University of Denmark, under Professor Johs. F. Munch-Petersen, and at the Department of Structural Engineering, under Professor Mogens Peter Nielsen. I wish to thank both for giving me the possibility of carrying out my licentiate studies and for their advice and help during the work.

In connection with my studies I received valuable assistance from many colleagues at the Institute of Building Design and the Structural Research Laboratory. In particular, Professor Mogens Peter Nielsen, Mr. Finn Bach and Mr. Mikael W. Bræstrup, of the latter department, were a constant source of inspiration and gave me the opportunity of participating in many useful discussions on plastic analysis of reinforced concrete.

CONTENTS

NOTATION

The following list gives the symbols most frequently used in this thesis and the sense in which they most often appear.

a	Length
b	Length
c	Length Cohesion
c'	Cohesion, reduced in relation to c
f	Ratio of reinforcement $\frac{F}{A}$ Loaded area under concentrated load
h	Length
k	$\frac{1+\sin\varphi}{1-\sin\varphi}$ in Coulomb's failure hypothesis Constant < 1
e	Length
p	Load per unit of length, or per unit of area
t	Length
A	Area of concrete
A_i	Internal work
A_{ia}	Contribution of reinforcement to internal work
A_{ib}	Contribution of concrete to internal work
A_y	External work
B	Cross-section from the "keys" in the keyed shear joint
F	Cross section of reinforcement "Active" area under concentrated load
I	First strain invariant = $\varepsilon_1 + \varepsilon_2 + \varepsilon_3$
N	Load
P	Load
P_{br}	Failure load
Q	Load

V	Deformation vector
W	Internal work per unit of volume
W_l	Internal work per unit of length of line of discontinuity
α	Angle between V and line of discontinuity
β	Angle specifying slope of line of discontinuity
δ	Height of deformation zone
ε	Longitudinal strain
$\varepsilon_1, \varepsilon_2, \varepsilon_3$	Principal strains
ε^+	Positive principal strain
ε_i	Strain vector
λ	Positive constant
μ	Coefficient of friction
ν	Poisson's ratio Efficiency factor
σ	Normal stress
$\sigma_1, \sigma_2, \sigma_3$	Principal stresses
σ_c	Uniaxial compression strength. For concrete, put equal to the cylinder strength
σ_f	Failure stress under concentrated load
σ_i	Stress vector
σ_t	Uniaxial tensile strength
σ_A	Separation strength
σ_F	Yield stress for reinforcement Under concentrated load; also the ultimate strength when the entire area F is loaded
σ_N	$\frac{N}{A}$
σ_T	Cube strength of concrete
σ_{br}	Ultimate load determined by an upper bound solution

σ'_t	Tensile strength reduced in relation to σ_t
σ'_N	$\frac{N}{\nu A}$
σ'_{br}	Ultimate load determined by a lower bound solution
τ	Shear stress
	$\frac{P}{A}$
τ_{br}	$\frac{P_{br}}{A}$
τ'_{br}	$\frac{P_{br}}{\nu A}$
φ	Angle of friction
φ'	Angle of friction reduced in relation to φ
φ_{xy}	Angular alteration in the xy-plane
ψ	Angle
	Airy's stress function
θ	Top angle in logarithmic spiral
Φ	Degree of reinforcement $\frac{F\sigma_F}{A\sigma_c}$
Φ'	$\frac{F\sigma_F}{\nu A\sigma_c}$
Φ^*	Equivalent degree of reinforcement $\Phi - \frac{\sigma_N}{\sigma_c}$

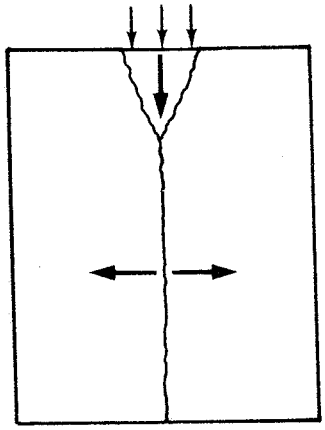

Fig. 1.1 Example of the fact that tests can show what failure mechanism can be expected.

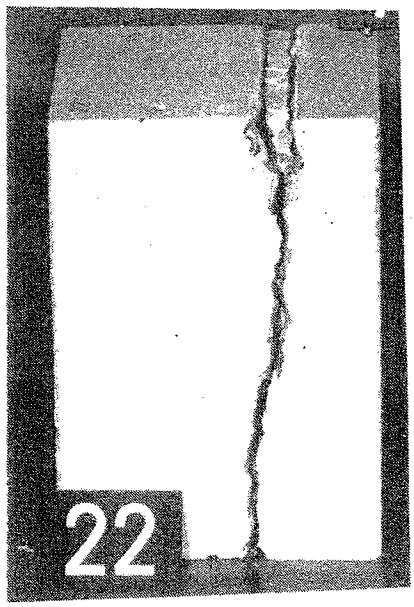

1. INTRODUCTION

During tests on moment-transmitting stirrup connections between reinforced concrete beams I became interested in limit state analysis for concrete, particularly in relation to connections between prefabricated concrete components.

Limit state analysis for concrete is difficult for a number of reasons, including the fact that concrete cannot be characterized as either distinctly elastic or distinctly plastic. Nevertheless, for the purposes of this thesis, concrete is regarded as a rigid, plastic material, which has as its yield criterion Coulomb's modified failure hypothesis.

Provided due attention is paid to the deformability of concrete, we find that we can get a very long way with ultimate load calculations by means of the theory of plasticity. On the other hand, it is owing to the deformability of concrete that results obtained by means of the theory of plasticity must only be used with extreme care until they have been verified by tests.

Here, the theory of plasticity is used almost exclusively for finding upper bounds for ultimate loads. This is done by calculating on the basis of failure mechanisms which there are often only a few reasonable ways of selecting. If we know from tests how a body fails, we thereby often have a good estimate of a failure mechanism. An excellent example of this is failure of a concrete prism under concentrated loading, see fig. 1.1.

We can obtain valuable results simply by considering a failure mechanism. An example is

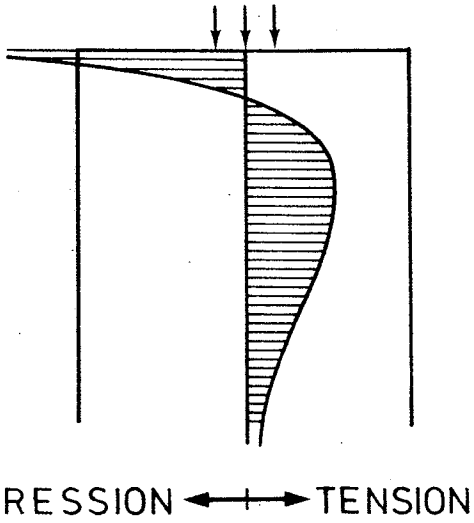

Fig. 1.2 Distribution of transverse stress beneath the load in accordance with the theory of elasticity.

again provided by the concentrated load. As described in chapter 7, we see clearly that transverse reinforcement is just as effective against failure when placed where elastic analysis gives transverse tension as where it gives transverse compression, see fig. 1.2.

As mentioned above, Coulomb's modified failure hypothesis is used as yield criterion for concrete. Both this and Coulomb's ordinary failure hypothesis are discussed in chapter 2. The modified failure criterion is compared with failure tests on concrete, and the stress-strain curves for concrete in uniaxial compression and uniaxial tension are discussed. The chapter contains nothing new and is only included to show that the modified failure hypothesis can be used for concrete.

In chapter 3 expressions are derived for the internal work per unit of volume for materials that obey Coulomb's failure hypothesis and Coulomb's modified failure hypothesis. In this chapter special attention is paid to discontinuity lines in displacements arising in plane stress fields and plane strain fields.

The chapter gives a general account of the theory of plasticity for Coulomb-materials and contains various original work. The expressions formulated here provide the background for the plastic analysis later in the thesis.

Chapter 4 is a short chapter which is presumably only of theoretical interest. It shows how the theory of plasticity can be used to find the load-carrying capacity of a construction joint in plain concrete. This chapter only contains really new considerations regarding construction joints in which pure sliding failure does not occur.

In chapter 5 complete formulae are established for the shear strength of reinforced concrete in which the reinforcement is normal to the shear section. In this chapter a quantity is introduced that takes account of the deformability. This was first done by Nielsen [69.1] in plastic shear analysis of reinforced concrete beams.

The actual content of the chapter is largely original, whereas the principle applied in the establishment of the formulae follows that used by Nielsen and Bræstrup [75.1] in upper-bound calculations of the shear strength of reinforced concrete beams.

Concentrated loads on plain concrete prisms are dealt with in chapter 6, which contains a plastic, an elastic and an empirical treatment of the problem.

The plastic failure analyses almost all lead to formulae that are only variants of one found earlier by Chen and Drucker [69.2]. This section thus has little new to offer readers. The ultimate carrying capacity of the concrete under concentrated loading can unfortunately not be determined by means of the formulae derived.

Ultimate load calculations by means of the theory of elasticity also prove to be impossible. The elastic calculations show, incidentally, that the tensile strength of concrete is less important than hitherto assumed,because failure starts with sliding failure.

We thus apparently still have to rely on empirical formulae for determining the ultimate load. A formula previously published is included in the empirical chapter, and here, too, the height of small prisms is discussed.

The corresponding problem, with reinforcement in the concrete prism, is dealt with in chapter 7. Here, on the basis of the theory of plasticity, an approximate expression is formulated for the ultimate load. However, the formula must be used with caution since it has not yet been adequately verified.

2. FAILURE HYPOTHESIS AND STRESS-STRAIN DIAGRAMS FOR CONCRETE

2.1 Coulomb's Failure Hypothesis

Coulomb's failure hypothesis (also known as the friction hypothesis) was presented in 1773 by C. A. Coulomb [1773.1], who had remarked that failure in stone prisms subjected to uni-axial compression took place along certain faces, as also occurred in the case of failure in earth behind retaining walls when these yielded to the pressure on them. These faces are called sliding surfaces, and this type of failure is known as sliding failure. Coulomb assumed that both internal cohesion, which is constant, and internal friction, which is proportional to the normal pressure on the sliding surface, had to be overcome in the sliding surface.

This assumption can be formulated as follows:

$$|\tau| = c - \mu\sigma = c - \sigma \tan\varphi \tag{2-1}$$

where

τ = the shear stress along the sliding surface

c = cohesion

μ = the coefficient of friction

σ = the normal stress perpendicular to the sliding surface (positive as tension)

φ = the angle of friction

However, Coulomb's failure hypothesis was first formulated mathematically by O. Mohr in connection with his general failure hypothesis from 1882 [1882.1].

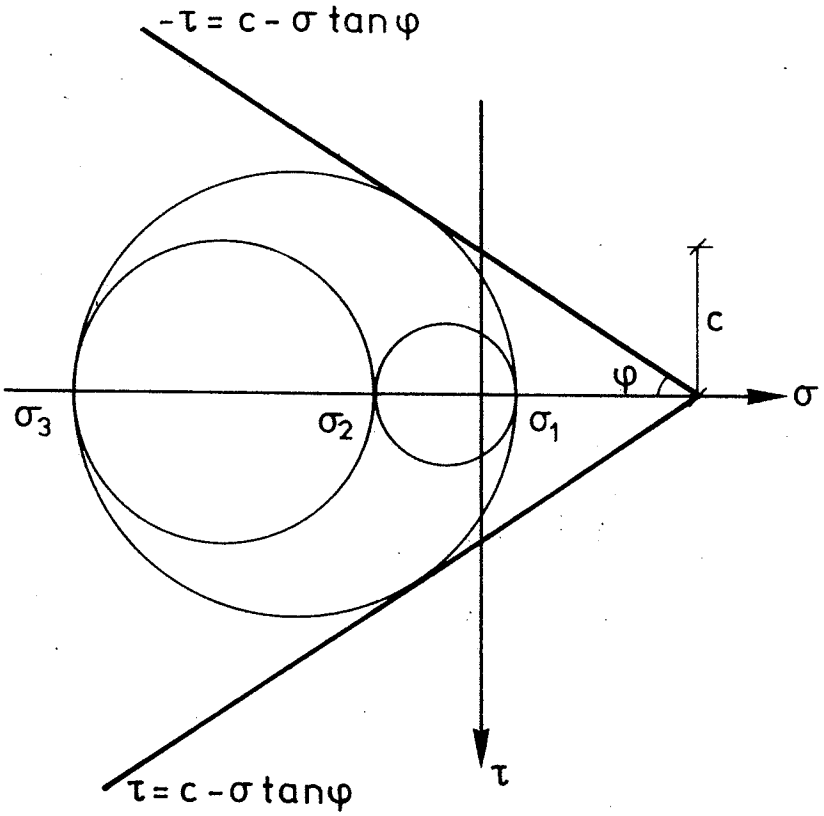

Fig. 2.1 Coulomb's failure hypothesis with Mohr's circles at one point.

According to Mohr's failure hypothesis the stresses in a sliding surface are assumed to satisfy the condition:

$$f(\sigma,\tau) = 0 \tag{2-2}$$

where $f(\sigma,\tau)$ is a characteristic function for the material. Coulomb's failure hypothesis is thus a special case of Mohr's hypothesis.

Figure 2.1 shows Coulomb's failure hypothesis depicted in a σ,τ-coordinate system. The figure includes Mohr's circles for the stresses at a point at which the failure hypothesis is satisfied.

By means of the figure we see that (2-1) can be written in principal stress form:

$$\frac{1}{2}\sigma_1 (1+\sin\varphi) - \frac{1}{2}\sigma_3 (1-\sin\varphi) - c\cos\varphi = 0 \tag{2-3}$$

which is valid for $\sigma_1 > \sigma_2 > \sigma_3$. If the mutual magnitudes of the principal stresses are altered, (2-3) must be altered correspondingly. In principal stress form, the failure hypothesis therefore consists of six equations, which have the same form as (2-3). In a $\sigma_1,\sigma_2,\sigma_3$ - coordinate system, the failure hypothesis constitutes an irregular, hexagonal pyramid, with its axis in the (1,1,1) direction. The apex of the pyramid is $\sigma_1 = \sigma_2 = \sigma_3 = c\cot\varphi$.

(2-3) can be written in the simpler form:

$$k\sigma_1 - \sigma_3 = 2c\sqrt{k} \tag{2-4}$$

where the constant k is given by

$$k = \left(\frac{\cos\varphi}{1-\sin\varphi}\right)^2 = \tan^2\left(\frac{\pi}{4} + \frac{\varphi}{2}\right) = \frac{1+\sin\varphi}{1-\sin\varphi} \tag{2-5}$$

The uniaxial compression strength σ_c is introduced as the stress field that is given by $(\sigma_1,\sigma_2,\sigma_3) = (0,0,-\sigma_c)$, and that precisely results in failure. We find from (2-4) and (2-5) that the following applies:

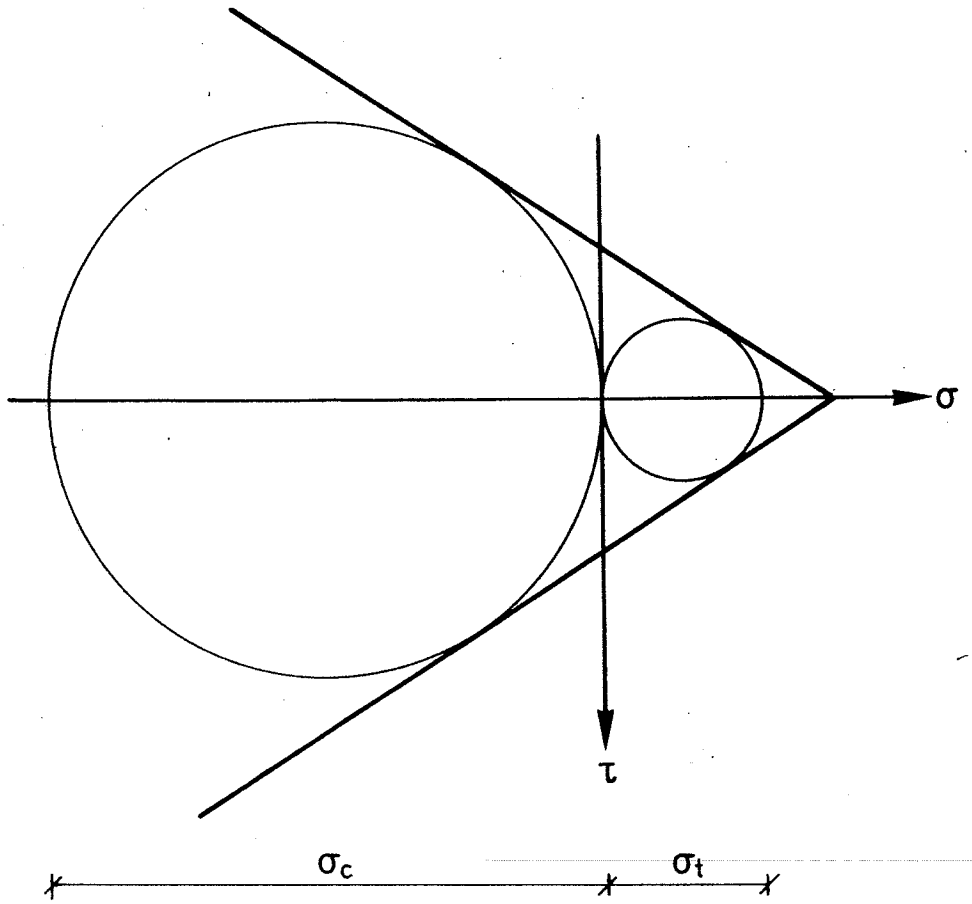

Fig. 2.2 Coulomb's failure hypothesis with Mohr's circles for uniaxial compression failure and uniaxial tension failure.

(2-6) $$\boxed{\sigma_c = \frac{2c\cos\varphi}{1-\sin\varphi}}$$

and that (2-4) can now be written as:

(2-7) $$\boxed{k\sigma_1 - \sigma_3 = \sigma_c}$$

In the same way as the uniaxial compression strength, the uniaxial tensile strength σ_t can be introduced as the stress field that is given by $(\sigma_1,\sigma_2,\sigma_3) = (\sigma_t,0,0)$ and that results in failure. From (2-7) we find

(2-8) $$k\sigma_t = \sigma_c$$

The failure hypothesis can then be written as

(2-9) $$\frac{\sigma_1}{\sigma_t} - \frac{\sigma_3}{\sigma_c} = 1$$

Coulomb's failure hypothesis is governed entirely by two parameters, e.g. c and φ in (2-1) or σ_c and σ_t in (2-9).

In figure 2.2, the failure hypothesis is depicted together with Mohr's circles for the stress fields applying in the cases of uniaxial compression failure and uniaxial tensile failure.

2.2 Coulomb's Modified Failure Hypothesis

The sliding hypothesis assumed by Coulomb can be supplemented by yet another hypothesis, viz, the separation failure hypothesis. In separation failure, the failure surfaces move away from each other perpendicular to the failure section. Separation failure occurs when the biggest tensile stress equals the separation resistance σ_A, i.e.

(2-10) $$\sigma_1 = \sigma_A$$

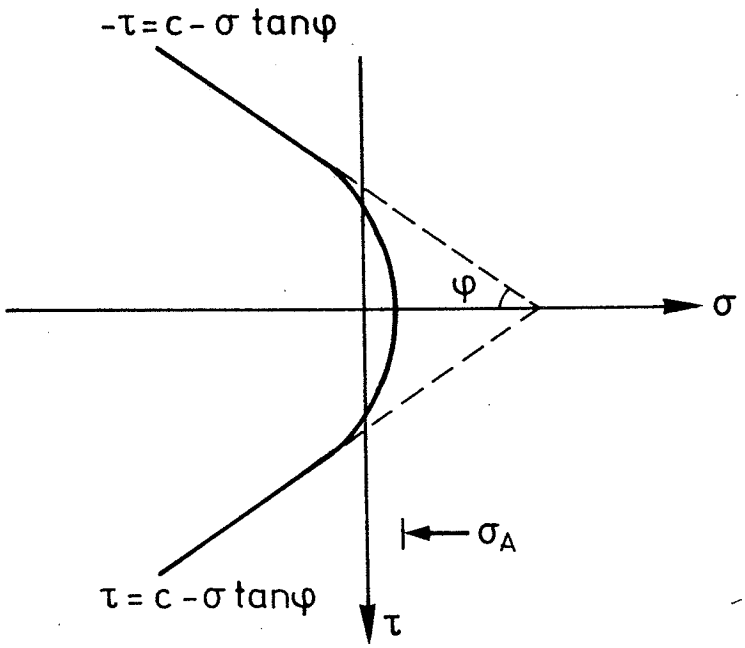

Fig. 2.3 Coulomb's modified failure hypothesis.

This failure hypothesis, which results from a combination of (2-7) and (2-10) is called Coulomb's modified failure hypothesis. In fig. 2.3 the failure hypothesis is depicted in a σ,τ-coordinate system. It consists of an arc that passes through $(\sigma,\tau) = (\sigma_A,0)$ and that is tangential to the straight lines, and a line segment that lies to the left of the tangent points.

In a $\sigma_1,\sigma_2,\sigma_3$-coordinate system, Coulomb's modified failure hypothesis constitutes an irregular pyramid with its axis in the direction (1,1,1) and cut off by three planes parallel with the coordinate planes.

It should be noted that the uniaxial tensile strength σ_t can be less than or equal to σ_A and that Coulomb's modified failure hypothesis requires three parameters to be determinate, e.g. k, σ_c and σ_A.

2.3 Failure Criterion for Concrete

Failure and yield criteria mean the criteria that must be satisfied for failure or yielding to commence.

We formulate failure and yield criteria in order to determine their parameters by means of simple test methods, after which we can evaluate the risk of failure or yielding in structures with complicated stress fields.

Here, we will examine the suitability of Coulomb's modified failure hypothesis with $\sigma_t = \sigma_A$ as failure criterion for concrete by comparing it with the results of some simple test methods. First, however, it is necessary to make a few, familiar reservations as regards the test methods, since, although

simple, these are not always entirely reliable.

The strength parameters resulting from the test methods depend on several factors, including the shape, size and age of the test specimen,and the method of curing applied. The strength parameters measured also depend on the test circumstances, for example, the relative humidity and the rate of loading.

The choice of test method is also important. For instance, it is a well known fact that the tensile strength measured for concrete depends on whether it is found by split tests, bending tests or uniaxial tensile tests. Lastly, there is also the question of whether the test specimen is sufficiently representative of the concrete in the finished structure. All in all, it can be said that the results obtained in simple tests deviate somewhat from the properties of the concrete in the finished structure. The failure hypothesis used for concrete must bear a reasonable relationship to these.

A stress-wise simple test is the triaxial compression test, in which a cylindrical test specimen is subjected to hydrostatic pressure, superposed by tension or compression in the axial direction of the cylinder. Tests carried out by Richart et al. [28.1] are depicted in fig. 2.4, which also shows tests carried out by the same authors on spirally reinforced cylinders [29. 1]. In the diagrams the cylinder compression strength is put equal to σ_c and $\sigma_1 > \sigma_2 > \sigma_3$. For the purposes of comparison, (2-7) is included, with k = 4, and it will be seen that there is good accordance.

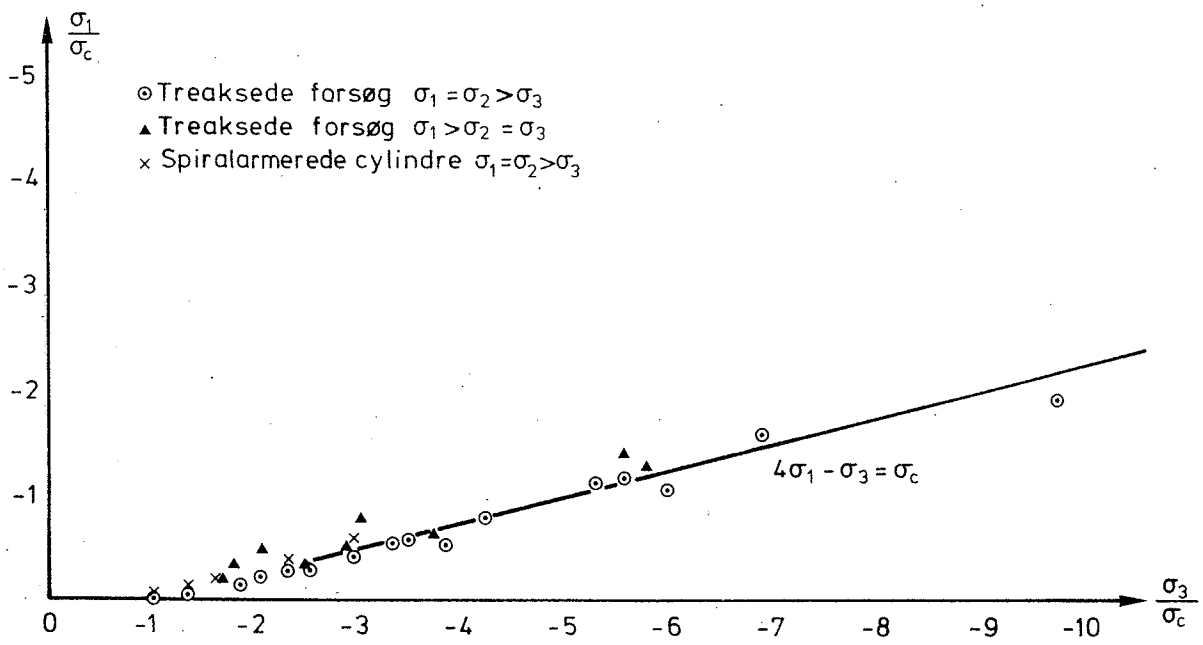

Fig. 2.4 Test results from [28.1] and [29.1].

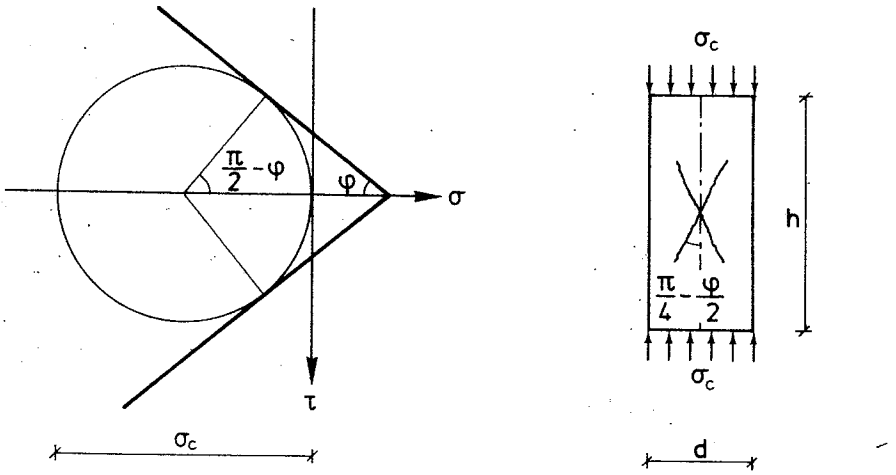

Fig. 2.5 Uniaxial compression tests.

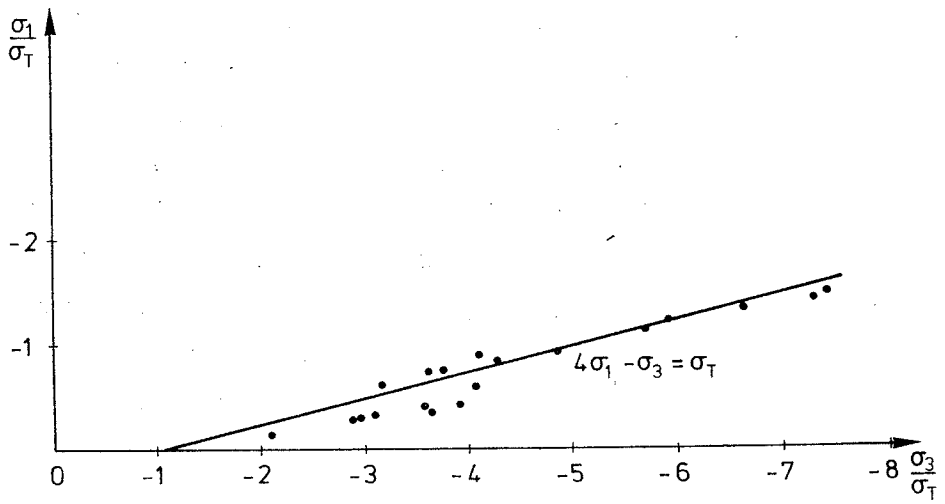

Fig. 2.6 Test results from [72.1].

Richart et al. themselves propose k = 4.1. Johansen [58.1] proposes k = 4.0, while Nielsen [55.1] suggests k = 5, also on the basis of tests, in which, like those referred to here, two of the principal stresses are identical.

Endebrock and Traina [72. 1] have carried out triaxial tests on test cubes in which all three principal stresses can be varied independently. The shape of the test specimens is unfortunate because the uniaxial compression strength is determined as the cube strength. If k = 4 is assumed, the angle of friction becomes $\varphi = 37^{o}$. In the case of uniaxial compression, the failure criterion is satisfied in sections forming the angle $\frac{\pi}{4} - \frac{\varphi}{2}$ with the loading direction, see figure 2.5. Failure can thus only develop freely when $h \geq 2d$, h and d being explained in figure 2.5. The cube compression strength is therefore greater than the cylinder strength, normally about 25%.

Figure 2.6 depicts Endebrock and Traina's test together with (2-7), where k = 4, although the cube strength is put equal to σ_c and $\sigma_1 > \sigma_2 > \sigma_3$. Accordance here is not quite as good as in fig. 2.4, but must be termed acceptable.

According to Coulomb's failure hypothesis the middle principal stress has no effect on the carrying capacity. However, tests show that it does have an effect, as witnessed, for instance, by biaxial compression tests. Fig. 2.7 shows the theoretical course of the failure criterion as found in biaxial compression tests by Liu et al. [72.2],, Endebrock and Traina [72.1] and Kupfer [73.1]. Coulomb's failure

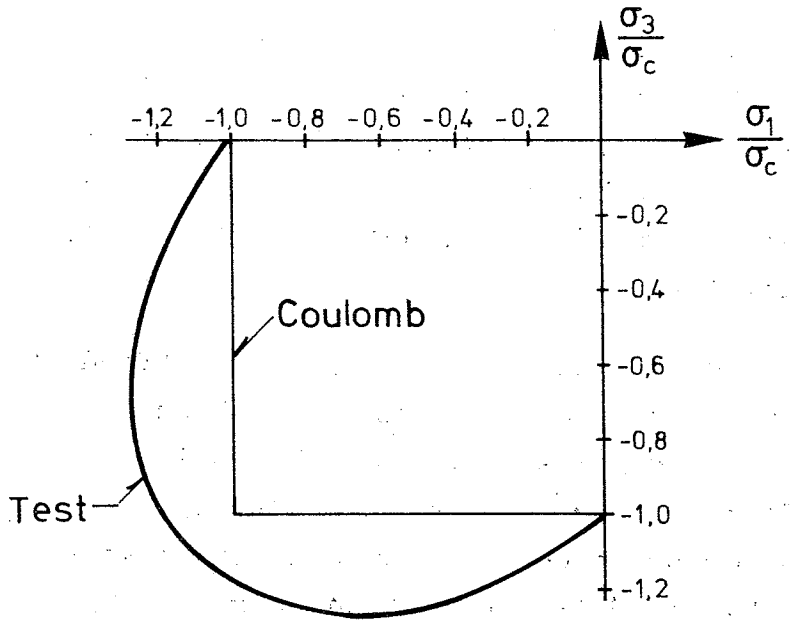

Fig. 2.7 Biaxial compression test and Coulomb's failure hypothesis in case of plane stress field and compression.

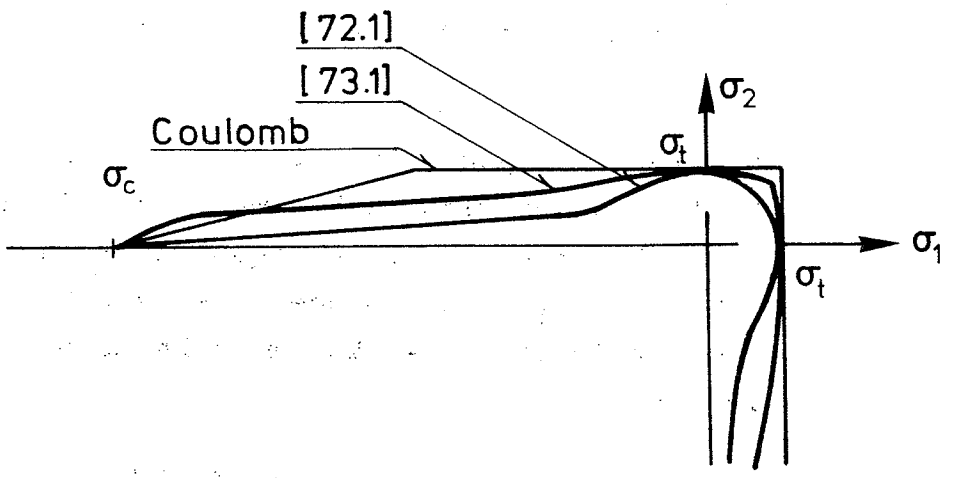

Fig. 2.8 Biaxial tensile tests and tensile/compressive tests, together with Coulomb's failure hypothesis.

hypothesis for compression and plane stress field is included for the purposes of comparison. The significance of the middle principal stress appears clearly from the figure. The tests thus show that $\sigma_3/\sigma_c = -1.2$ to -1.4 for $\sigma_1/\sigma_c = -0.6$, whereas Coulomb's failure hypothesis says $\sigma_3/\sigma_c = -1.0$.

There are fewer tests for determination of the failure criterion for concrete in the case of tensile stresses than in the case of compression stresses. Figure 2.8 shows the theoretical appearance as found in [72.1] and [73.1] in biaxial tests. Coulomb's modified failure hypothesis is included for the purposes of comparison, and it will be seen that the failure hypothesis is a little on the unreliable side when tensile stresses occur.

It can thus be ascertained that Coulomb's modified failure hypothesis does not completely describe the failure criterion for concrete. However, the hypothesis must anyway be described as usable because the deviations are often moderate, which, as previously mentioned, must be regarded in relation to the great dependence of the strength properties on the test circumstances.

When the results derived in the following from the failure hypothesis are compared with tests, φ will normally be put at 37°, corresponding to $k = 4.0$. For the uniaxial compression strength σ_c, the cylinder compression strength will be used because tests show that the ultimate compression strength only falls slightly with increasing h for $h < 2d$, cf. fig. 2.5. The uniaxial tensile strength σ_t is rarely measured, and it is therefore difficult to specify a suitable value since both bending tensile tests and the commonly used split

tensile tests result in excessive values, see, for example, Wright [52.2] and Jensen and Nielsen [75.2]. In finished structures this is further complicated by the fact that the tensile strength can be zero locally on account of cracks. σ_t is often assumed to be zero, but in the case, for instance, of concentrated loads, this gives misleading results, see chapter 6. In the few cases in which σ_t is used, an explanation of the value adopted will be given.

2.4 Stress-Strain Curves for Concrete

The stress-strain diagram for concrete subjected to uniaxial tensile stresses and uniaxial compression stresses is the graphical representation of the relationship between the uniaxial stress and the strain in the same direction as the stress.

Just as in the case of the failure criterion, many factors influence the stress-strain diagram. Despite this, however, we can ascertain a number of general characteristics for the stress-strain diagrams.

In uniaxial tension, concrete is almost linear-elastic right up to failure. In compression, the stress-strain diagram is curved (hollow downwards), and maximum compression stress is reached at a strain of about -0.2%. After the maximum, the stress-strain curve falls and failure occurs at a strain of -0.3% to -0.5%. For concrete with a high compression strength the stress-strain diagram normally has a smaller curvature, and the ultimate strain is also smaller. Thus, a very strong concrete has almost a brittle compression failure. Typical stress-strain diagrams are shown in fig. 2.9.

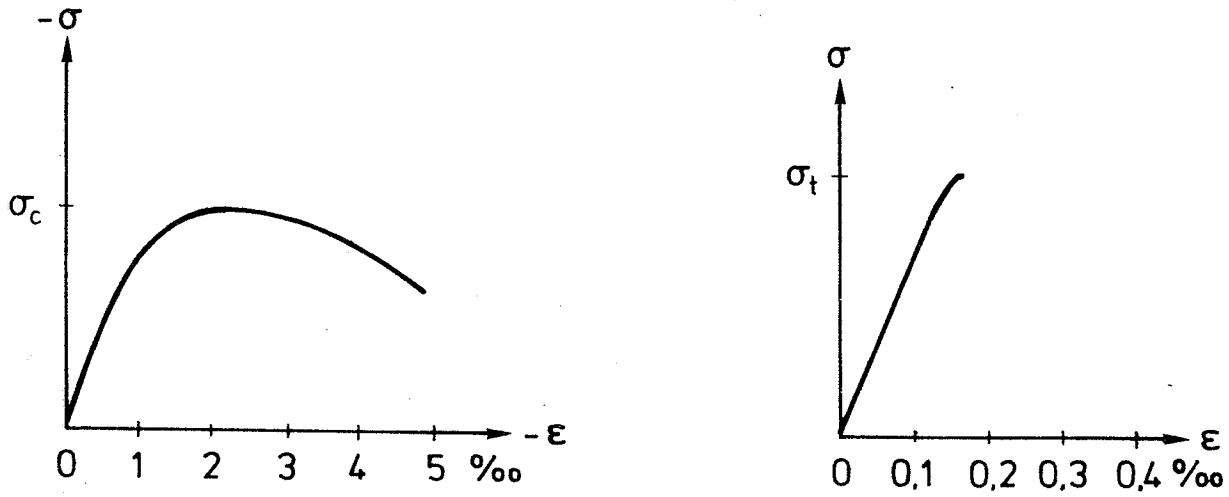

Fig. 2.9 Typical compressive and tensile stress-strain curves.

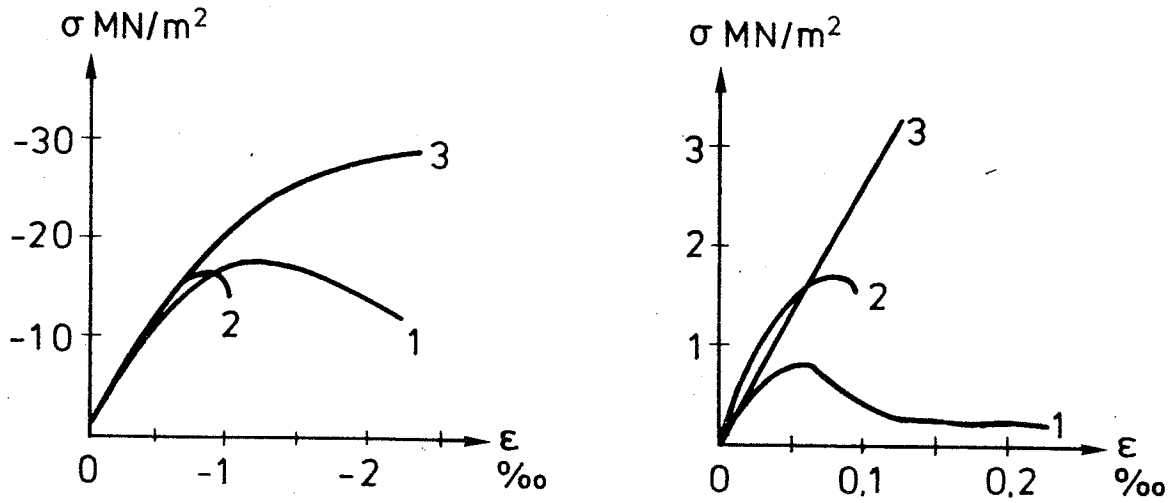

Fig. 2.10 Compressive and tensile stress-strain diagrams for three types of concrete. From [66.1].

However, we also encounter stress-strain diagrams that deviate considerably from those described here. In flexural tests, Nylander and Sahlin [55.2] have measured ultimate strains of -4.0% to -5.0%. Other extreme stress-strain diagrams are shown in fig. 2.10, in accordance with Hughes and Chapmann [66.1].

It will thus be seen that an idealization of concrete to a rigid, perfectly plastic material is a very drastic step to take. However, such idealization may be warranted if, together with the failure criterion adopted, it leads to simple and viable methods of calculation. In the following chapters it will be shown that the idealization is acceptable in many cases.

3. THEORY OF PLASTICITY FOR COULOMB-MATERIALS

3.1 Assumptions

This chapter contains a short study of the theory for rigid-plastic materials. In the following sections expressions will be derived for the internal work per unit volume for rigid-plastic materials whose yield criteron obeys Coulomb's failure hypothesis or Coulomb's modified failure hypothesis. Such materials will be designated Coulomb-materials or modified Coulomb-materials. Section 3.6 contains a brief discussion of the possibilities for plastic calculations of concrete and reinforced concrete.

The yield criterion for a material shall here be taken to mean the stress combination that results in yielding of the material. Expressed in terms of the principal stresses, the yield criterion can be written as follows:

$$f(\sigma_1,\sigma_2,\sigma_3) = 0 \tag{3-1}$$

The signs in $f(\sigma_1,\sigma_2,\sigma_3)$ are chosen such that we get $f < 0$ for stress fields in which yielding cannot occur. When, as here, we work with the rigid-plastic material model, this means that there is no deformation for $f < 0$. $f = 0$ means that plastic deformation can just take place. $f > 0$ corresponds to stress fields which the material cannot sustain.

In a 3-dimensional representation, with σ_1,σ_2 and σ_3 as coordinate axes, (3-1) produces a surface, the so-called yield surface. The corresponding curve for a plane stress field is called the yield surface.

The relationship between the strains that can occur at a given stress field that satisfies (3-1) is determined by the yield law

$$\varepsilon_i = \lambda \frac{\partial f}{\partial \sigma_i} \qquad (i = 1,2,3) \tag{3-2}$$

If we regard (3-2) as a vector in the $\sigma_1,\sigma_2,\sigma_3$-coordinate system, it is a normal vector to the yield surface. If the plastic work $\sigma_i \cdot \varepsilon_i \geq 0$ is required, we get $\lambda \geq 0$. (3-2) is thus an outwards-directed normal to the yield surface (3-1), and the yield law is therefore often called the normality criterion. Note that the direction of the deformations, but not their size, is determined.

The normality criterion is an assumption made in the theory of plasticity. It has been substantiated in various ways by v. Mises [28.2], Gvozdev [38.1] and Drucker [51.1]. The substantiation requires the yield surface to be convex, which is satisfied for Coulomb-materials and modified Coulomb-materials.

Here, the yield criteron and yield law are expressed by principal stresses and strains. However, they can be expressed in more general terms by means of generalized stresses and strains, as done by Gvozdev [38.1] and Prager [52.2].

If the yield surface is a differentiable surface, the normality criteron uniquely determines the direction of the strain vector to a given stress field on the yield surface. If the yield surface consists of piecewise differentiable surfaces, the strain vector for stress fields lying on the curve of intersection of two surfaces must be located in the angle between the normals to the adjacent surfaces.

We will now define some concepts that will prove useful in the following.

A statically permissible stress field is a stress field which satisfies the equilibrium conditions and the statical boundary conditions.

A safe stress field is a stress field in which $f \leq 0$ throughout.

A geometrically admissible failure figure is a deformation field that satisfies the compatibility conditions and the geometrical boundary conditions.

The carrying capacity of a body consisting of a rigid-plastic material is the load at which plastic deformations become possible. The carrying capacity is also called the yield load.

We will now look at the extremum principles, which constitute an important tool in the determination of the carrying capacity of bodies consisting of perfectly plastic materials (including rigid-plastic materials). The extremum principles have been demonstrated by Gvozdev [38.1], Hill [51.2] and Drucker et al. [52.3].

The extremum principles can, for example, be formulated as follows:

The Upper-Bound Theorem:

The load found from the equation of work for an arbitrary, geometrically admissible failure figure is greater than or equal to the yield load of the body.

The Lower-Bound Theorem:

The load belonging to a safe and statically permissible stress field is smaller than or equal to the yield load of the body.

The Uniqueness Theorem:

If there are both a geometrically admissible failure figure and a safe and statically permissible stress field corresponding to a load, then the load is equal to the yield load of the body.

A load that is greater than or equal to the yield load of a body is called an upper bound for the yield load. Correspondingly, a lower bound is a load that is smaller than or equal to the yield load.

In this thesis, use will principally be made of the method that leads to upper bounds - the upper-bound method. For this, as mentioned in the upper-bound theorem, we use the equation of work, and in the following, expressions will be derived for the internal work for Coulomb-materials and modified Coulomb-materials that are subjected to deformations. The equation of work is not identical with the principle of virtual work because the stresses belonging to a chosen deformation need not satisfy the equilibrium conditions.

3.2 Internal Work for Coulomb-materials

In accordance with (2-3) the yield criterion for a Coulomb-material can be written as

$$(3\text{-}3) \qquad f(\sigma_1,\sigma_2,\sigma_3) = \tfrac{1}{2}\sigma_1(1+\sin\varphi)-\tfrac{1}{2}\sigma_3(1-\sin\varphi)-c\cos\varphi = 0$$

when $\sigma_1 \geq \sigma_2 \geq \sigma_3$.

We see that (3-3) has the same form as (3-1), whereby the related strains can be found directly from the normality criterion (3-2). Here, we get

$$\varepsilon_1 = \lambda_1 \frac{1}{2}(1+\sin\varphi), \quad \varepsilon_2 = 0, \tag{3-4}$$

$$\varepsilon_3 = \lambda_1 \frac{1}{2}(1-\sin\varphi)$$

The internal work for a material that is deformed with the strains $(\varepsilon_1, \varepsilon_2, \varepsilon_3)$ is

$$A = \int_V (\sigma_1\varepsilon_1 + \sigma_2\varepsilon_2 + \sigma_3\varepsilon_3)dV = \int_V W\,dV \tag{3-5}$$

where W is the internal work per unit volume (the dissipation).

With (3-4) we get here

$$W = \lambda_1(\tfrac{1}{2}\sigma_1(1+\sin\varphi) - \tfrac{1}{2}\sigma_3(1-\sin\varphi)) \tag{3-6}$$

which, by means of (3-3), can be written as

$$W = \lambda_1 c \cos\varphi \tag{3-7}$$

By means of the positive strain in (3-4), (3-7) can be written as

$$W = 2c \frac{\cos\varphi}{1+\sin\varphi} \varepsilon_1 \tag{3-8}$$

$$= 2c \tan(\frac{\pi}{4} - \frac{\varphi}{2})\varepsilon_1$$

For the first strain invariant I_ε we get

$$I_\varepsilon = \varepsilon_1 + \varepsilon_2 + \varepsilon_3 = \lambda_1 \sin\varphi \tag{3-9}$$

From (3-9) we can thus conclude:

Coulomb-materials yield during volumetric enlargement

By means of (3-9) we can also write (3-7) as

$$W = c \cot\varphi \; I_\varepsilon \tag{3-10}$$

The above has been derived for $\sigma_1 \geq \sigma_2 \geq \sigma_3$, i.e. for one of the six sides of the pyramid constituted by the yield surface in a $\sigma_1, \sigma_2, \sigma_3$-coordinate system. Analogous formulae to (3-8) - (3-10) can be established for the other sides when we substitute ε_1 in (3-8) by the corresponding positive strain.

At the secant between two sides of the yield surface the strain vector will be an arbitrary positive linear combination of the strain vectors belonging to the the two sides. Let us now consider the secant between (3-4) and

$$\tfrac{1}{2}\sigma_2(1+\sin\varphi) - \tfrac{1}{2}\sigma_3(1-\sin\varphi) - c\cos\varphi = 0 \tag{3-11}$$

the related strains are found to be

$$\varepsilon_1 = \lambda_1 \tfrac{1}{2}(1+\sin\varphi), \quad \varepsilon_2 = \lambda_2 \tfrac{1}{2}(1+\sin\varphi) \tag{3-12}$$

$$\varepsilon_3 = -(\lambda_1+\lambda_2) \tfrac{1}{2}(1-\sin\varphi)$$

Analogously with (3-7), we find

$$W = \lambda_1 c\cos\varphi + \lambda_2 c\cos\varphi \tag{3-13}$$

By means of the positive strains in (3-12), (3-13) can be written as

(3-14) $$W = 2c \frac{\cos\varphi}{1+\sin\varphi} (\varepsilon_1+\varepsilon_2)$$

The first strain invariant I_ε is found from (3-12), and inserting this in (3-13) we see that (3-10) is also valid here.

Similar calculations can also be performed in the case of the other secants. When the vertex of the yield surface ($\sigma_1 = \sigma_2 = \sigma_3 = c \cot\varphi$), is neglected, the dissipation can be written as

(3-15) $$W = 2c \frac{\cos\varphi}{1+\sin\varphi} \Sigma \varepsilon^+$$

(3-16) $$\boxed{W = c \cot\varphi \, I_\varepsilon}$$

Here, ε^+ means the positive principal strains.

At the vertex of the yield surface (3-16) is valid, but not (3-15), as can be seen directly by considering the strain vector $\varepsilon_1 = \varepsilon_2 = \varepsilon_3 > 0$ belonging to the vertex. In this case, the sum of the positive strains is equal to the first strain variant, and (3-15) thereby gives a different result than (3-16). (3-15) is given by Chen [69.3], who does not, however, draw attention to the fact that it is not valid at the vertex.

In general, therefore, the dissipation for a Coulomb-material can be written as (3-16).

Example 3.1 Uniaxial Extension

A cubical body consisting of a Coulomb-material is subjected to a load σ acting on one side of it. The body is restrained so

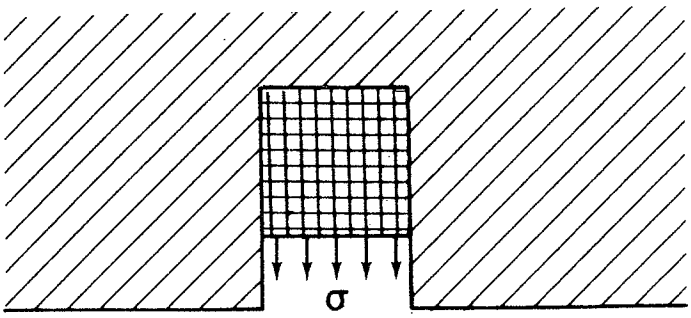

Fig. 3.1 Cube-shaped test specimen from example 3.1.

that it can only deform in the same direction as that in which the imposed stress acts, see. fig. 3.1.

In order to find an upper bound $\sigma > \sigma_{br}$ for the carrying capacity, we imagine the free side moved a distance Δl in the positive direction of the stress. Taking the edge length of the body as equal to 1, we find the principal strains to be

(a) $$\varepsilon_1 = \frac{\Delta l}{l} \ , \ \varepsilon_2 = \varepsilon_3 = 0$$

We thus have uniaxial extension.

We now use the equation of work, where the external work A_y is put equal to the internal work A_i. Using (3-16) and the fact that the volume of the body is l^3, we find

(b) $$\sigma_{br} \, l^2 \, \Delta l = c \cot\varphi \, (\frac{\Delta l}{l} + 0 + 0) l^3$$

The yield stress is thus found to be

(c) $$\sigma_{br} = c \cot\varphi$$

This value is an upper bound for the ultimate load; however, we can easily find a lower bound by letting the body be subjected to hydrostatic tension. The hydrostatic tension that exactly satisfies the yield criterion is

(d) $$\sigma_1 = \sigma_2 = \sigma_3 = c \cot\varphi$$

The upper and lower bounds are thus identical, and the ultimate load is thereby determined by (c).

The stress field hydrostatic tension therefore belongs to the deformation field uniaxial extension, whereas the reverse can naturally not be concluded.

3.3 Plane Deformation Field in Coulomb-Material

It will be seen from (3-4) that one of the principal strains is zero on one of the sides of the yield surface for a Coulomb-material.

In the following we will consider the case in which $\varepsilon_3 = 0$, and where the yield criterion is

$$\text{(3-17)} \qquad \tfrac{1}{2}\sigma_1(1+\sin\varphi) - \tfrac{1}{2}\sigma_2(1-\sin\varphi) - c\cos\varphi = 0$$

Calculations of the following type can naturally be performed for all six sides of the yield surface.

For the strains for (3-17), we have the following:

$$\text{(3-18)} \qquad \varepsilon_1 = \lambda\frac{1}{2}(1+\sin\varphi) \;,\; \varepsilon_2 = -\lambda\frac{1}{2}(1-\sin\varphi)$$

$$\text{(3-19)} \qquad \varepsilon_1 - \varepsilon_2 = \lambda$$

For the strains in an x,y-coordinate system perpendicular to the 3rd main axis, we have

$$\text{(3-20)} \qquad \left.\begin{matrix}\varepsilon_1\\ \varepsilon_2\end{matrix}\right\} = \frac{1}{2}(\varepsilon_x+\varepsilon_y \pm \sqrt{(\varepsilon_x-\varepsilon_y)^2 + \varphi_{xy}^2}$$

$$\text{(3-21)} \qquad \varphi_{max} = (\varepsilon_1-\varepsilon_2)$$

By inserting (3-19) in (3-7) and making use of (3-20) and (3-21), we can also write the dissipation in a plane deformation field as

(3-22) $$W = (\varepsilon_1 - \varepsilon_2) c \cos\varphi$$

(3-23) $$W = \varphi_{max}\, c \cos\varphi$$

(3-24) $$W = c \cos\varphi \sqrt{(\varepsilon_x - \varepsilon_y)^2 + \varphi_{xy}^2}$$

The above formulae are given by Chen [69.3]. Like (3-15), they are not valid for $\sigma_1 = \sigma_2 = \sigma_3 = c \cot\varphi$. Use should therefore be made of the general expression (3-16) for plane deformation fields.

We will now consider a plane, homogeneous deformation field occurring in a narrow zone of height δ between two rigid parts, marked I and II in figure 3.2.

Part II moves V in relation to part I, as shown in figure 3.2. In the deformation zone we find the strains

(3-25) $$\varepsilon_y = \frac{V}{\delta} \sin\alpha \ , \ \varepsilon_x = 0 \ , \ \varphi_{xy} = \frac{V}{\delta} \cos\alpha$$

The principal strains are

(3-26) $$\left.\begin{matrix} \varepsilon_1 \\ \varepsilon_2 \end{matrix}\right\} = \frac{V}{2\delta} (\sin\alpha \pm 1)$$

From (3-26) we obtain

(3-27) $$\frac{\varepsilon_1}{\varepsilon_2} = \frac{\sin\alpha+1}{\sin\alpha-1}$$

If the vertex of the yield surface is neglected, (3-18) must at the same time be satisfied, which leads to $\alpha = \varphi$.

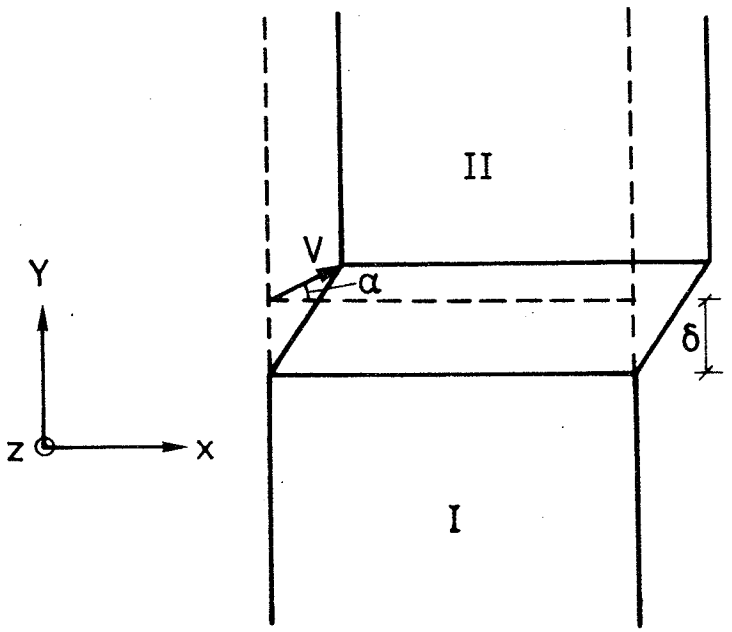

Fig. 3.2 Deformation zone between two rigid parts.

Putting the thickness at unity in the deformation zone in figure 3.2, we can write the internal work per unit length by means of (3-26) and $\alpha = \varphi$. For W we use (3-16).

(3-28) $$\boxed{W_1 = V\, c \cos\varphi}$$

(3-28) is independent of the height δ, and this has led to introduction of the convenient discontinuity lines, where $\delta \to 0$, but V is retained and (3-28) is still an expression of the internal work per unit of length. The discontinuity lines can be regarded as idealized states in line with the well-known yield lines in slab theory.

Discontinuities with $\alpha > \varphi$ also exist, corresponding to the stress field at the vertex of the yield surface. For such lines, use must be made of

(3-29) $$W_1 = V\, c \cot\varphi \sin\alpha$$

instead of (3-28).

The criterion $\alpha \geq \varphi$ in plane deformation fields means that:

> In plane deformation fields in a Coulomb-material, displacement along a discontinuity line is always accompanied by a movement perpendicular to the line.

Example 3.2 Line Failure along a Logarithmic Spiral.

A geometrically admissible failure pattern in plane deformation fields in a Coulomb-

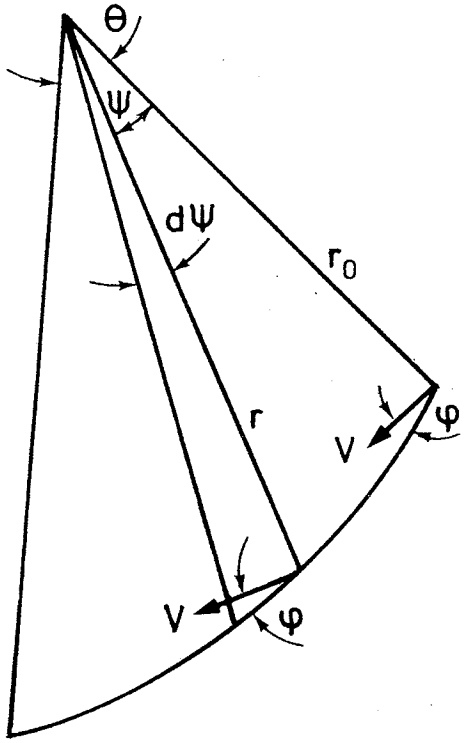

Fig. 3.3 Failure along logarithmic spiral.

material is failure along a discontinuity line, which has the shape of a logarithmic spiral, see fig. 3.3. The failure is chosen such that the body turns as a rigid body around the pole of the spiral, and the angle between the movement at a point and the logarithmic spiral is φ .

The logarithmic spiral is given by

(a) $$r = r_o e^{\psi \tan\varphi}$$

Every point along the spiral has a movement V that is proportional to the length of r at the location in question and that stands at right-angles to r, i.e.

(b) $$V = V_o e^{\psi \tan\varphi}$$

We will now formulate an expression for the internal work along a spiral discontinuity line, using the notation from fig. 3.3.

We consider a small angle $d\psi$.

The corresponding length of the spiral is

(c) $$s = \frac{r\, d\psi}{\cos\varphi}$$

For $d\psi$ we find the internal work from (c) and (3-28)

(d) $$dW = V c r\, d\psi$$

Using (a) and (b) and integrating from 0 to θ we find the internal work for failure along a spiral with vertical angle θ :

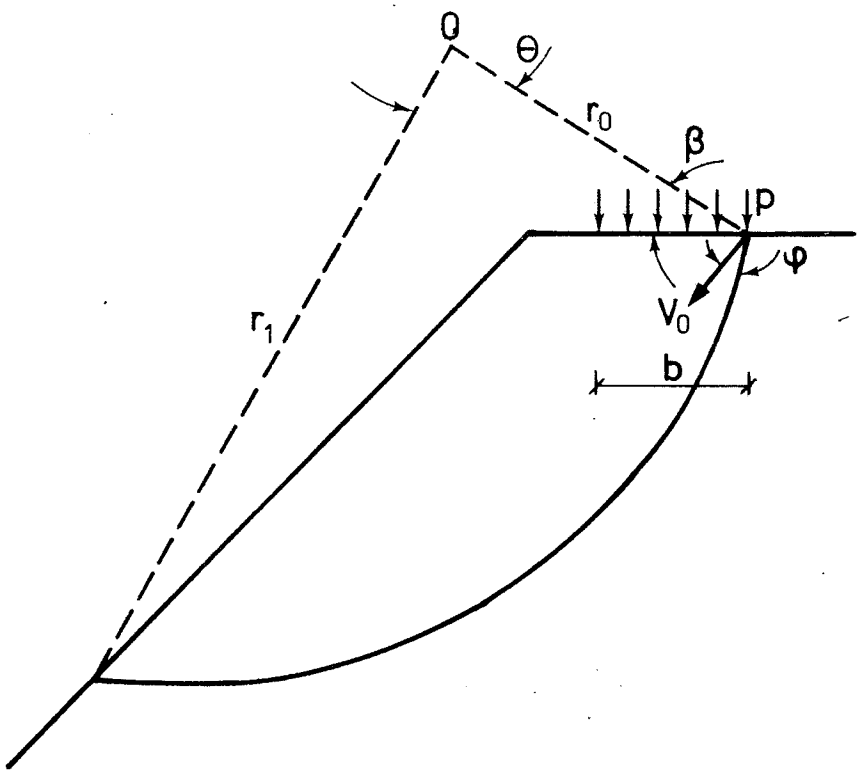

Fig. 3.4 Slope with failure along spiral.

(e) $$\boxed{W = \tfrac{1}{2} c V_o r_o \cot\varphi \, [e^{2\theta\tan\varphi} - 1]}$$

The thickness is here put at 1.

It should be noted that a logarithmic spiral (including a straight line) satisfies the requirement regarding a constant angle φ between the movement and the discontinuity line. This is a requirement that applies everywhere on the yield surface except at the vertex.

The type of failure considered is the same as that known as line failure in geotechnical calculations.

If, on the other hand, we have zone failure in a logarithmic spiral, i.e. a type of failure in which the whole of the spiral fails, the following expression is valid for the internal work:

(f) $$W = c V_o r_o \cot\varphi \, [e^{2\theta\tan\varphi} - 1]$$

Here, too, (b) is valid for V.

The expression has been found by Chen [69.3] and others.

Example 3.3 Carrying Capacity of Slope (Stability)

Let us consider a load p located on a surface, near a sloping edge. An upper bound for p can be found by assuming a failure pattern as shown in fig. 3.4. The failure pattern is a logarithmic spiral that turns like a rigid body about the pole O. O is specified by the parameters β and r_o. V_o at A forms the angle φ with the tangent of the spiral at A.

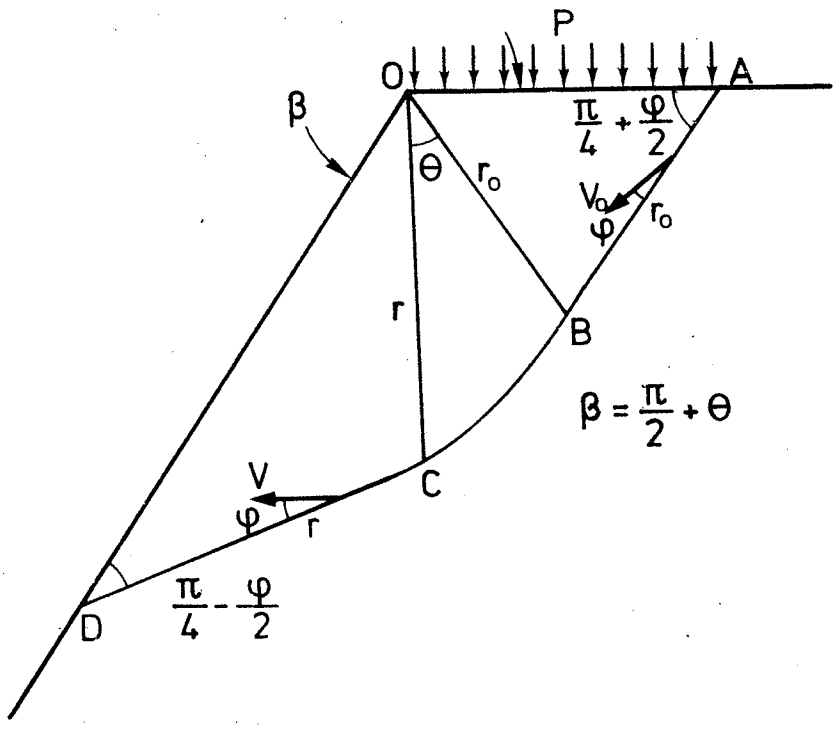

Fig. 3.5 Failure mechanism in slope.

The equation of work can be written with the notation from fig. 3.4. It should be noted, however, that θ depends on β, r_o and the geometry of the loaded body.

The average vertical displacement of p is

(a) $$V_p = V_o \cos\alpha\left(1 - \frac{b}{2r_o\cos\alpha}\right)$$

The external work is

(b) $$A_y = p\,b\,V_o \cos\alpha \left(1 - \frac{b}{2r_o\cos\alpha}\right)$$

The internal work is found from (e) in example 3.2.

(c) $$A_i = \tfrac{1}{2}c\,V_o\,r_o \cot\varphi\,[e^{2\theta\tan\varphi}-1]$$

From $A_y = A_i$ we find the following upper bound for p:

(d) $$p = c\cot\varphi \frac{r_o^2}{2r_o\,b\cos\alpha - b^2}\,[e^{2\theta\tan\varphi}-1]$$

This solution is identical with that found in geotechnical stability calculations in respect of a weightless body, as described, for example, by Harremoës et al. [70.1] and Lundgren and Brinch Hansen [58.2].

Example 3.4 Carrying Capacity of a Slope

We will now consider a slope that is loaded as shown in fig. 3.5. As failure pattern we take two equilateral triangles that move as rigid bodies. Between them we place a logarithmic spiral, which must have zone failure.

Along the line AB there is the movement V_o, which forms the angle φ with the discontinuity

line. Along BC V increases at the same time as it turns, and along CD it has the value

(a) $$V = V_o e^{\theta \tan\varphi}$$

The external work is found to be

(b) $$A_y = p\, 2r_o \cos(\tfrac{\pi}{4} + \tfrac{\varphi}{2}) V_o \cos(90-(\tfrac{\pi}{4} + \tfrac{\varphi}{2})+\varphi)$$

$$= p\, r_o V_o (1-\sin\varphi)$$

There are three contributions to the internal work. The contributions from the discontinuity lines AB and CD are found from (3-28), and the contribution from the zone failure in is found from (f) in example 3.2.

The following applies

(c) $$r = r_o e^{\theta \tan\varphi}$$

and hence,

(d) $$A_i = c\, r_o V_o \cos\varphi + c\, r_o e^{\theta\tan\varphi} V_o e^{\theta\tan\varphi} \cos\varphi + c\, r_o V_o \cot\varphi [e^{2\theta\tan\varphi}-1]$$

Using $A_y = A_i$, we find

(e) $$p = \frac{c}{1-\sin\varphi}[\cos\varphi-\cot\varphi+(\cos\varphi-\cot\varphi)e^{2\theta\tan\varphi}]$$

After some rewriting and introduction of $\theta = \beta - \frac{\pi}{2}$, we find

(f) $$p = c \cot\varphi [\tan^2(\tfrac{\pi}{4} + \tfrac{\varphi}{2}) e^{(2\beta-\pi)\tan\varphi}-1]$$

In the case where $\beta = \pi$, (f) becomes

(g) $$p = c \cot\varphi [\tan^2(\tfrac{\pi}{4} + \tfrac{\varphi}{2}) e^{\pi\tan\varphi}-1]$$

which is identical with the solution found by Prandtl in 1920 [20.1]. The above example is reproduced from Chen [69.3].

3.4 Plane Deformation Field in Modified Coulomb-Material

In a plane deformation field in a modified Coulomb-material, where $\varepsilon_3 = 0$ and $\sigma_1 \geq \sigma_3 \geq \sigma_2$, the yield criterion is composed of the following two criteria:

$$\tfrac{1}{2}\sigma_1(1+\sin\varphi)-\tfrac{1}{2}\sigma_2(1-\sin\varphi)-c\cos\varphi = 0 \tag{3-30}$$

$$\sigma_1 - \sigma_A = 0 \tag{3-31}$$

Here, (3-30) corresponds to sliding failure, and the corresponding dissipation is found from (3-16). For discontinuity lines, (3-28) applies. (3-31) corresponds to separation failure, and the corresponding strains are found by means of (3-2) to be

$$\varepsilon_1 = \lambda' \qquad \varepsilon_2 = 0 \tag{3-32}$$

For separation failure the dissipation is

$$W = \sigma_A \varepsilon_1 \tag{3-33}$$

In the case of the deformation zone in fig. 3.2, we see from (3-26) that, as anticipated, separation failure occurs at $\alpha = \frac{\pi}{2}$. The internal work per unit length is found from (3-33) and (3-26) to be independent of δ, and is

$$W = \sigma_A V \tag{3-34}$$

When both (3-30) and (3-31) are satisfied simultaneously, the corresponding strains are

found from (3-18) and (3-32):

(3-35) $$\varepsilon_1 = \tfrac{1}{2}\lambda(1+\sin\varphi)+\lambda' \quad \varepsilon_2 = -\tfrac{1}{2}\lambda(1-\sin\varphi)$$

The dissipation is

(3-36) $$W = \sigma_1 \varepsilon_1 + \sigma_2 \varepsilon_2$$

By inserting (3-35) in (3-36) we find, as both (3-10) and (3-31) are satisfied:

(3-37) $$W = \lambda c \cos\varphi + \lambda' \sigma_A$$

We again consider the deformation zone in fig. 3.2, where (3-26) and (3-35) must be satisfied.

If $\lambda' = 0$ we get pure sliding failure, and (3-28) is valid. If $\lambda = 0$, we get separation failure, and (3-34) is valid. If both $\lambda' \neq 0$ and $\lambda \neq 0$, we get $\frac{\pi}{2} > \alpha > \varphi$. λ and λ' can be found from (3-26) and (3-35), and inserting these quantities in (3-37), we find that the work per unit length is independent of δ . We obtain

(3-38) $$\boxed{W_1 = V\left(\frac{1-\sin\alpha}{1-\sin\varphi}\, c\cos\varphi + \frac{\sin\alpha-\sin\varphi}{1-\sin\alpha}\,\sigma_A\right), \quad \alpha \geq \varphi}$$

It will be seen that (3-28) also applies in cases in which $\alpha = \varphi$ and $\alpha = \frac{\pi}{2}$. The formula thus gives the internal work per unit of length of a discontinuity line in a modified Coulomb-material.

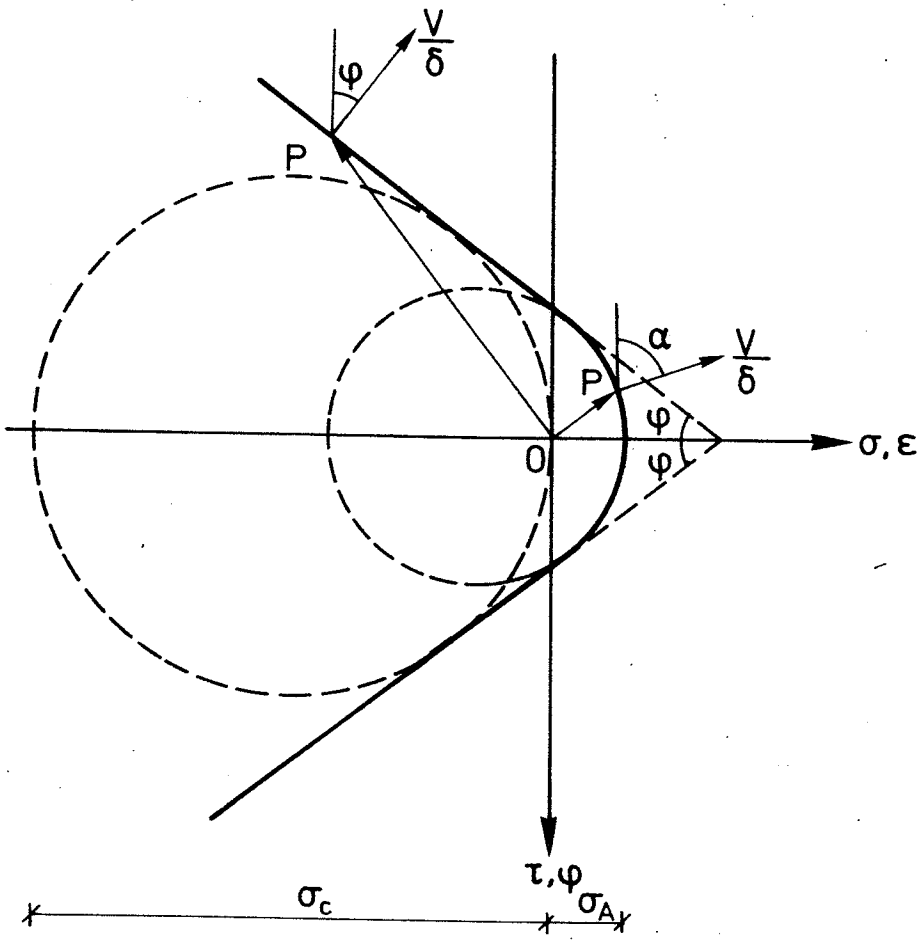

Fig. 3.6 Failure criterion with strain vectors.

By means of (2-6) we can rewrite (3-38) to include the uniaxial compression strength . We thereby find

$$(3\text{-}39) \qquad \boxed{W_1 = V\left(\frac{1-\sin\alpha}{2}\sigma_c + \frac{\sin\alpha-\sin\varphi}{1-\sin\varphi}\sigma_A\right), \qquad \alpha \geq \varphi}$$

In the above we use the separation strength σ_A. If the uniaxial tensile failure takes the form of separation failure, $\sigma_t = \sigma_A$, and in this case, σ_t can be inserted in (3-38) and (3-39).

Example 3.5 Drucker, Prager and Chen's Solution

Drucker and Prager [52.4] have found (3-28) and (3-38) for $\sigma_A = 0$ by considering the yield criteron for a Coulomb-material and a modified Coulomb-material in a σ,τ-coordinate system. Chen and Drucker [69.2] have found (3-28) in the same way.

The normality criterion, together with (3-25), shows that V must form an angle $\alpha \geq \varphi$ with the discontinuity line, see fig. 3.6. The internal work per unit length of a discontinuity line is found as δ multiplied by the vector product of the stress vector and the strain vector.

$$(a) \qquad W_1 = \delta\, \vec{OP}\, \frac{\vec{V}}{\delta}$$

The results from a plane deformation field in discontinuity lines are thus not new, but have not previously been derived on the basis of the yield criterion in principal stress form.

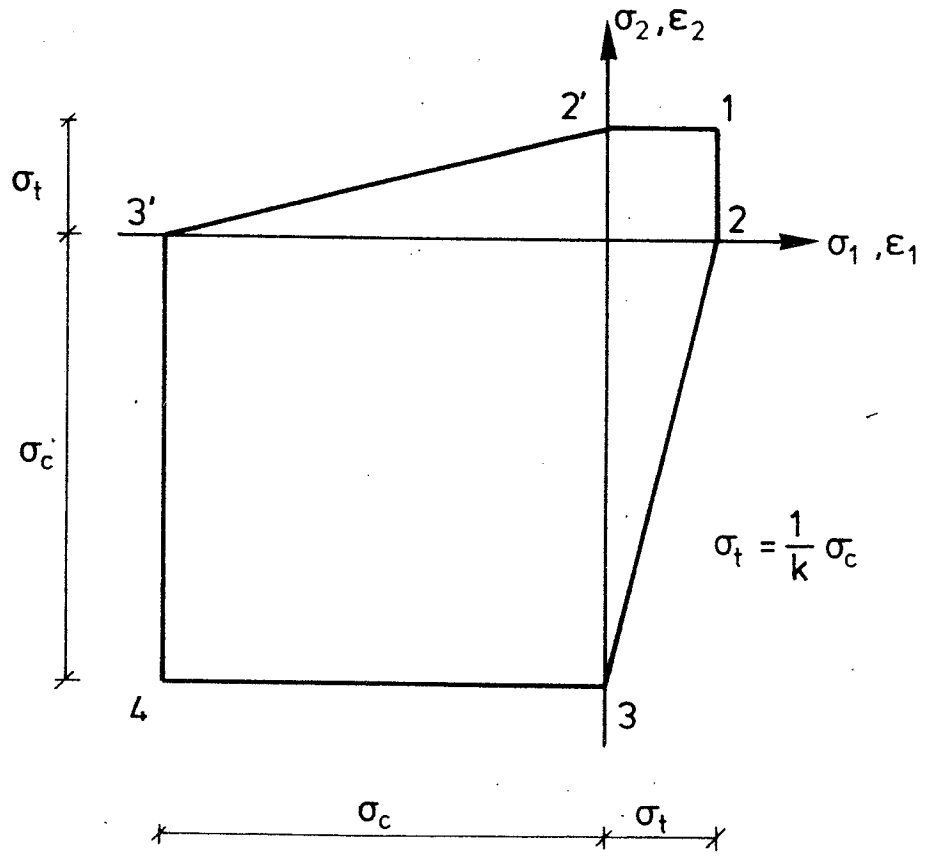

Fig. 3.7 Failure criterion for Coulomb-material with $\sigma_3 = 0$ and for modified Coulomb material with $\sigma_3 = 0$ and $\sigma_t < \sigma_A$.

3.5 Plane Stress Field

Now let us consider the deformation zone in fig. 3.2 again. We assume that both the plane stress field and the deformation field in the deformation zone are homogeneous. The problem can now be treated as a plane problem since we only consider what is going on in the plane of the paper.

For a Coulomb-material or modified Coulomb-material, where $\sigma_A > \sigma_t$, the yield criterion in a plane stress field, where $\sigma_3 = 0$, is shown in fig. 3.7. A strain coordinate system is inserted, corresponding to the stress coordinate system, and it is now easy to determine where a strain field which we wish to introduce belongs because the strain vector must be normal to the yield curve.

The strains in the deformation zone under consideration are again given by (3-26), and we see that $\varepsilon_1 > 0$ and $\varepsilon_2 \leq 0$, i.e. we find ourselves in the area 1-2-3 in fig. 3.7. However, at point 1, the strain vector can only be parallel with the ε_1-axis. The following formulae can be established for the dissipation in the area in question:

At point 3:

$$W = -\sigma_c \varepsilon_2 \qquad \varepsilon_2 \leq -\frac{1}{k}\varepsilon_1 \tag{3-40}$$

At point 2:

$$W = \sigma_t \varepsilon_1 \qquad \varepsilon_2 \geq -\frac{1}{k}\varepsilon_1 \tag{3-41}$$

Along 2-3:

(3-42) $$W = \sigma_t \varepsilon_1 = -\sigma_c \varepsilon_2 \qquad \varepsilon_2 = -\frac{1}{k}\varepsilon_1$$

Along 1-2 and at 1:

(3-43) $$W = \sigma_t \varepsilon_1 \qquad \varepsilon_2 = 0$$

We introduce (3-26) for the strains, and the last relationship in (2-5) for k. It will then be seen that (3-42) is satisfied when $\alpha = \varphi$.

From formulae (3-40) - (3-43) we find the work per unit length $W_1 = W\delta$ in the deformation zone to be

(3-44) $$W_1 = \tfrac{1}{2}\sigma_c V (1-\sin\alpha), \qquad \alpha \leq \varphi$$

(3-45) $$W_1 = \tfrac{1}{2}\sigma_c V \frac{1-\sin\varphi}{1+\sin\varphi} (1+\sin\alpha), \qquad \alpha \geq \varphi$$

Here, (3-44) gives the internal work per unit length at 3 and along 2-3, and (3-45) gives the internal work per unit length at 2, along 1-2 and along 2-3. The expressions are independent of δ ; therefore, as in the case of plane deformation fields, we can introduce discontinuity lines in plane stress fields, where $\delta \to 0$.

For a modified Coulomb-material, where $\sigma_t = \sigma_A$, the yield criterion for a plane stress field is shown in fig. 3.8. 1-2-3 are once more possible locations for the strain vector from the deformation zone in fig. 3.2.

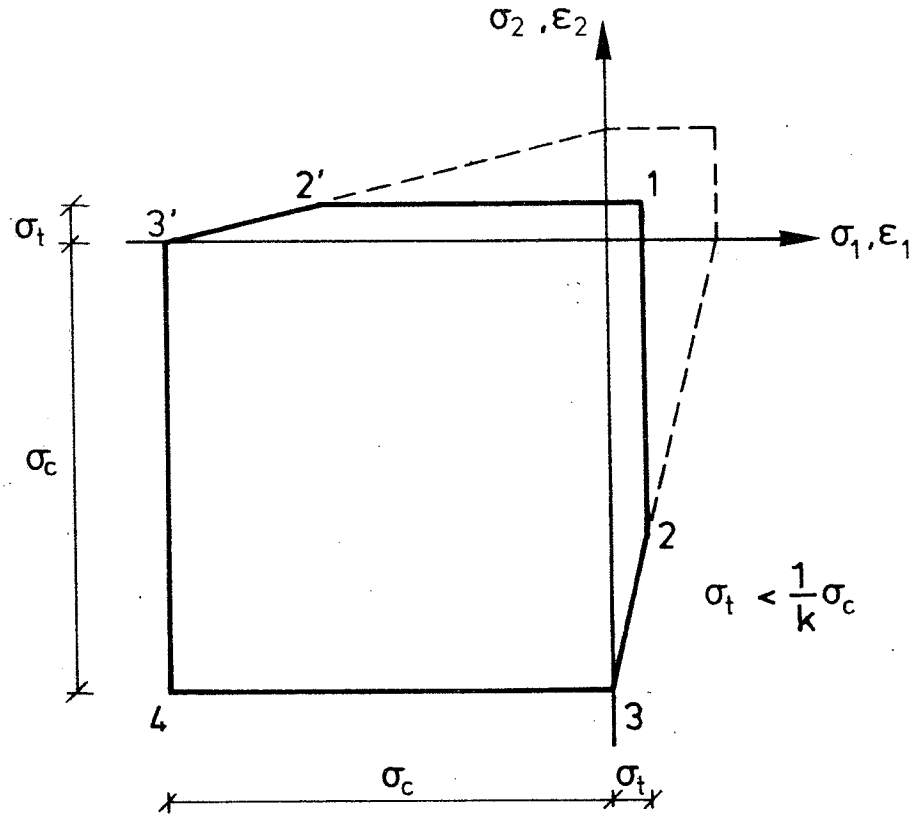

Fig. 3.8 Failure criterion for modified Coulomb-material with $\sigma_3 = 0$ and $\sigma_t = \sigma_A$.

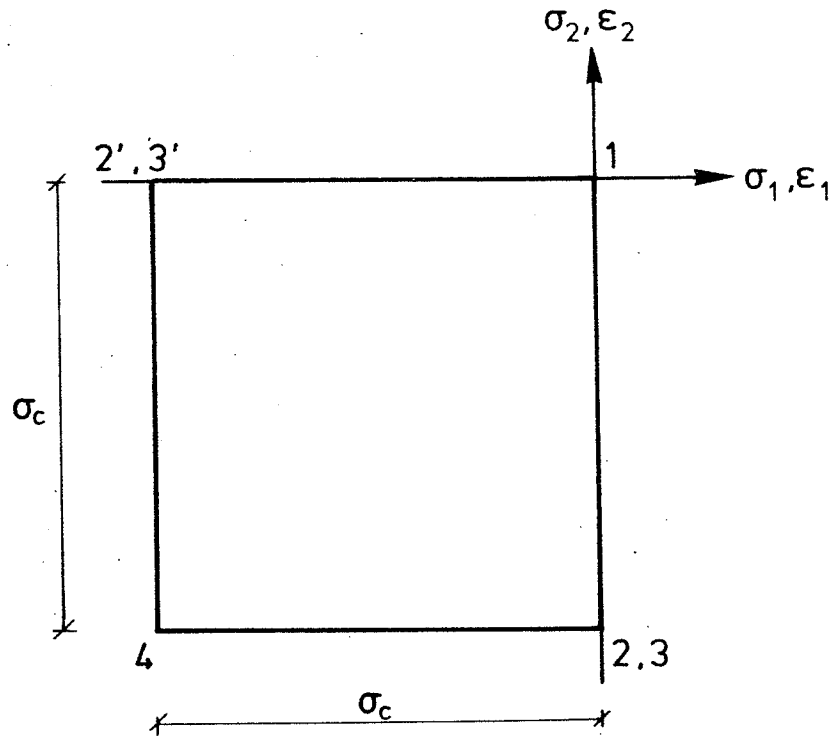

Fig. 3.9 Failure criterion for modified Coulomb-material with $\sigma_3 = 0$ and $\sigma_t = 0$.

The coordinates to 2 are

(3-46) $$(\sigma_1,\sigma_2) = (\sigma_t, k\sigma_t - \sigma_c)$$

At this point, the dissipation is

(3-47) $$W = \sigma_t \varepsilon_1 + (k\sigma_t - \sigma_c)\,\varepsilon_2 \qquad \varepsilon_2 \geq -\frac{1}{k}\,\varepsilon_1$$

As previously, (3-40), (3-42) and (3-43) apply along the remainder of the yield curve, although only the last relation in (3-42) is valid.

We can now find the internal work per unit length of a discontinuity line for the modified Coulomb-material in the same way as in the case of the Coulomb-material.

We obtain:

(3-48) $$W_1 = \tfrac{1}{2}\sigma_c V (1-\sin\alpha) \qquad \alpha \leq \varphi$$

(3-49) $$W_1 = \tfrac{1}{2}\sigma_c V (1-\sin\alpha) + \frac{\sin\alpha-\sin\varphi}{1-\sin\varphi}\,\sigma_t V \qquad \alpha \geq \varphi$$

(3-48) gives the internal work per unit length at 3 and along 2-3, and (3-49) gives the internal work per unit length at 2, along 1-2 and along 2-3.

In fig. 3.9 the yield criterion is shown for a plane stress field and $\sigma_t = 0$. Only negative strains contribute to the dissipation, and this contribution can be written

(3-50) $$W = \tfrac{1}{2}\sigma_c(|\varepsilon_1|+|\varepsilon_2|-(\varepsilon_1+\varepsilon_2))$$

The internal work per unit length of a discontinuity line can be found from (3-50) and (3-26) to be

$$W_1 = \tfrac{1}{2}\sigma_c V (1-\sin\alpha) \tag{3-51}$$

The same result would naturally also be found from (3-48) and (3-49) for $\sigma_t = 0$. (3-50) and (3-51) have been derived by Nielsen [69.4] in connection with his work on reinforced concrete diaphragms.

It should be noted that (3-49) is identical with (3-39) for $\sigma_t = \sigma_A$, and further, that (3-44) and (3-45) are identical with (3-28) for $\alpha = \varphi$. Thus, in some areas of the yield curve for a plane stress field, the corresponding strain field will also be plane. For the yield criterion in fig. 3.7 this naturally applies when $\alpha = \varphi$. For the yield criteria in fig. 3.8 and 3.9 it applies when $\alpha \geq \varphi$.

On the other hand, it cannot be concluded that there is a plane stress field when there is a plane deformation field where (3-28) or (3.39) apply.

The above is conditional on the middle principal stress having no influence in the case of the yield criteria used here.

Example 3.6 Approximation at Discontinuity Lines

We will again consider the deformation zone in fig. 3.2, and assume that there is a plane stress field. In this example, we will see what happens in the deformation zone when we leave the plane theory.

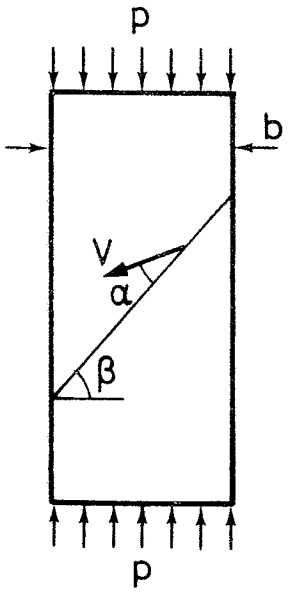

Fig. 3.10 Compressed diaphragm with failure mechanism.

The body with the deformation zone now extends at right-angles to the plane of the paper, and in the homogeneous deformation zone there will be a strain ε_3, which is not zero, except in the special case in which we have both plane stress and plane deformation field.

Therefore, if we have a plane stress field corresponding to point 3 in fig. 3.7, 3.8 or 3.9, there must be inhomogeneous transitional zones between the homogeneous deformation field and the rigid parts I and II in fig. 3.2. The contribution from these transitional zones to the internal work is thus neglected when we use the formulae in section 3.5.

Example 3.7 The Compression Test

A diaphragm subjected to uniaxial compression p is considered. The yield criterion is that shown in fig. 3.9. Failure is assumed to take place along a discontinuity line with the slope β, see fig. 3.10. The movement V forms the angle α with the discontinuity line.

The external work A_y is found to be

(a) $$A_y = p\,b\,V\cos(90 - (\beta-\alpha))$$

The internal work from the discontinuity line is found from (3-51):

(b) $$A_i = \tfrac{1}{2}\sigma_c\,V\,(1-\sin\alpha)\,\frac{b}{\cos\beta}$$

From $A_y = A_i$ we obtain

(c) $$p = \tfrac{1}{2}\sigma_c\,\frac{1-\sin\alpha}{\cos\beta\,\sin(\beta-\alpha)}$$

(c) is an upper bound for the carrying capacity, and by minimizing with regard to α and β, we find the minimum for

(d) $$\beta = \frac{\pi}{4} + \frac{\alpha}{2}$$

As expected, the minimum is found to be

$$p = \sigma_c$$

3.6 Plastic Properties of Concrete

Here, we will very briefly look into the question of how well concrete satisfies the conditions for being calculated in accordance with the rules established in this chapter for the modified Coulomb-material, with $\sigma_t = \sigma_A$.

In section 2.3, test results for concrete were compared with Coulomb's modified failure hypothesis, and were found to be in reasonable agreement with this. The hypothesis can thus be used as yield criterion because the simple ultimate strength tests fit the hypothesis. On the other hand, fig. 2.8 seems to indicate that the yield criterion for concrete is not always convex when there are tensile stresses. However, one should be cautious about drawing this conclusion because existing test results are ambiguous on this point, and it is difficult to carry out the tests satisfactorily.

The simple compression and tensile stress-strain curves for concrete were dealt with in section 2.4, where we saw that idealization of concrete to a rigid-plastic material was a drastic idealization.

In reality, elastic strains will also occur; however, in the rigid-plastic model, we only consider the ultimate state in which yield stress is reached at so many points and in such big zones that a geometrically admissible yield pattern can be developed.

In order to be able to use this approach, the elastic strains must be small in relation to the plastic strains. In section 2.4 we saw that this is not the case for concrete, either in uniaxial compression or in uniaxial stress. We also saw that, for compression, the stress falls after achieving its maximum value and that, for tension, there is seldom any capacity for continued deformation after the maximum stress has been reached.

The contribution to the internal work from zones with separation failure will thus usually be negligible. The contribution from sliding failure will often be less than determined by the formulae in this chapter because the whole of the yield surface will not be fully active. To take this into account we can introduce an efficiency factor $\nu \leq 1$, by which a yield surface must be multiplied to arrive at an equivalent fully utilized yield surface.

This can also be done by multiplying σ_c by ν, whereby we get an equivalent yield stress over the entire area. This has been done by Nielsen [69.1] in connection with the formulation of a lower-bound solution for the carrying capacit of beams in shear.

Finally, attention must here be drawn to the fact that the normality criterion requires a volumetric enlargement during yielding. Some volumetric enlargement has been found in tests,

but none of the available results either confirms or disproves the normality criterion.

The results found in plastic calculations must therefore be used with care because it has not yet been determined whether the assumptions for the plastic calculations actually exist. However, to the extent that tests support the calculations, the results can naturally always be used.

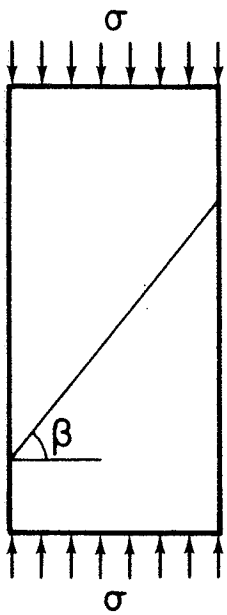

Fig. 4.1 Construction joint in concrete body.

4. UNREINFORCED CONSTRUCTION JOINT

4.1 Introduction

In this chapter we shall consider a construction joint placed so that it forms an angle β with a normal to the loading direction, see fig. 4.1. The plane of the construction joint is perpendicular to the plane of the paper.

A construction joint normally means a weakening of the carrying capacity of the body along the construction joint itself. Assuming that Coulomb's failure hypothesis can also be used as yield criterion for the construction joint, we can take this weakness into account by introducing new values for c and φ to apply in the construction joint. If the construction joint is made with a certain degree of roughness, φ will often be the same as in monolithic concrete, as will be demonstrated in examples in this and the following chapter. In such cases we can introduce $c' < c$ in the construction joint, but retain the size of the angle of friction.

4.2 Sliding Failure

We will now look at a failure mechanism in which sliding failure occurs along the construction joint, whereby we get a plane deformation field and the discontinuity line coincides with the construction joint. We shall therefore use the strength parameters of the construction joint for the calculations.

The deformation vector V forms the angle φ' with the discontinuity line. φ' is the angle of friction applying to the construction joint.

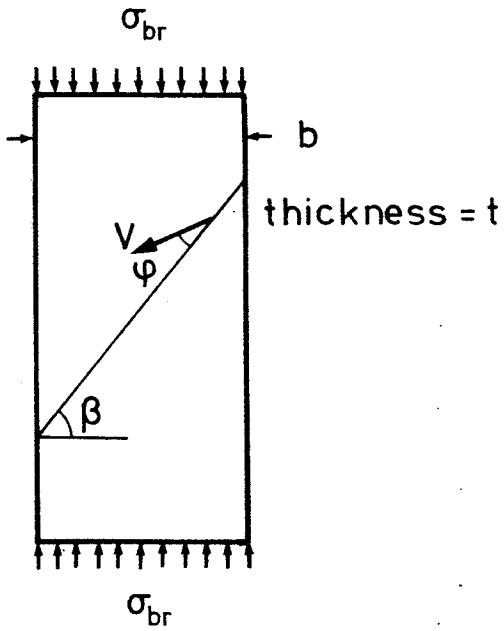

Fig. 4.2 Sliding failure in construction joint.

As mentioned, this angle need not be equal to the angle of friction φ for the monolithic concrete.

With the notation from fig. 4.2, we find the external work to be

(4-1) $$A_y = \sigma_{br}\, b\, t\, V \cos(90-\beta+\varphi')$$

The internal work is found from (3-28):

(4-2) $$A_i = V\, c'\cos\varphi' \frac{b}{\cos\beta}\, t$$

From these expressions we find an upper bound for the carrying capacity:

(4-3) $$\sigma_{br} = \frac{\cos\varphi'}{\cos\beta\, \sin(\beta-\varphi')}\, c'$$

The minimum carrying capacity is found when the construction joint has the slope $\beta = \frac{\pi}{4} + \frac{\varphi'}{2}$, and is

(4-4) $$\sigma_{br,min} = \frac{2c'\cos\varphi'}{1-\sin\varphi'}$$

Comparison with (2-6) shows that $\sigma_{br,min}$ is the compression strength for a concrete with the strength properties of the construction joint.

If the slope of the construction joint is increased or reduced in relation to $\beta = \frac{\pi}{4} + \frac{\varphi'}{2}$, the strength will increase. However, it can never be greater than σ_c for the monolithic concrete. If β is of such a size that we get $\sigma_{br} > \sigma_c$ from (4-3), failure will simply occur outside the construction joint. In the case of such failure, the carrying capacity will be $\sigma_{br} = \sigma_c$.

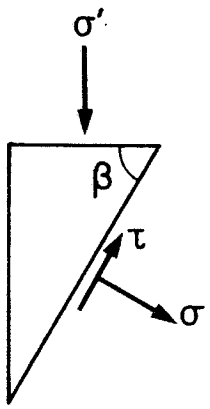

Fig. 4.3 Stresses along construction joint.

Incidentally, this carrying capacity is found whether we assume a plane stress field or a plane deformation field in the case of failure of the monolithic concrete. For a plane stress field this is shown in example 3.7, and for the plane deformation field, it appears from (4-3) and (4-4), in which c' and φ' must be substituted by c and φ in the case of monolithic concrete. (4-3) is then the general upper-bound expression, which has minimum (4-4) for $\beta = \frac{\pi}{4} + \frac{\varphi}{2}$.

This accordance between the carrying capacity in a plane deformation field and that in a plane stress field results from the fact that the middle principal stress does not form part of the yield criterion - a factor that is discussed in detail in section 3.5.

The upper bound found for the carrying capacity (3-14) is an exact solution, as will be seen from the following lower-bound considerations.

In the construction joint the yield criterion is

$$|\tau| = c' - \sigma \tan\varphi' \tag{4-5}$$

An external load σ results in a shear force and a normal force in the construction joint. Asssuming that these are uniformly distributed along the construction joint, we obtain the following relationship between the external load σ' and the stresses (σ,τ) in the construction joint with the slope β (see fig. 4.3):

$$\sigma = -\sigma' \cos^2\beta \tag{4-6}$$

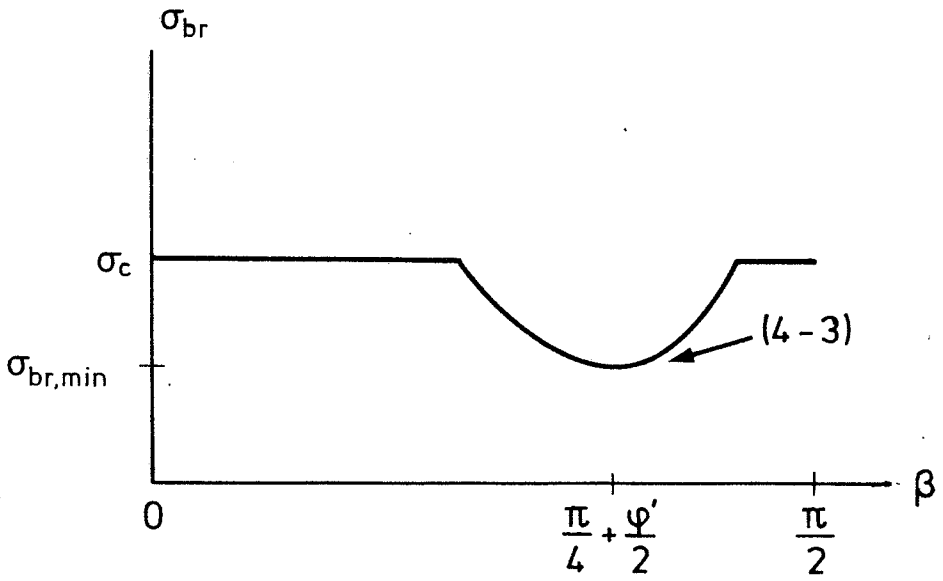

Fig. 4.4 Dependence of the carrying-capacity on the slope of the construction joint. Type of failure: slidi failure.

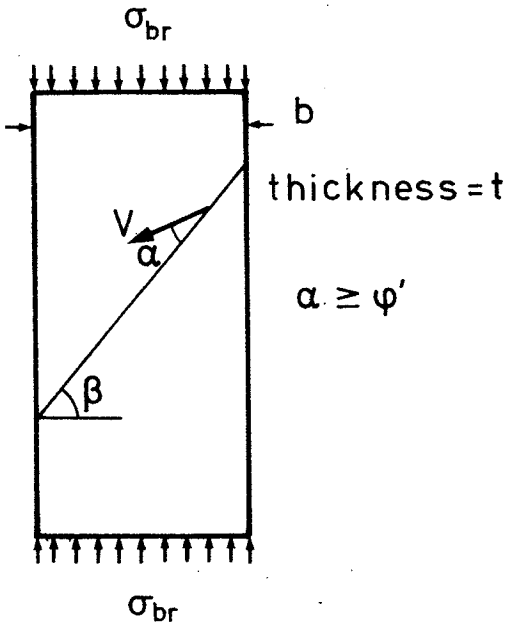

Fig. 4.5 Failure in construction joint.

(4-7) $$\tau = \sigma' \sin\beta \cos\beta$$

A lower bound for the ultimate load σ'_{br} is found by putting $\sigma' = \sigma'_{br}$ in (4-6) and (4-7) and inserting these in (4-5).

(4-8) $$\sigma'_{br} \sin\beta \cos\beta = c' - \sigma'_{br} \cos^2\beta \tan\varphi'$$

This can be rewritten

(4-9) $$\sigma'_{br} = \frac{c'\cos\varphi'}{\cos\beta \sin(\beta-\varphi')}$$

The upper bound (4-3) and the lower bound (4-9) are thus identical, and the solution found is therefore the exact solution.

The dependence of the carrying capacity on the slope β of the construction joint is depicted in fig. 4.4. The horizontal parts of the graph correspond to failure outside the construction joint, and the curved part corresponds to sliding failure in the joint.

4.3 Sliding and Separation Failure

Let us now look at the case in which the yield criterion for the construction joint obeys Coulomb's modified failure hypothesis.

The yield pattern at failure in the construction joint is as shown in fig. 4.5, and the internal work is found by means of (3-38), although with use of c' and φ'.

The contributions to the equation of work are

(4-10) $$A_y = \sigma_{br}\, b\, t\, V \cos(90-\beta+\alpha)$$

(4-11) $$A_i = V\left(\frac{1-\sin\alpha}{1-\sin\varphi'}\, c'\cos\varphi' + \frac{\sin\alpha-\sin\varphi'}{1-\sin\varphi'}\, \sigma_t'\right) \frac{b}{\cos\beta}\, t$$

From this an upper bound for the carrying capacity is found to be

(4-12) $$\sigma_{br} = \frac{(1-\sin\alpha)\, c'\cos\varphi' + \sigma_t' (\sin\alpha-\sin\varphi')}{\cos\beta\, \sin(\beta-\alpha)\,(1-\sin\varphi')}$$

In this, σ_t' denotes the tensile strength perpendicular to the construction joint. This tensile strength will normally be smaller than the tensile strength of the monolithic concrete. To facilitate the calculations we express the tensile strength as part of the compression strength for a concrete with the properties of the construction joint, i.e. as a part of (4-4):

(4-13) $$\sigma_t' = k\, \frac{2c'\cos\varphi'}{1-\sin\varphi'}$$

where the constant $k < 1$. For monolithic concrete, this is often about $\frac{1}{10}$. (4-12) then becomes

(4-14) $$\sigma_{br} = \frac{c'\cos\varphi'}{(1-\sin\varphi')\cos\beta\, \sin(\beta-\alpha)} \cdot \left(1-\sin\alpha + \frac{2k(\sin\alpha-\sin\varphi')}{1-\sin\varphi'}\right)$$

In this expression, α is a variable, and the minimum is found at

(4-15) $$\tan(\beta-\alpha) = \frac{(1-\sin\varphi)(1-\sin\alpha)+2k(\sin\alpha-\sin\varphi)}{(1-\sin\varphi)\cos\alpha-2k\cos\alpha}$$

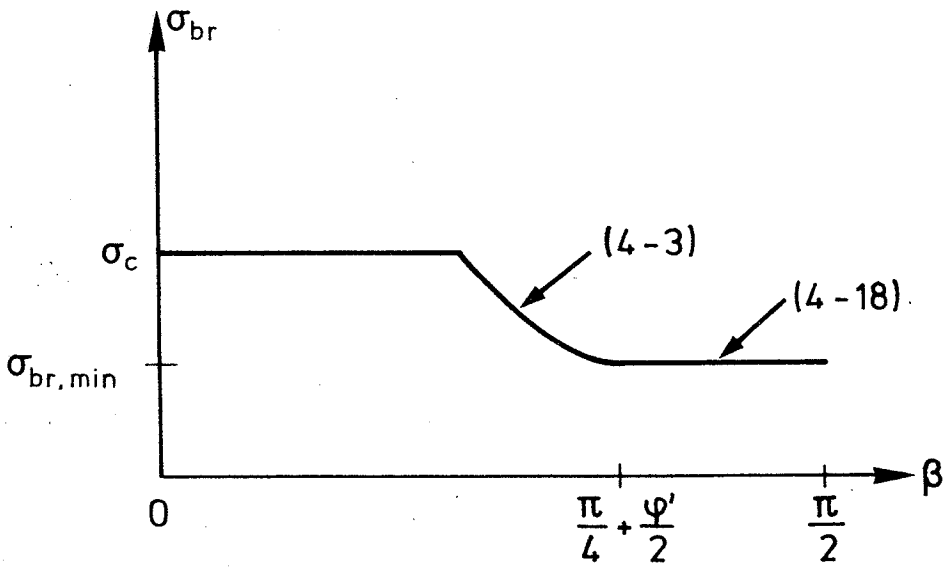

Fig. 4.6 Dependence of carrying capacity on slope of construction joint. Type of failure: sliding failure and separation failure, $\sigma_t' = 0$.

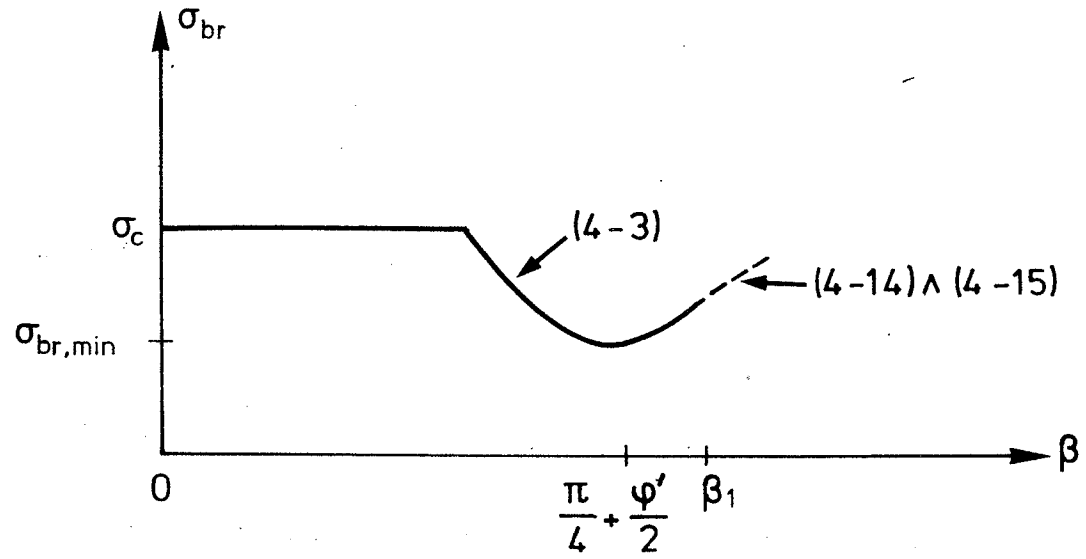

Fig. 4.7 Dependence of carrying capacity on slope of construction joint. Type of failure: sliding failure and separation failure, $\sigma_t' > 0$.

The equations apply when $\alpha \geq \varphi'$. In normal sliding failure $\alpha = \varphi'$ and (4-3) is still valid.

We will first consider the case in which the the tensile strength perpendicular to the construction joint is zero, i.e. $k = 0$. (4-14) and (4-15) then become

$$\sigma_{br} = \frac{c'\cos\varphi'(1-\sin\alpha)}{(1-\sin\varphi')\cos\beta\sin(\beta-\alpha)} \tag{4-16}$$

$$\tan(\beta-\alpha) = \frac{1-\sin\alpha}{\cos\alpha} \tag{4-17}$$

From (4-17) we find the minimum when $\alpha = 2\beta - \frac{\pi}{2}$:

$$\sigma_{br} = \frac{2c'\cos\varphi'}{1-\sin\varphi'} \tag{4-18}$$

As mentioned, (4-18) applies when $\alpha \geq \varphi'$, i.e. when the construction joint has a slope of $\beta \geq \frac{\pi}{4} + \frac{\varphi'}{2}$. For a construction joint with a smaller slope (4-2) applies, although such that $\sigma_{br} < \sigma_c$, where σ_c is the compression strength of the monolithic concrete.

The carrying capacity found is shown in fig. 4.6.

Next, we will look at the case in which $\sigma_t' > 0$, i.e. $k > 0$. In this case, (4-14) and (4-15) apply for $\alpha \geq \varphi'$ and (4-3) applies for $\alpha = \varphi'$.

At the limit of the validity of the formulae the slope β_1 of the construction joint is given by

$$\tan(\beta_1-\varphi') = \frac{(1-\sin\varphi')^2}{(1-\sin\varphi')\cos\varphi'-2k\cos\varphi'} \tag{4-19}$$

This can be rewritten

$$(4\text{-}20) \qquad \tan(\beta_1-\varphi') = \tan(\frac{\pi}{4} - \frac{\varphi'}{2}) \frac{1-\sin\varphi'}{1-\sin\varphi'-2k}$$

As we have $k > 0$, the factor on $\tan(\frac{\pi}{4} - \frac{\varphi'}{2})$ will exceed unity, and (4-20) thereby shows that the slope of the construction joint at the transition from (4-3) to (4-14) and (4-15) is

$$\beta_1 > \frac{\pi}{4} + \frac{\varphi'}{2}$$

An increase in the tensile strength of the construction joint (~ increase in k) thus increases the realm of validity of (4-3). The principle of the dependence of the carrying capacity is shown in fig. 4.7.

Example 4.1 Test by Johansen

Johansen's test [30.1] from 1930 is one of the oldest (if not the oldest) of the tests on construction joints.

In the tests the bottom part of the test specimen is cast with its slanting surface against a steel plate treated with paraffin. After 7 or 14 days, the slanting surface is moistened and the top part of the test specimen is cast in place.

The test results are depicted in a τ,σ - coordinate system, where τ,σ are the stresses at failure in the construction joint, cf. (4-6) and (4-7). This representation has the advantage that the sliding failure criterion for

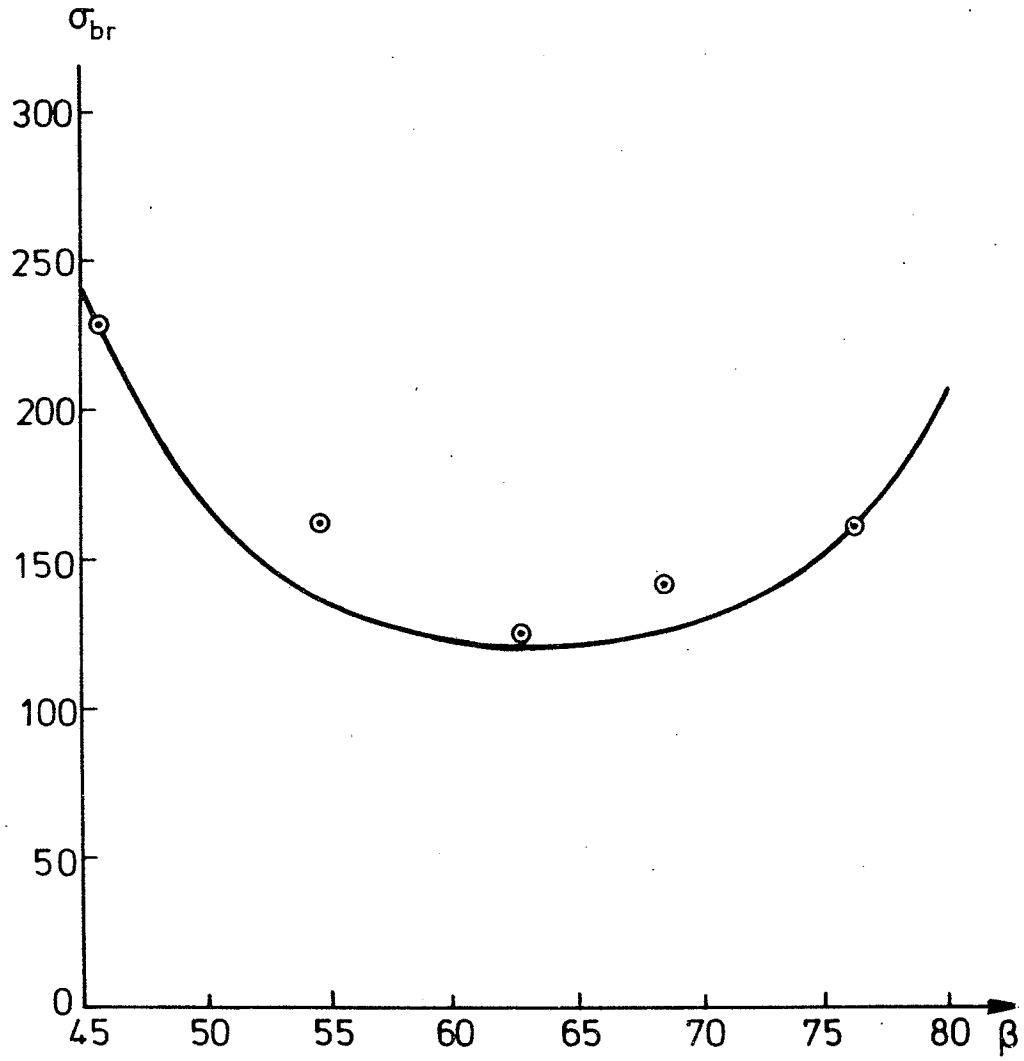

Fig. 4.8 Johansen's test results and (4-3) with c' = 3 MN/ and $\tan\varphi$ = 0.75.

the construction joint (4-5) is depicted as a straight line, and the values for c' and φ' are easy to read off. On the other hand, the importance of the slope of the construction joint is not so clear, and it is difficult to see any influence from a low tensile strength.

From the figure and the information contained in [30.1] , we find, by means of (4-6) and (4-7) the relationship between the ultimate load σ_{br} and the angle of slope β of the construction joint. These are shown in fig. 4.8 together with (4-3), in which c' = 3MN/m^2 and tan φ' = 0.75 (φ' = 37^o). (Johansen himself gave c' = 3MN/m^2 and φ' = 0.8).

The test results shown are the average of four, apart from β = 45.6^o, where one of the test results was excluded because it was distinctly lower than the others.

The results accord well with (4-3), which was only to be expected as (4-3) is identical with the well-known (4-5). This was demonstrated in the lower-bound considerations at the end of section 4.1.

The monolithic concrete had the strength σ_c = 30 MN/m^2, corresponding to c = 7.5 MN/m^2 when φ = 37^o. The construction joint has thus resulted in a 60% reduction in c.

An assessment of the formulae established in section 4.2 has not been possible owing to lack of test results.

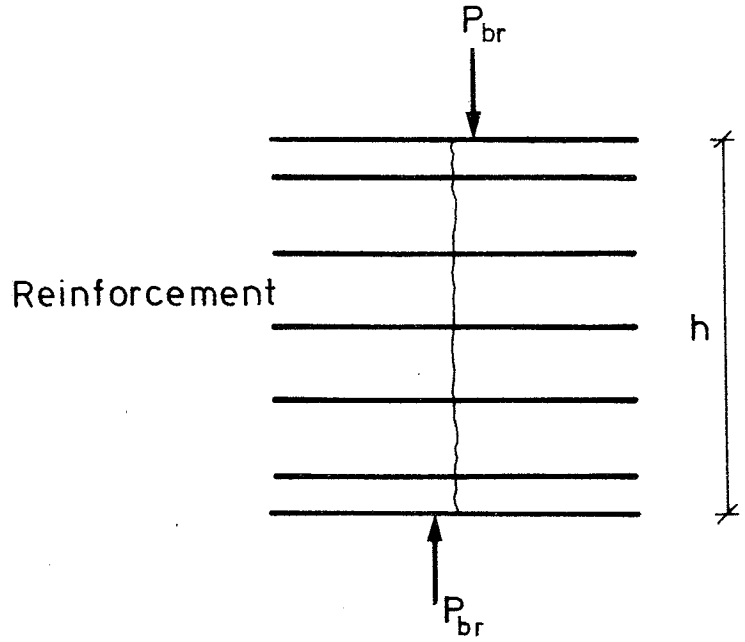

Fig. 5.1 Shear failure.

5. SHEAR

5.1 Introduction

In this chapter we will consider some problems relating to the carrying capacity of reinforced concrete. Like the concrete, the reinforcement is considered to be rigid-plastic with the yield stress σ_F. It is similarly assumed that the reinforcement can only resist forces in the longitudinal direction.

Figure 5.1 shows the principle of the shear problem we wish to consider. A body is loaded by two forces acting in opposite directions, and failure occurs by one part of the body moving downwards and away from the other part. This movement takes place along a discontinuity line between the external loads. Reinforcement with a total area F is placed perpendicular to the discontinuity line.

The height of the shear failure is denoted by h, see fig. 5.1, and the width perpendicular to the plane of the paper is denoted by b. As the cross-section of the concrete is much bigger than F, the cross-section becomes $b \cdot h$. The degree of reinforcement is introduced as the ratio between the tensile yield strength of the reinforcement and the compression strength of the concrete perpendicular to the line between the two external loads, i.e.

$$\Phi = \frac{F \sigma_F}{h b \sigma_c} \tag{5-1}$$

The external load P is assumed to be uniformly distributed over the cross-section, so that the shear stress τ is given by

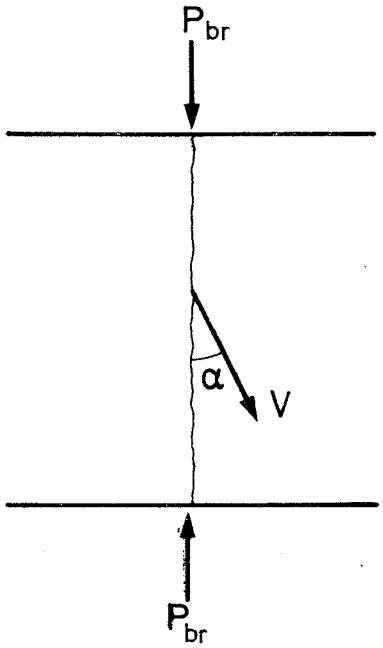

Fig. 5.2 Failure pattern.

(5-2) $$\tau = \frac{P}{b\,h}$$

The subsequent calculations will be carried out as upper-bound calculations. In the formulation of the equation of work there will now be two contributions to the internal work, one from the reinforcement and the other from the concrete. Initially, we will consider the concrete as a material with a yield criterion that obeys Coulomb's modified failure hypothesis. In section 5.5 we will introduce a factor by means of which we seek to take into account the fact that the concrete cannot be made fully effective.

Here, we will only consider the case with reinforcement perpendicular to the discontinuity line. Inclined reinforcement can naturally be dealt with in the same way.

5.2 Plane Deformation Field

The failure pattern in fig. 5.2 can be used, and as we have a plane deformation field, we know that the angle α between V and the discontinuity line is greater than or equal to the angle of friction φ. The calculations are split into two parts, depending on whether $\alpha = \varphi$ or $\alpha > \varphi$.

$\alpha = \varphi$

The contributions to the equation of work are

(5-3) $$A_y = P_{br}\, V \cos\varphi$$

From the concrete we find from (3-39)

(5-4) $$A_{ib} = \frac{1-\sin\varphi}{2}\, \sigma_c\, V\, h\, b$$

As the reinforcement can only resist forces acting in the longitudinal direction, we have

(5-5) $$A_{ia} = F\,\sigma_F\,V\sin\varphi$$

From $A_y = A_{ia} + A_{ib}$ we find, by introducing (5-1) and (5-2),

(5-6) $$\frac{\tau_{br}}{\sigma_c} = \frac{1-\sin\varphi}{2\cos\varphi} + \Phi\tan\varphi$$

In a Φ, $\frac{\tau_{br}}{\sigma_c}$ -coordinate system, (5-6) is a straight line.

$\underline{\alpha \geq \varphi}$

Analogously with (5-3) and (5-5) we find

(5-7) $$A_y = P_{br}\,V\cos\alpha$$

(5-8) $$A_{ia} = F\,\sigma_F\,V\sin\alpha$$

The contribution from the concrete is again found from (3-39).

(5-9) $$A_{ib} = \left(\frac{1-\sin\alpha}{2}\,\sigma_c + \frac{\sin\alpha-\sin\varphi}{1-\sin\varphi}\,\sigma_t\right)V\,h\,b$$

The complete equation of work gives, analogously with (5-6):

(5-10) $$\frac{\tau_{br}}{\sigma_c} = \frac{1-\sin\alpha}{2\cos\alpha} + \frac{\sin\alpha-\sin\varphi}{(1-\sin\varphi)\cos\alpha}\,\frac{\sigma_t}{\sigma_c} + \Phi\tan\alpha$$

This is an upper bound, in which α is variable. The value of α, which gives the minimum, is found after some calculation to be

$$\sin\alpha = 1 - 2\,\frac{(\Phi + \frac{\sigma_t}{\sigma_c})\ (1-\sin\varphi)}{1-\sin\varphi - 2\,\frac{\sigma_t}{\sigma_c}\sin\varphi} \tag{5-11}$$

The minimum for (5-10) is then found to be

$$\frac{\tau_{br}}{\sigma_c} = \sqrt{(\Phi + \frac{\sigma_t}{\sigma_c})\left(\frac{1-\sin\varphi - 2\,\frac{\sigma_t}{\sigma_c}\sin\varphi}{1-\sin\varphi} - (\Phi + \frac{\sigma_t}{\sigma_c})\right)} \tag{5-12}$$

In a Φ, $\frac{\tau_{br}}{\sigma_c}$-coordinate system, (5-12) is a circle with its centre at

$$(\Phi, \frac{\tau_{br}}{\sigma_c}) = (\frac{1}{2} - \frac{1}{\sin\varphi}\,\frac{\sigma_t}{\sigma_c}\ ,\ 0) \tag{5-13}$$

The radius of the cirlce is

$$r = \frac{1}{2} - \frac{\sigma_t}{\sigma_c}\,\frac{\sin\varphi}{1-\sin\varphi} \tag{5-14}$$

The condition for validity of (5-12) is that $\alpha > \varphi$, i.e.

$$\sin\alpha > \sin\varphi \tag{5-15}$$

From (5-15) and (5-11) we find that (5-12) is valid when

$$\Phi < \frac{1-\sin\varphi}{2} - (1+\sin\varphi)\,\frac{\sigma_t}{\sigma_c} \tag{5-16}$$

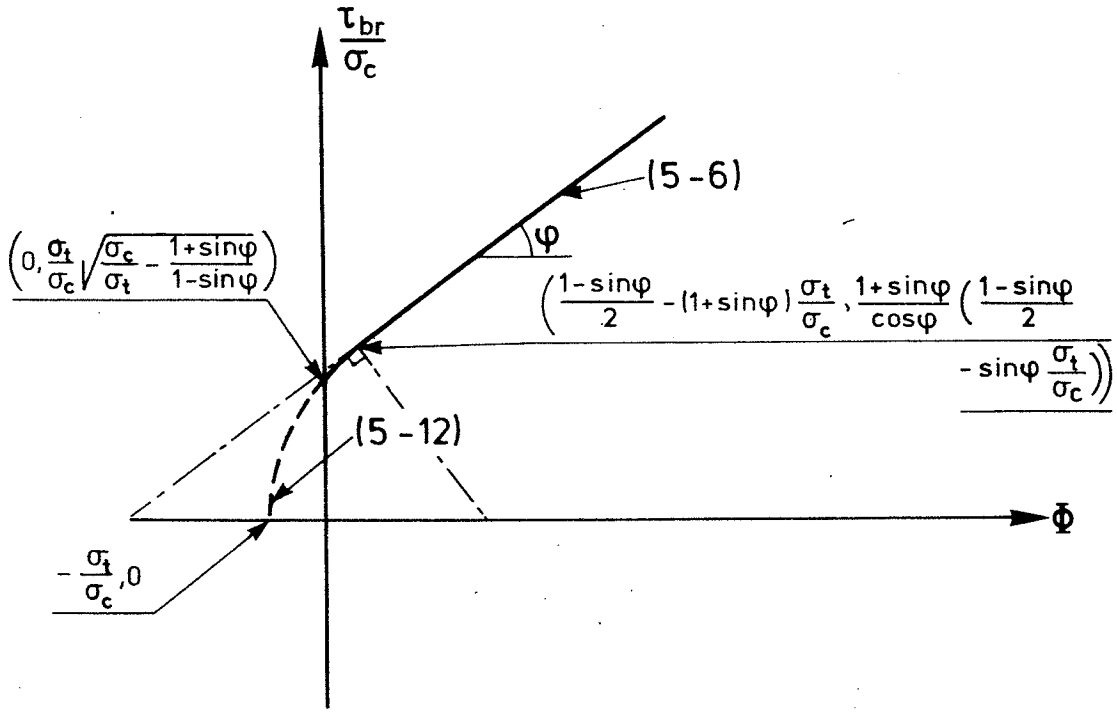

Fig. 5.3 Carrying capacity in plane strain field.

The transition from the straight line (5-6) to the circle (5-12) is located at the point at which the line is tangential to the circle. This point is

$$(5\text{-}17)\quad (\Phi, \frac{\tau_{br}}{\sigma_c}) = (\frac{1-\sin\varphi}{2} - (1+\sin\varphi)\frac{\sigma_t}{\sigma_c}\ ,$$

$$\frac{1+\sin\varphi}{\cos\varphi}\ (\frac{1-\sin\varphi}{2} - \sin\varphi\ \frac{\sigma_t}{\sigma_c}))$$

(5-6) and (5-12) are depicted in fig. 5.3, in which some characteristic points are given. For $\Phi < 0$ the curve is drawn with a dotted line since it has no physical meaning (see, however, section 5.4). Besides this, note the close analogy of the curve with Coulomb's modified failure hypothesis, fig. 2.3.

5.3 Plane Stress Field

We will now consider a problem that is entirely analogous with the foregoing, apart from the assumption of a plane stress field. The contribution from the concrete to the internal work is found from (3-48) and (3-49), the failure criterion being that shown in fig. 3.8. The calculations are split up into 4 cases, depending on the angle α in fig. 5.2

$\alpha = 0$

In this case there is no contribution from the reinforcement to the internal work because the movement takes place perpendicular to the reinforcement. The contribution from the concrete is found from (3-48), whereby we get

(5-18) $$A_y = P_{br} V$$

(5-19) $$A_i = A_{ib} = \tfrac{1}{2}\sigma_c V h b$$

The result thus becomes

(5-20) $$\frac{\tau_{br}}{\sigma_c} = \frac{1}{2}$$

It should be noted that (5-20) is independent of the degree of reinforcement Φ .

$\underline{0 \leq \alpha \leq \varphi}$

The three contributions to the equation of work are:

(5-21) $$A_y = P_{br} V \cos\alpha$$

(5-22) $$A_{ib} = \tfrac{1}{2}\sigma_c V (1-\sin\alpha) h b$$

(5-23) $$A_{ia} = F \sigma_F V \sin\alpha$$

An upper bound for the carrying capacity is thus found to be

(5-24) $$\frac{\tau_{br}}{\sigma_c} = \frac{1-\sin\alpha}{2\cos\alpha} + \Phi \tan\alpha$$

The minimum for (5-24) is found for

(5-25) $$\sin\alpha = 1-2\Phi$$

and is

(5-26) $$\frac{\tau_{br}}{\sigma_c} = \sqrt{\Phi(1-\Phi)}$$

In a Φ, $\frac{\tau_{br}}{\sigma_c}$ -coordinate system, (5-26) is a circle with its centre at

(5-27) $$(\Phi, \frac{\tau_{br}}{\sigma_c}) = (0, \frac{1}{2})$$

The radius of the circle is

(5-28) $$r = \frac{1}{2}$$

(5-26) is valid for $0 < \alpha < \varphi$, i.e.

(5-29) $$0 < \sin\alpha < \sin\varphi$$

From (5-29) and (5-25) we find the sphere of validity for (5-26) to be

(5-30) $$\frac{1-\sin\varphi}{2} < \Phi < \frac{1}{2}$$

In the $\Phi, \frac{\tau_{br}}{\sigma_c}$-coordinate system, (5-20) is tangential to (5-26) at the point

(5-31) $$(\Phi, \frac{\tau_{br}}{\sigma_c}) = (\frac{1}{2}, \frac{1}{2})$$

$\underline{\alpha = \varphi}$

Apart from alteration of α to φ, the contribution to the equation of work is equal to (5-21), (5-22) and (5-23), and instead of (5-24), we find

(5-32) $$\frac{\tau_{br}}{\sigma_c} = \frac{1-\sin\varphi}{2\cos\varphi} + \Phi\tan\varphi$$

(5-32) is identical to (5-6) and is a straight line in a $\Phi, \frac{\tau_{br}}{\sigma_c}$-coordinate system. (5-32) is tangential to the circle (5-26) at one end of the sphere of validity of the circle, i.e.

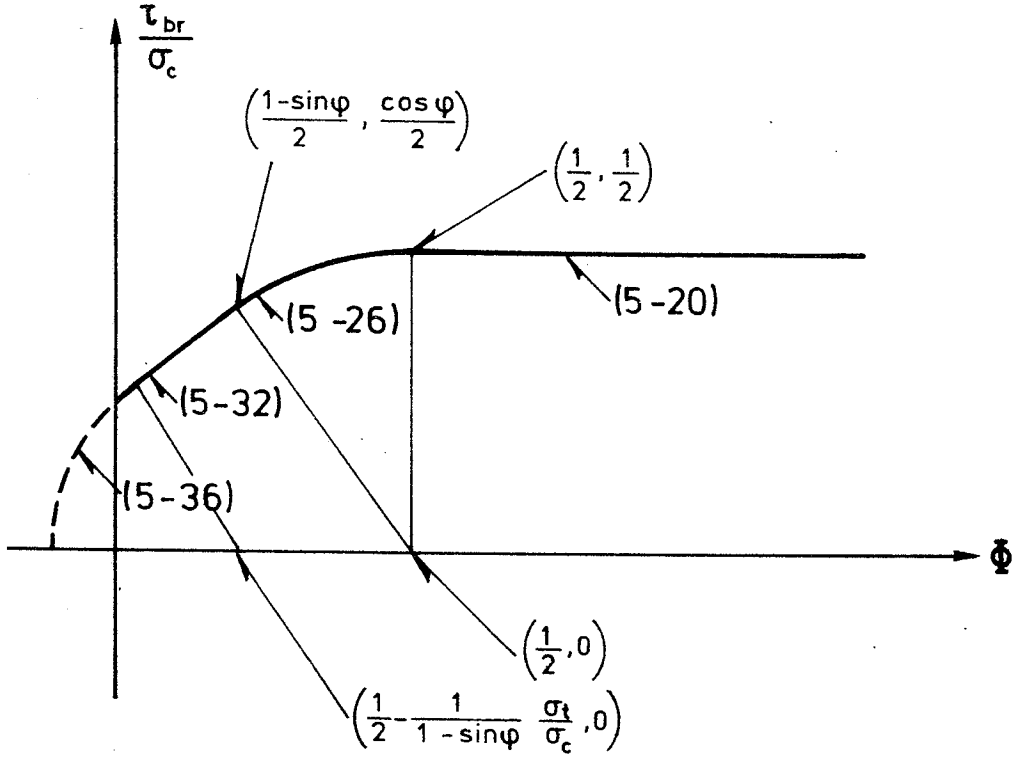

Fig. 5.4 Carrying capacity in plane stress field.

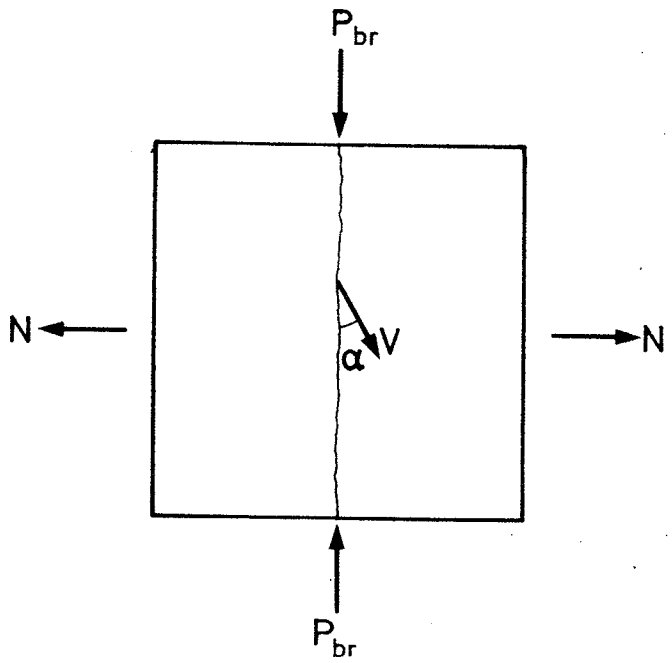

Fig. 5.5 Failure mechanism for shear with normal force.

$$(5\text{-}33) \qquad (\Phi, \frac{\tau_{br}}{\sigma_c}) = (\frac{1-\sin\varphi}{2}, \frac{\cos\varphi}{2})$$

$\underline{\alpha \geq \varphi}$

The contribution from the concrete to the equation of work is found from (3-49) as

$$(5\text{-}34) \qquad A_{ib} = (\frac{1-\sin\alpha}{2}\sigma_c + \frac{\sin\alpha-\sin\varphi}{1-\sin\varphi}\sigma_t) V h b$$

The other contributions to the equation of work are identical to (5-21) and (5-23). An upper bound for the carrying capacity can then be found to be

$$(5\text{-}35) \qquad \frac{\tau_{br}}{\sigma_c} = \frac{1-\sin\alpha}{2\cos\alpha} + \frac{\sin\alpha-\sin\varphi}{(1-\sin\varphi)\cos\alpha}\frac{\sigma_t}{\sigma_c} + \Phi\tan\alpha$$

The equation is identical to (5-10); therefore, we know the minimum

$$(5\text{-}36) \qquad \frac{\tau_{br}}{\sigma_c} = \sqrt{(\Phi + \frac{\sigma_t}{\sigma_c})(\frac{1-\sin\varphi - 2\frac{\sigma_t}{\sigma_c}\sin\varphi}{1-\sin\varphi} - (\Phi + \frac{\sigma_t}{\sigma_c}))}$$

(5-36) is a circle that is valid when (5-16) is satisfied. The circle is tangential to (5-32) at a point given by (5-17).

For $\alpha \geq \varphi$ the formulae for the carrying capacity in plane stress field are identical to those in plane deformation fields. This is yet another example of the fact that a plane stress field is accompanied in a number of cases by a plane deformation field. As mentioned in section 3.5, this is because the middle principal stress is of no signifi-

cance in Coulomb's failure hypothesis and modified failure hypthesis.

The formulae for the carrying capacity in a plane stress field are shown in fig. 5.4. A few characteristic values are indicated (see also fig. 5.3).

5.4 Influence of Normal Force

An external normal force, as shown in fig. 5.5, can easily be taken into account.

With a given value of the normal force N, the external work in the yield pattern shown gives

$$A_y = P_{br} V \cos\alpha + N V \sin\alpha \tag{5-37}$$

The internal work from the concrete is simply denoted by A_{ib} and is dependent on α but is otherwise identical to the expressions used in sections 5.2 and 5.3. As usual, the contribution from the reinforcement is found to be

$$A_{ia} = F \sigma_F V \sin\alpha \tag{5-38}$$

The equation of work thereby gives

$$P_{br} V \cos\alpha + N V \sin\alpha = A_{ib} + F \sigma_F V \sin\alpha \tag{5-39}$$

We now introduce the stress σ_N as the uniformly distributed normal stress originating from N, i.e.

$$\sigma_N = \frac{N}{b h} \tag{5-40}$$

(5-39) can then be written as

$$(5\text{-}41) \qquad \frac{\tau_{br}}{\sigma_c} = \frac{1}{\cos\alpha}\frac{A_{ib}}{V\sigma_c} + (\Phi - \frac{\sigma_N}{\sigma_c})\tan\alpha$$

This expression is completely analogous with the corresponding expressions in sections 5.2 and 5.3. The only difference is that Φ is now replaced by $\Phi - \frac{\sigma_N}{\sigma_c}$. If we introduce

$$(5\text{-}42) \qquad \Phi^* = \Phi - \frac{\sigma_N}{\sigma_c}$$

all the formulae calculated earlier can be used by inserting Φ^* instead of Φ.

As expected, the formulae show that an external compressive force increases the carrying capacity. The increase is equivalent to an increase in the reinforcement corresponding to a yield strength that is equivalent to the external compressive force.

In the same way, a tensile force corresponds to removal of reinforcement.

In fig. 5.3 and 5.4, a normal force manifests itself in shearing of the $\frac{\tau_{br}}{\sigma_c}$ axis.

5.5 Shear in Concrete

The foregoing calculations have been performed for a rigid-plastic modified Coulomb material. The ultimate strain is limited and the elastic strains are of the same order of magnitude as the plastic strains. Furthermore, the compressive stress-strain curve of the concrete

falls at higher strains than that corresponding to $\sigma = \sigma_{max} = \sigma_c$.

These factors mean that we cannot expect a failure section to result in as big a contribution from the concrete to the resistance capacity as indicated by the formulae in section 3.

For a given structure we can now introduce a factor (efficiency factor) $\nu \leq 1$, which must be multiplied by the area b h in order to obtain an equivalent area which we can reckon will give a full contribution to the internal work. That means that all the foregoing formulae will be valid if we replace τ_{br}, Φ and σ_N by

$$\tau'_{br} = \frac{P_{br}}{\nu b h} \tag{5-43}$$

$$\Phi' = \frac{F \sigma_F}{\nu b h \sigma_c} \tag{5-44}$$

$$\sigma'_N = \frac{N}{\nu b h} \tag{5-45}$$

The relationship between these quantities and the corresponding unmarked quantities is found to be

$$\tau'_{br} = \frac{1}{\nu} \tau_{br} \tag{5-46}$$

$$\Phi' = \frac{1}{\nu} \Phi \tag{5-47}$$

$$\sigma'_N = \frac{1}{\nu} \sigma_N \tag{5-48}$$

As it is the unmarked quantities that are most convenient to work with, the formulae

are written by means of these. The procedure is to replace all τ_{br}, Φ and σ_N in the calculated formulae by τ'_{br}, Φ' and σ'_N, after which (5-46) to (5-48) are used to get the formulae expressed by means of τ_{br}, Φ and σ_N. A systematic survey of the formulae is given in section 5.6.

With the introduction of the efficiency factor ν we may be said to have moved somewhat away from the upper-bound method. However, the upper-bound method alone cannot be used for determination of carrying capacity. It must either be combined with lower-bound solutions, or we must verify the applicability of the upper-bound solutions by tests.

An evaluation of the formulae in section 5.6 by means of test results must, in the first instance, take the form of a comparison of the nature of the relationship between the carrying capacity and the degree of reinforcement. If the relationship can be compared to fig. 5.3 or fig. 5.4, we must then investigate which values of ν we can reckon on in different cases.

What is most important for this thesis is to show that the theory developed can be used in a large number of cases. The examples here in chapter 5 therefore primarily demonstrate that the carrying capacity in the cases in question can be compared to fig. 5.3 and fig. 5.4. A detailed study of ν has not been carried out, but a number of conclusions that can be reached on the basis of the existing tests are included in the individual cases.

5.6 List of Formulae

The formulae calculated in sections 5.3 and 5.4, with the modifications required in the case of concrete, are then as follows:

Plane deformation field

$$\frac{\tau_{br}}{\sigma_c} = \sqrt{(\Phi+\nu\,\frac{\sigma_t}{\sigma_c})\,(\nu\,\frac{1-\sin\varphi-2\,\frac{\sigma_t}{\sigma_c}\sin\varphi}{1-\sin\varphi} - (\Phi+\nu\,\frac{\sigma_t}{\sigma_c}))} \tag{5-49}$$

for

$$\Phi \leq \nu\left(\frac{1-\sin\varphi}{2} - (1+\sin\varphi)\frac{\sigma_t}{\sigma_c}\right) \tag{5-50}$$

For bigger Φ we have

$$\frac{\tau_{br}}{\sigma_c} = \nu\,\frac{1-\sin\varphi}{2\cos\varphi} + \Phi\tan\varphi \tag{5-51}$$

Plane stress field

$$\frac{\tau_{br}}{\sigma_c} = \sqrt{(\Phi+\nu\,\frac{\sigma_t}{\sigma_c})\,(\nu\,\frac{1-\sin\varphi-2\,\frac{\sigma_t}{\sigma_c}\sin\varphi}{1-\sin\varphi} - (\Phi+\nu\,\frac{\sigma_t}{\sigma_c}))} \tag{5-52}$$

for

$$\Phi \leq \nu\left(\frac{1-\sin\varphi}{2} - (1+\sin\varphi)\,\frac{\sigma_t}{\sigma_c}\right. \tag{5-53}$$

$$\frac{\tau_{br}}{\sigma_c} = \nu\,\frac{1-\sin\varphi}{2\cos\varphi} + \Phi\tan\varphi \tag{5-54}$$

$-\sigma_t$	φ	$\frac{\tau_{br}}{\sigma_c}$	
0	φ	$\sqrt{\Phi(\nu-\Phi)}$ $\nu\frac{1-\sin\varphi}{2\cos\varphi}+\Phi\tan\varphi$	$\Phi \leq \nu\frac{1-\sin\varphi}{2}$ $\Phi \geq \nu\frac{1-\sin\varphi}{2}$
σ_t	37^o	$\sqrt{\left(\Phi+\nu\frac{\sigma_t}{\sigma_c}\right)\left(\nu\left(1-3\frac{\sigma_t}{\sigma_c}\right)-\left(\Phi+\nu\frac{\sigma_t}{\sigma_c}\right)\right)}$ $0{,}25\,\nu+0{,}75\,\Phi$	$\Phi \leq \nu\left(0{,}2-1{,}6\frac{\sigma_t}{\sigma_c}\right)$ $\Phi \geq \nu\left(0{,}2-1{,}6\frac{\sigma_t}{\sigma_c}\right)$
0	37^o	$\sqrt{\Phi(\nu-\Phi)}$ $0{,}25\,\nu+0{,}75\,\Phi$	$\Phi \leq 0{,}2\,\nu$ $\Phi \geq 0{,}2\,\nu$
$\frac{\sigma_c}{10}$	37^o	$\sqrt{(\Phi+0{,}1\nu)(0{,}7\nu-(\Phi+0{,}1\nu))}$ $0{,}25\,\nu+0{,}75\,\Phi$	$\Phi \leq 0{,}04\nu$ $\Phi \geq 0{,}04\nu$

Table 5.1 Formulae for carrying capacity in plane strain field.

σ_t	φ	$\frac{\tau_{br}}{\sigma_c}$	
0	φ	$\sqrt{\Phi(\nu-\Phi)}$ $0{,}5\,\nu$	$\Phi \leq 0{,}5\,\nu$ $\Phi \geq 0{,}5\,\nu$
σ_t	37^o	$\sqrt{(\Phi+\nu\frac{\sigma_t}{\sigma_c})\left(\nu(1-3\frac{\sigma_t}{\sigma_c})-(\Phi+\nu\frac{\sigma_t}{\sigma_c})\right)}$ $0{,}25\,\nu+0{,}75\,\Phi$ $\sqrt{\Phi(\nu-\Phi)}$ $0{,}5\,\nu$	$\Phi \leq \nu(0{,}2-1{,}6\frac{\sigma_t}{\sigma_c})$ $\nu(0{,}2-1{,}6\frac{\sigma_t}{\sigma_c} \leq \Phi \leq 0{,}2\,\nu)$ $0{,}2\,\nu \leq \Phi \leq 0{,}5\,\nu$ $\Phi \geq 0{,}5\,\nu$
0	37^o	$\sqrt{\Phi(\nu-\Phi)}$ $0{,}5\,\nu$	$\Phi \leq 0{,}5\,\nu$ $\Phi \geq 0{,}5\,\nu$
$\frac{\sigma_c}{10}$	37^o	$\sqrt{(\Phi+0{,}1\,\nu)(0{,}7\,\nu-(\Phi+0{,}1\nu))}$ $0{,}25\,\nu+0{,}75\,\Phi$ $\sqrt{\Phi(\nu-\Phi)}$ $0{,}5\,\nu$	$\Phi \leq 0{,}04\,\nu$ $0{,}04\,\nu \leq \Phi \leq 0{,}2\,\nu$ $0{,}2\,\nu \leq \Phi \leq 0{,}5\,\nu$ $\Phi \geq 0{,}5\,\nu$

Table 5.2 Formulae for carrying capacity in plane stress field.

for

$$(5\text{-}55)\quad \nu\left(\frac{1-\sin\varphi}{2} - (1+\sin\varphi)\,\frac{\sigma_t}{\sigma_c}\right) \leq \Phi \leq \nu\,\frac{1-\sin\varphi}{2}$$

$$(5\text{-}56)\quad \frac{\tau_{br}}{\sigma_c} = \sqrt{\Phi(\nu-\Phi)}$$

for

$$(5\text{-}57)\quad \nu\,\frac{1-\sin\varphi}{2} \leq \Phi \leq \nu\,\frac{1}{2}$$

$$(5\text{-}58)\quad \frac{\tau_{br}}{\sigma_c} = \nu\,\frac{1}{2}$$

for

$$(5\text{-}59)\quad \Phi \geq \nu\,\frac{1}{2}$$

Tables 5.1 and 5.2 show the formulae for the carrying capacity with characteristic values for φ and σ_t. It will be noted that (5-52) approaches (5-56) for decreasing values of σ_t, and that they are identical for $\sigma_t = 0$. It will also be noted that test results with degrees of reinforcement $\Phi \leq \nu\,\frac{1-\sin\varphi}{2}$ do not enable us to decide whether we should assume a plane stress field or a plane deformation field.

In the case of normal forces, the formulae derived can be used provided Φ is substituted by Φ^*, which is found from (5-42).

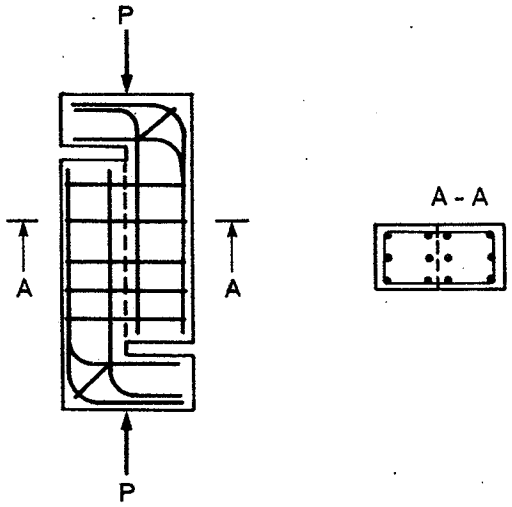

Fig. 5.6 Shear tests from [69.5].

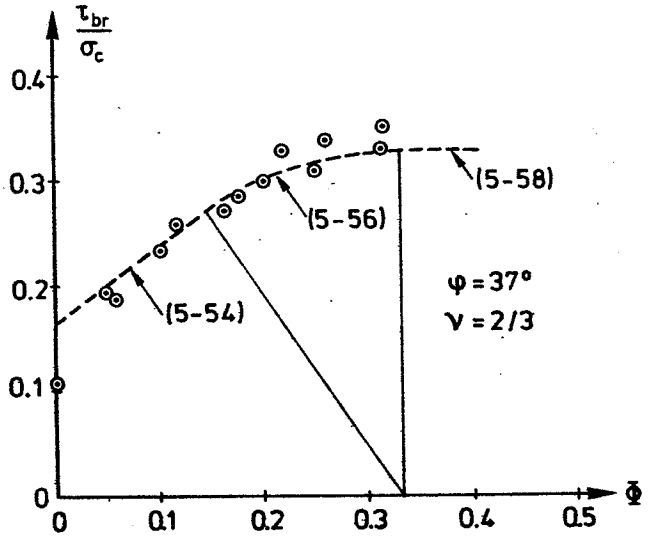

Fig. 5.7 Results with monolithic test specimens from [69.5]

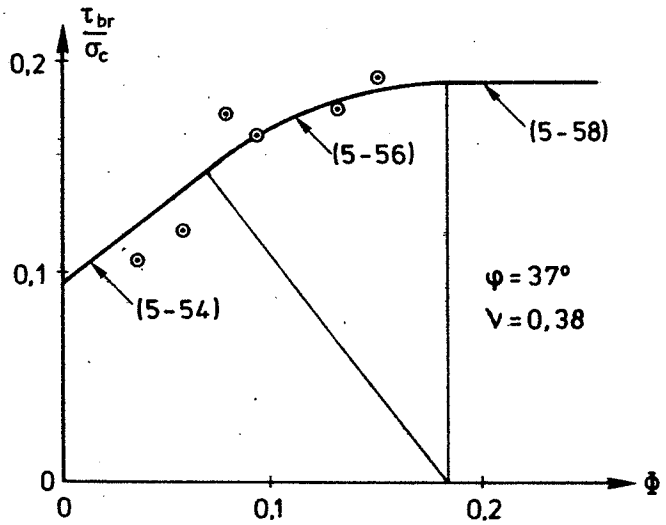

Fig. 5.8 Results from monolithic test specimens from [72.3]

Example 5.1 Shear in Monolithic Concrete

Hofbeck, Ibrahim and Mattock [69.5] have performed tests with monolithic test specimens of the appearance shown in fig. 5.6.

The dependence of the carrying capacity on the degree of reinforcement in shown in fig. 5.7. This figure also shows the curves found for the carrying capacity in a plane stress field, where φ is put at 37° and $\nu = 2/3$.

The value used for φ is the one normally used for concrete. ν is chosen so that accordance between tests and the formulae is good. (5-52) is not plotted because an estimated tensile strength of $\frac{1}{10}$ of the compression strength gives only a small difference between (5-52) and (5-54) for $0 \leq \Phi \leq 0.04\nu$, see fig. 5.4.

Apart from $\Phi = 0$, the agreement between the formulae for the carrying capacity and the test results is exceptionally good.

That the carrying capacity for $\Phi = 0$ is lower than predicted by the theory may be due to one or more of the following factors: the negligible yield strength in tension enters the picture; the tensile strength is lower than assumed; it may be a statically normal deviation.

Mattock and Hawkins [72.3] have carried out six tests with specimens subjected to tensile loading but otherwise in accordance with the principle in fig. 5.6. However, the shape of the test specimens was slightly different, so we cannot expect the same efficiency factor as in Hofbeck et al.

The results of the tests are plotted in fig. 5.8, together with the curves for the carrying capacity for a plane stress field. Again, $\varphi = 37^{o}$ and (5-52) is omitted. ν is put at 0.38.

There are only a few results and there is some dispersion on them. It will be seen that accordance with the theory is acceptable, although not as good as in fig. 5.7.

Rajendran and Morley [74.1] have also assessed Hofbeck et. al.'s tests [69.5] by means of the theory of plasticity.

By putting the tensile strength at zero and using a plane stress field, they have found (5-26) as a lower bound for the carrying capacity. Incidentally, they mention - without showing it - that there is a failure pattern that results in the same carrying capacity as the lower bound, such that (5-26) is a correct solution when $\sigma_t = 0$.

In order to get the test results to fit the theory, Rajendran and Morley also use a lower ultimate strength of concrete than the measured value. This corresponds entirely to the efficiency factor introduced here.

Rajendran and Morley only work with plane stress fields. This has led them to the conclusion that the theory of plasticity cannot explain the difference between the carrying capacity of the test specimens described here and corresponding specimens that have cracked along the shear plane. As we shall see in example 5.2, the difference can be explained by using the formulae for a plane deformation field.

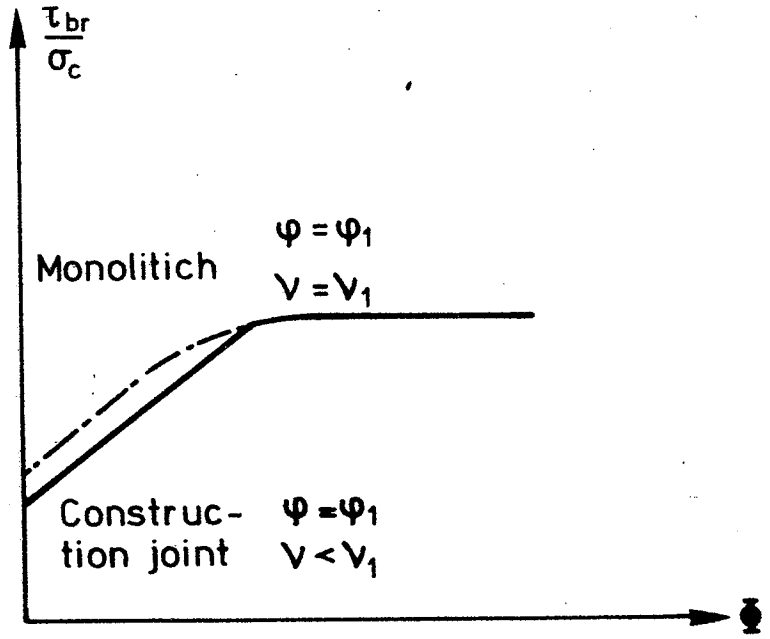

Fig. 5.9 Principle of carrying capacity of construction joint.

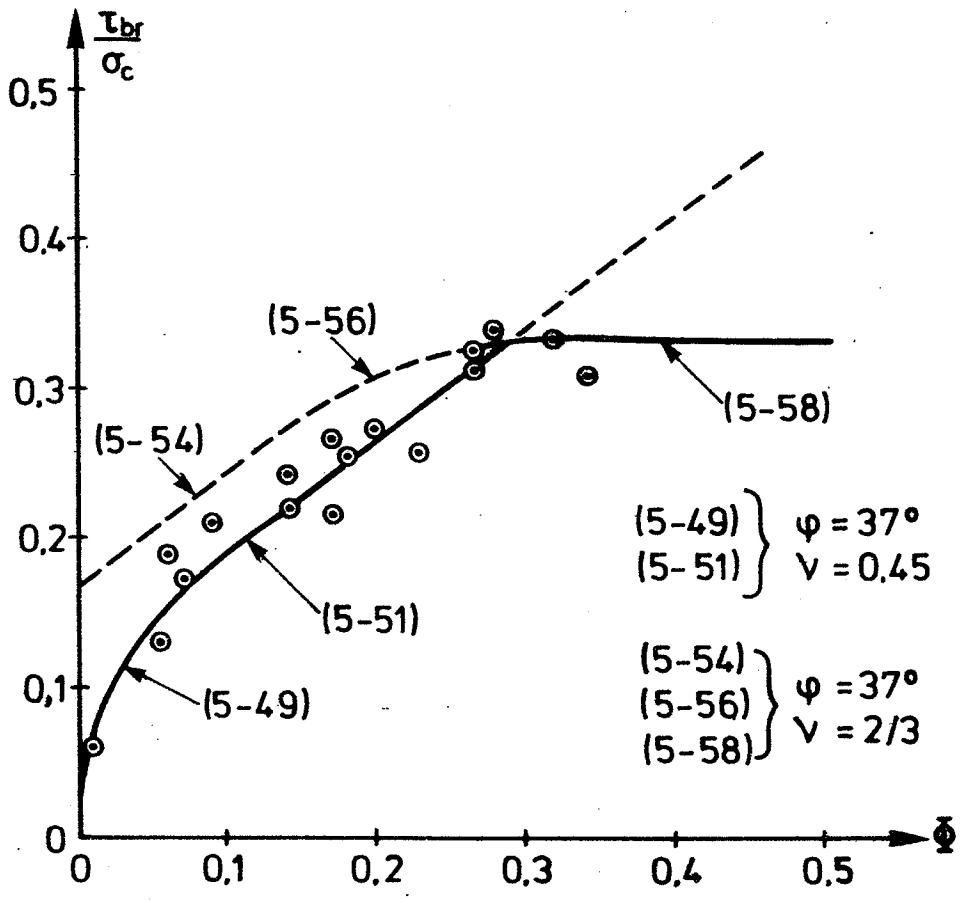

Fig. 5.10 Results with cracked test specimens from [69.5].

Example 5.2 Shear in Reinforced Construction Joint

We consider fig. 5.6 again and assume that the shear section is weakened in relation to the monolithic concrete. The weakening may, for example, take the form of a construction joint.

The weakening introduced manifests itself by a smaller cohesion c in the construction joint than in the monolithic concrete. Example 4.1 shows that φ, on the other hand, can often be expected to be the same in the construction joint as in the monolithic concrete.

For the construction joint this means that the efficiency factor ν is apparently smaller than for the corresponding case in monolithic concrete. Furthermore, failure in the construction joint will occur as a plane deformation field when the degree of reinforcement is suitable low. With high degrees of reinforcement, the failure will be as in monolithic concrete and thus also with an efficiency factor corresponding to this. This change from failure in the construction joint to failure in the monolithic body is entirely analogous to the corresponding change in the unreinforced construction joint in chapter 4. The principle of the relationship between the carrying capacity and the degree of reinforcement is shown in fig. 5.9.

Hofbeck, Ibrahim and Mattock [69.5]have performed tests corresponding to the monolithic tests shown in fig. 5.6. In the shear section they have merely introduced a weakness, viz, a split crack, established in accordance with same principle as applies in the split test

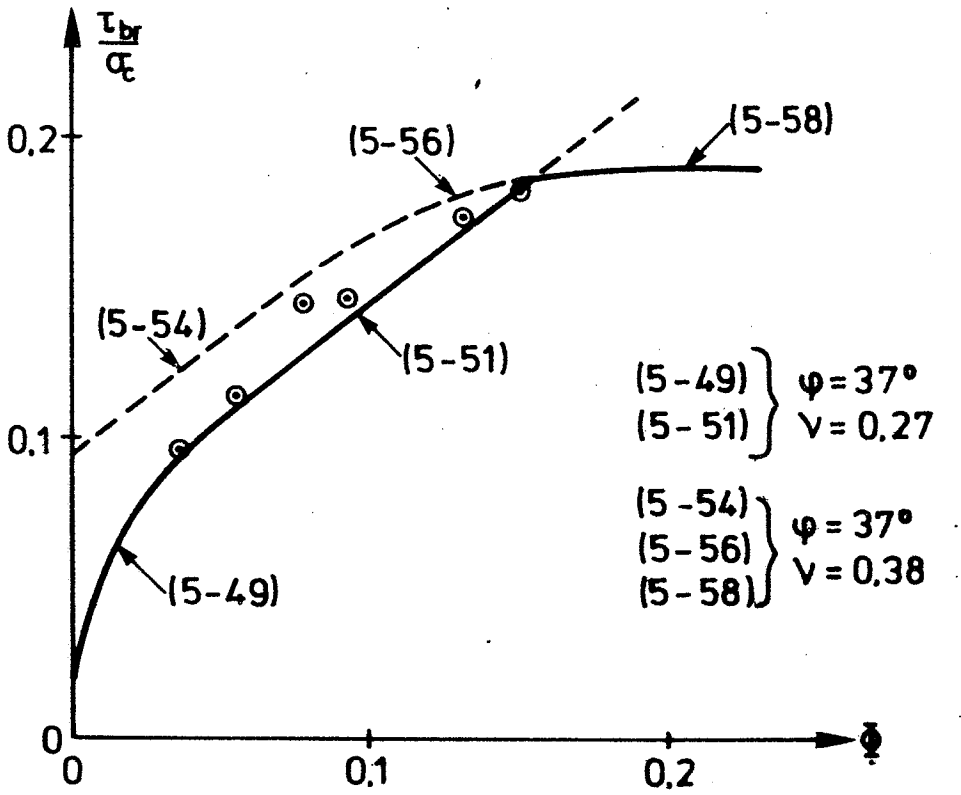

Fig. 5.11 Results with cracked test specimens from [72.3].

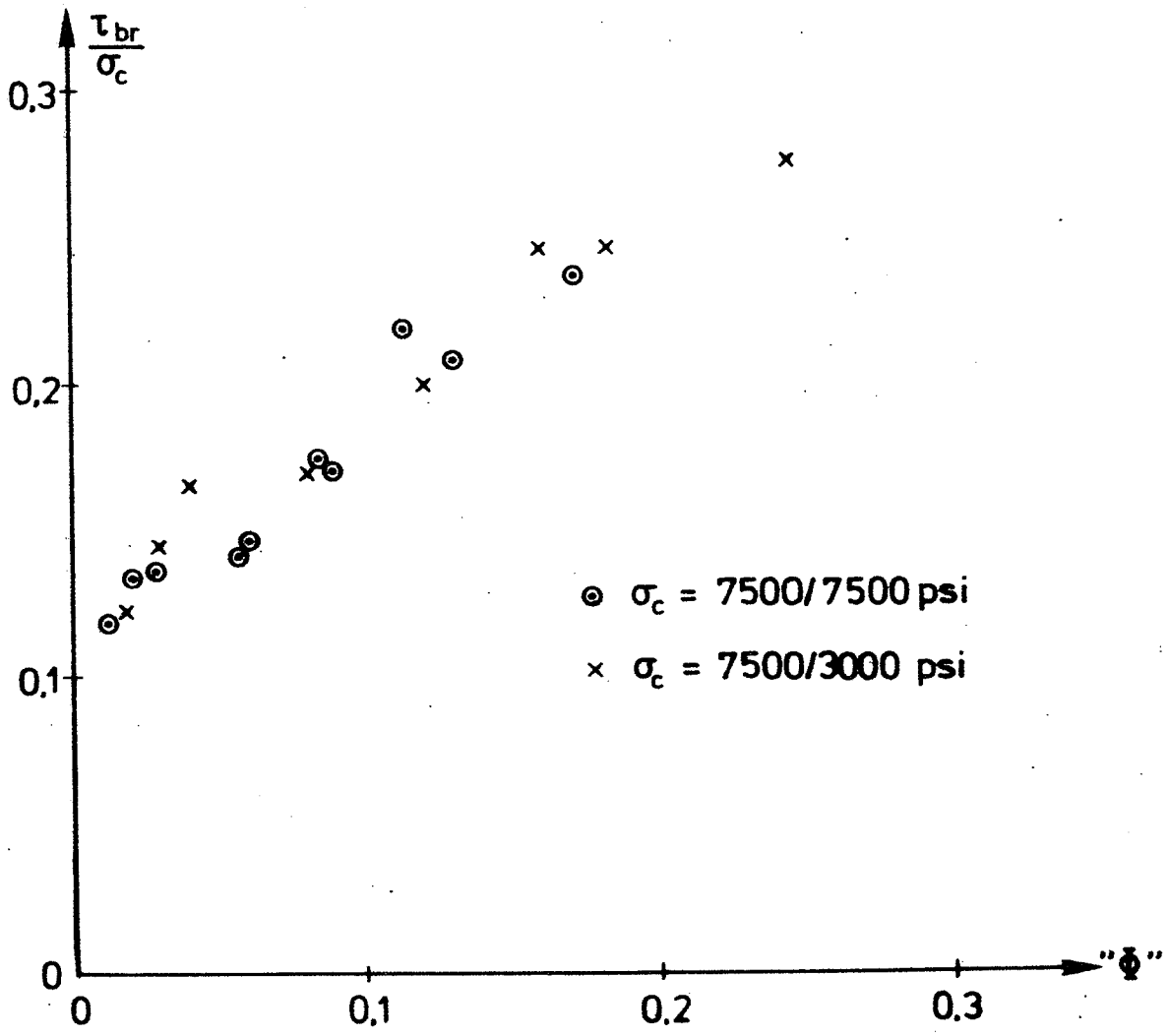

Fig. 5.12 Tests with construction joints from [60.1].

for determination of the split tensile strength of concrete.

The test results are plotted in fig. 5.10. The formulae for the carrying capacity for a plane deformation field are plotted, with $\varphi = 37^{o}$ and $\sigma_t = 0$. (The tensile strength of the concrete is zero perpendicular to the shear section). ν is put at 0.45, corresponding to about 70% of the efficiency factor in the monolithic case. The curves for the carrying capacity for a plane stress field, i.e. the carrying capacity for monolithic test specimens, is also shown. This curve is equivalent to that shown in fig. 5.7.

The carrying capacity is determined from the set of curves that gives the lowest carrying capacity. For $\Phi < 0.28$, failure occurs with a plane deformation field, and $\nu = 0.45$, and for $\Phi >$ about 0.28, failure occurs as in the monolithic case, i.e. with plane stress field and $\nu = 2/3$.

It will be seen that the test results accord well with the theory.

Mattock and Hawkins [72.3] have also performed tests with cracked test specimens, which, apart from this, correspond to their tests with monolithic test specimens and tension, which are dealt with in example 5.1.

The results are shown in fig. 5.11, together with the curves for the carrying capacity, which are analogous to those shown in fig. 5.10. The curve for plane deformation field is plotted with $\nu = 0.27$, i.e. here, too, an efficiency factor of 70% of that from the monolithic case.

Here, too, it will be seen that the test results accord well with the theory.

Anderson [60.1] has carried out tests with real construction joints. The test specimen was, in principle, as shown in fig. 6.5. One half, i.e. up to the shear section, was cast first. After curing, the rough shear section was scrubbed with cement mortar and the second half was cast.

The test data are extremely sparse, the results being given in a figure with the shear strength τ_{br} as a function of the area of reinforcement F in relation to the area of the concrete b·h. In addition, it is stated that the first half of the test specimen was cast with concrete with σ_c = 7500 psi ($\sim$ 52 MN/m^2), and the second half with concrete with either σ_c = 7500 psi or σ_c = 3000 psi ($\sim$ 21 MN/m^2).

If we estimate a yield stress for the reinforcement, the test results can be plotted in our usual coordinate system. The yield stress is estimated at σ_F = 53000 psi (370 MN/mm^2), and the results are depicted in fig. 5.12, the mean strength σ_c = 5300 psi (37 MN/m^2) being used for the test specimens of concrete with different strengths. It should be noted that the results from the two series are largely identical in this plot.

As the test specimens in the two series were identical apart from the concrete strength, we can assume same ν in the two series. We cannot find ν from the test results because the yield stress for the reinforcement is estimated. On the other hand, we can see from fig. 5.12 that the strength in a construction joint

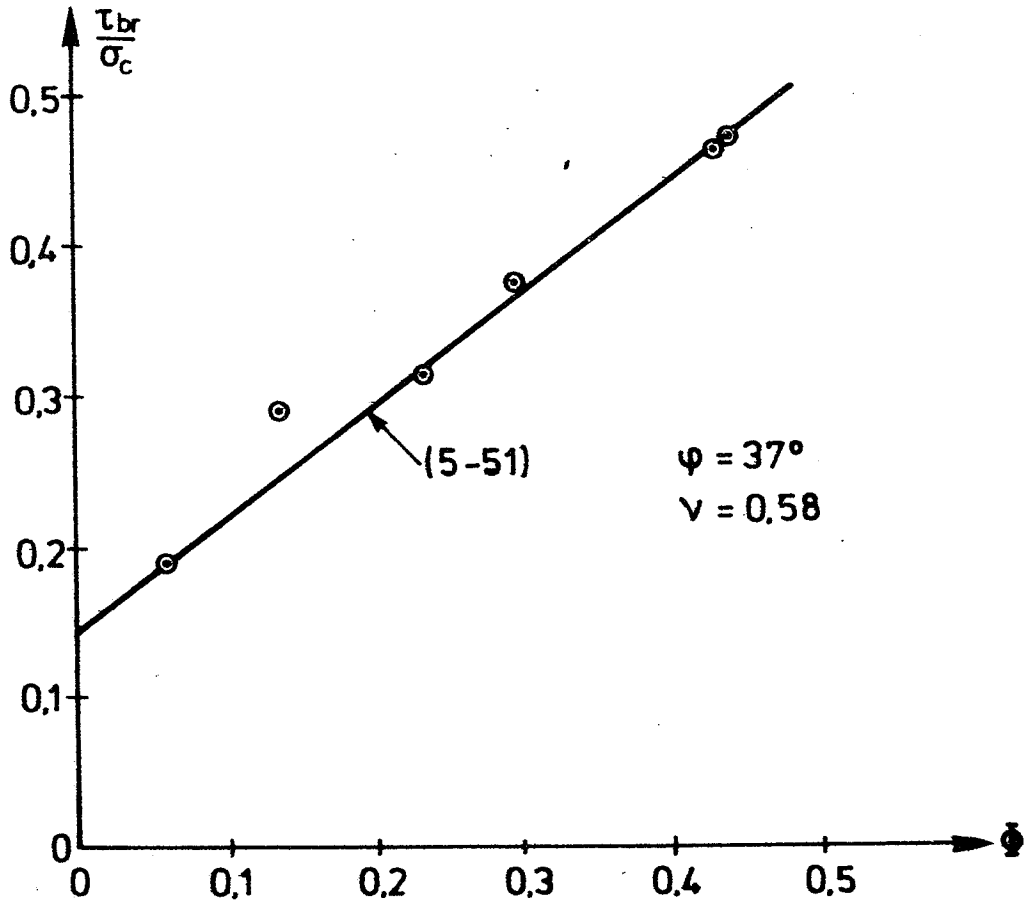

Fig. 5.13 Tests with construction joints from [74.2].

between concrete with two different strengths can be determined by means of the average strength of the two types of concrete.

Caution must be exercised when using this conclusion because it must be remembered that construction joints can be made so strong that failure will occur in the weakest concrete as monolithic failure.

Houborg and Sørensen [74.2] have carried out tests with three types of construction joints in connection with an examination project at the Structural Research Laboratory of the Technical University of Denmark. One half of the test specimen was cast with the shear section upwards. The shear section was treated in one of the following three ways:

1) Floated with steel rail and then steel-trowelled.
2) Floated with steel rail.
3) Floated with steel rail and then brushed with a steel brush after about 2 hours.

After two days, the opposite part of the test specimen was cast.

The results from the tests with the construction joints treated in accordance with method 3 are depicted in fig. 5.13. The results accord well with the assumption of a plane deformation field, as can be seen from the plotted line, which is (5-15) with $\nu = 0.58$ and $\varphi = 37^{\circ}$.

The construction joints treated according to method 1 and method 2 proved to give a lower carrying capacity than those treated according to method 3. This is actually not particu-

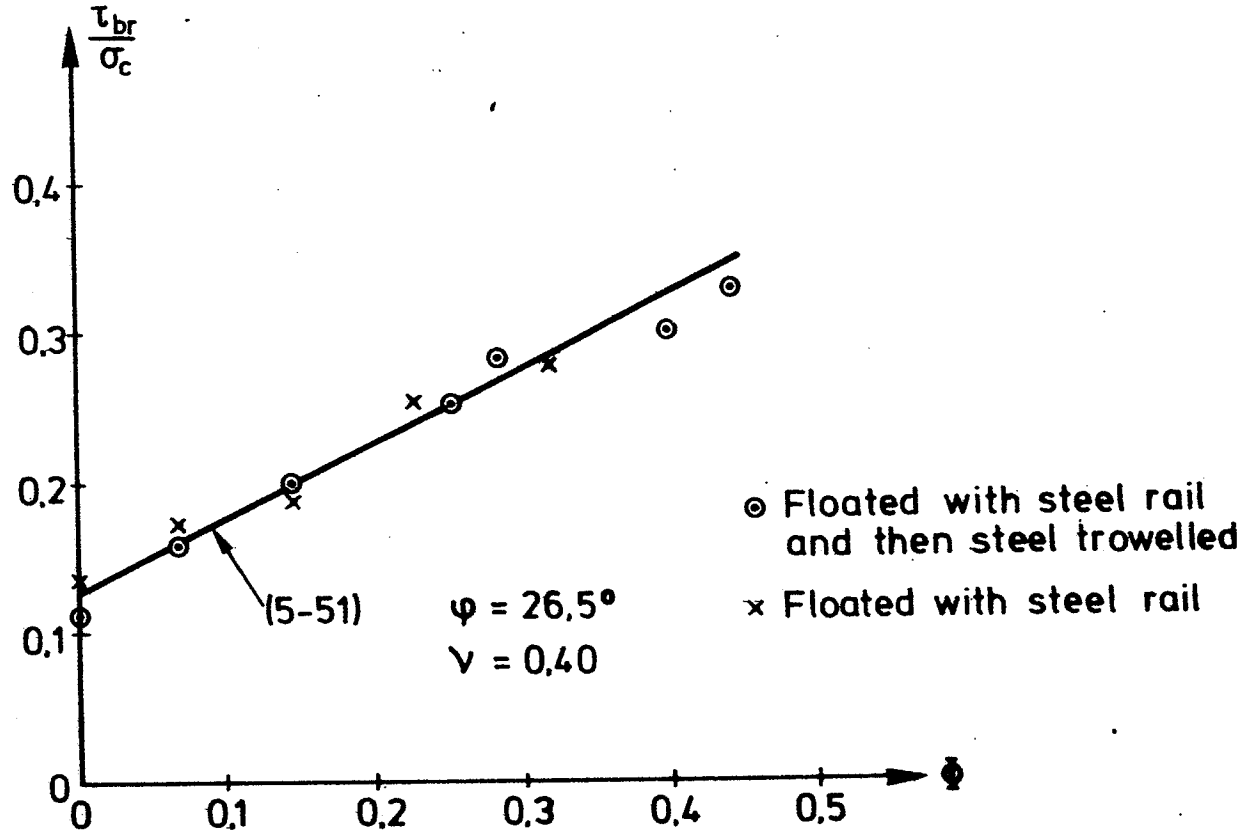

Fig. 5.14 Tests with smooth construction joints from [74.2].

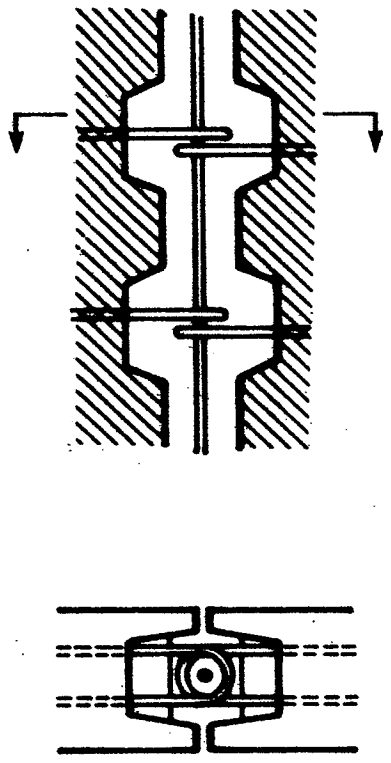

Fig. 5.15 Principle of keyed, reinforced wall joint.

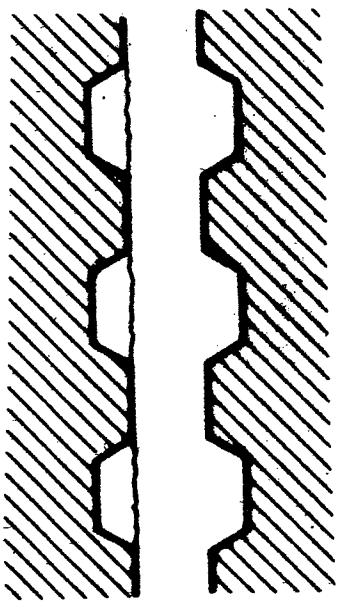

Fig. 5.16 Failure in keyed edge

larly surprising. What is more surprising is the fact that method 1 and method 2 are equally good, as can be seen from fig. 5.14. It will also be seen from the figure that the assumption of a plane deformation field is good, except that the angle of friction is now reduced to about 26.5^{o} and ν is similarly reduced.

As trowelling presumably gives the smoothest type of construction joint that can occur, the tests therefore indicate that the angle of friction in a construction joint can always be assumed to be bigger than 26^{o}.

Example 5.3 Shear Strength of Keyed Shear Joints

In prefabricated, large panel buildings, structural wall components are often connected by means of a keyed, reinforced shear joint. The principle is shown in fig. 5.15.

The wall components are placed side by side, after which the vertical reinforcement is inserted between the stirrups. Finally, the joint is cast with joint mortar. The keyed shear joint is a special case of a construction joint, where, however, only the keyed area is active at failure, see fig. 5.16.

Putting the tensile strength normal to the joint at zero, we can easily see (see [75.3]) that the formulae for plane deformation field lead to:

(a) $$\frac{\tau_{br}}{\sigma_c} = \sqrt{\Phi(\nu \frac{B}{A} - \Phi)}$$

(b) $$\frac{\tau_{br}}{\sigma_c} = \nu \frac{B}{A} \frac{1-\sin\varphi}{2\cos\varphi} + \Phi \tan\varphi$$

The boundary between the validity of the two formulae is given by

$$\Phi = \nu \frac{B}{A} \frac{1-\sin\varphi}{2} \qquad (c)$$

In the formulae the usual designations are used, and $\frac{B}{A}$ is the key-ratio. Here, A is the entire cross-section of the joint mortar and B is the cross-section of the keys in the joint mortar, i.e. the part in which failure has occurred in fig. 5.16. The efficiency factor ν is still a measure of how large a part of the yield surface B can be assumed to contribute fully.

The shear strength of keyed shear joints has been investigated by tests for many years. One group of researchers [74.3] has studied a large number of test results and, on this basis, has arrived at an empirical formula

$$\frac{\tau_{br}}{\sigma_c} = 0{,}09 \frac{B}{A} + \Phi \qquad \text{for } 0{,}01 \leq \Phi \leq 0{,}08 \qquad (d)$$

It will be seen that, apart from the limits, (d) is identical with (b) when $\varphi = 45^{\circ}$ and $\nu = 0.43$. The range of validity of (d) is confined to the area covered by the tests.

However, the theory shows that we do not have a straight line in the entire area, but that, for small Φ, we have a circle that passes through $(\Phi, \frac{\tau_{br}}{\sigma_c}) = (0, 0)$. The test results relating to this circle have presumably been one of the reasons for choosing a slightly low factor in front of $\frac{B}{A}$ in (d). A more realistic value for ν would be 0.55 instead of 0.43. The formulae for the carrying capacity

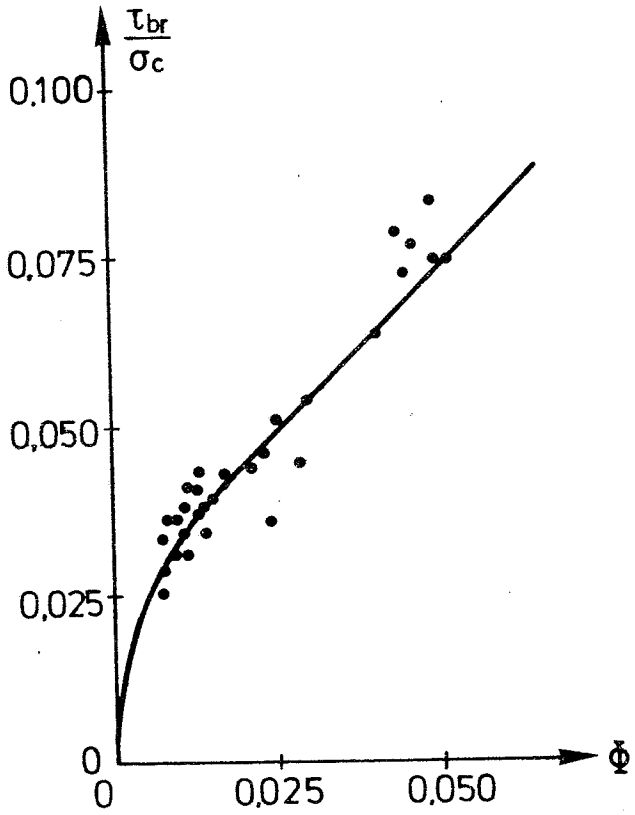

Fig. 5.17 Test by Pommeret (from [74.3]), with $\frac{B}{A} = 0.22$ and (e) and (f).

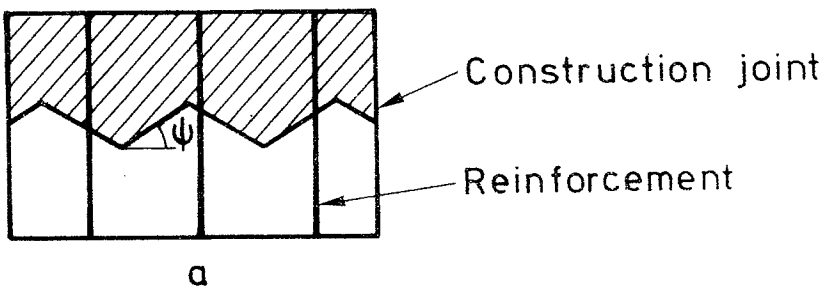

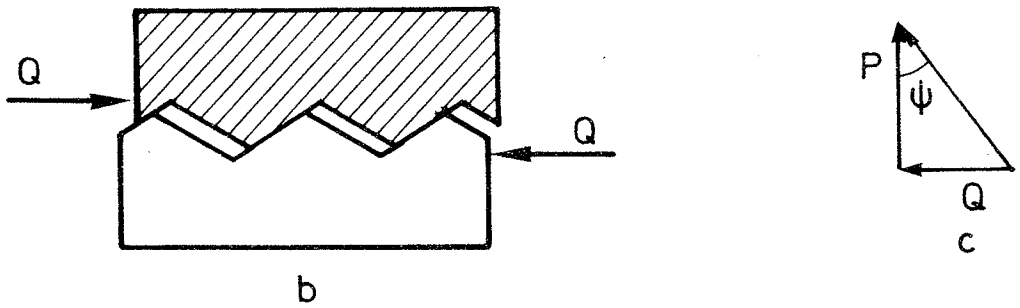

Fig. 5.18 Shear in construction joint.

thereby become

(e) $$\frac{\tau_{br}}{\sigma_c} = \sqrt{\Phi(0{,}55\ \frac{B}{A} - \Phi)} \qquad \Phi \leq 0{,}08\ \frac{B}{A}$$

(f) $$\frac{\tau_{br}}{\sigma_c} = 0{,}11\ \frac{B}{A} + \Phi \qquad \Phi \geq 0{,}08\ \frac{B}{A}$$

Fig. 5.17 shows some test results with $\frac{B}{A} = 0.22$ by Pommeret [71.1], here taken from [74.3]. The figure also shows (e) and (f), and it will be seen that there is excellent agreement.

Example 5.4. The Shear-Friction Theory

The shear-friction theory is often used in USA for calculating certain shear problems, e.g. the shear strength of construction joints. As the formulae resulting from the shear-friction theory greatly resemble the formulae derived here for plane deformation fields, the theory will be discussed and commented on here.

Birkeland and Birkeland [66.2] advanced the shear-friction theory in 1966, on the assumption that a construction joint was serrated and that the serrations had the angle ψ, see fig. 5.18a. As will be seen from fig. 5.18b, shear of the upper part in relation to the lower part requires lateral expansion. This gives rise to deformations and thus to stresses in the transverse reinforcement. Failure occurs when the reinforcement yields.

By assuming that the compression between the "serrations"stands at right-angles to these, we find, with the notation from fig. 5.18c,

(a) $$Q = P \tan\psi = F \sigma_F \tan\psi$$

Here, F is the area of the transverse reinforcement.

We can introduce the shear stress by dividing by the concrete area A

(b) $$\tau_{br} = \frac{F}{A} \sigma_F \tan\psi = f \sigma_F \tan\psi$$

where the designation f is introduced for the ratio of reinforcement $\frac{F}{A}$.

For $\tan\psi$ Birkeland and Birkeland gave 0.8 to 1.0 for an ordinary construction joint and for concrete against steel, 1.4 for a rough construction joint and 1.7 for monolithic concrete. As upper bound for τ_{br}, they recommended 800 psi (5.5 MN/m^2), the test results being limited to $\tau_{br} \leq 800$ psi.

Mast [68.1] also gives $\tan\psi = 1.4$ for a rough construction joint, but gives 0.7 for smooth construction joints and 0.7-1.0 for concrete against steel.

Comparison of (b) with various shear tests, e.g. some of those mentioned in example 5.1, has since resulted in both Birkeland [71.2] and Mattock and Hawkins [72.3] putting $\tau_{br} = 0.2 \sigma_c$ as upper bound for validity of (b).

The derived formula (b) is equivalent to (5-51), apart from the fact that contribution from the concrete is omitted in (b). In a

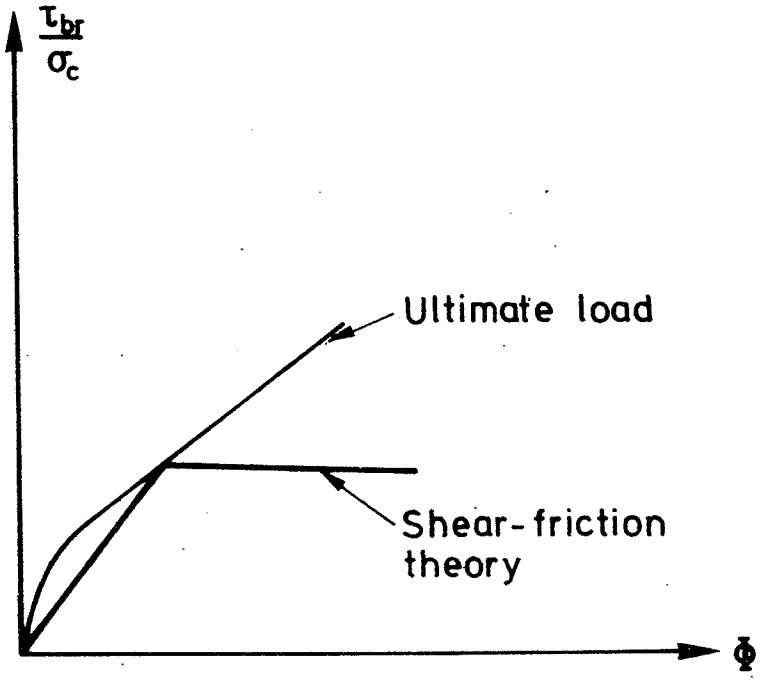

Fig. 5.19 Comparison of ultimate carrying capacity with the shear-friction theory.

Φ , $\frac{\tau_{br}}{\sigma_c}$ -coordinate system this means that (b) passes through (0,0). It is immediately clear from fig. 5.19 why the big values have been obtained for $\tan\psi$ and the upper bound for the validity of (b), regardless of whether comparison has been made with tests in which there is a plane deformation field or tests in which there is a plane stress field.

The tensile strength of concrete has always presented serious problems, and the approximation is therefore often made of neglecting it. Therefore, in tests to determine the carrying capacity (e.g. [69.5] and [72.3], see example 5.1), it was found preferable to split the test specimens first, so that the tensile strength perpendicular to the shear section in fig. 5.6 was zero. Without reinforcement, the shear strength must therefore be zero, and a formula for the carrying capacity must therefore pass through $(\Phi, \frac{\tau_{br}}{\sigma_c}) = (0, 0)$. This requirement is satisfied by (b).

However, splitting means that we force the test specimen, in the case of low degrees of reinforcement, to fail in a plane deformation field instead of in a plane stress field, as described in example 5.1. An effort is then made to describe the ultimate strength in a plane deformation field by means of a straight line through $(\Phi, \frac{\tau_{br}}{\sigma_c}) = (0, 0)$, which leads to the big slopes, since there is no contribution from the concrete.

In order to get the straight line to fit the test results better, Mattock and Hawkins [72.3] proposed an alternative calculation of the cracked test specimens

(c)
$$\tau_{br} = 200 + 0{,}8f\sigma_f \qquad \text{(psi)}$$
$$(\tau_{br} = 1{,}38 + 0{,}8f\sigma_f) \qquad (\text{MN/m}^2))$$

At the same time as the straight line was thus lifted and given smaller slope (from $\tan\psi = 1.4$ to $\tan\psi = 0.8$), the upper limit of validity was altered from $\tau_{br} = 0{,}2\sigma_c$ to $\tau_{br} = 0{,}3\sigma_c$.

Mattock [74.4] has since further raised the line by proposing

(d)
$$\tau_{br} = 400 + 0{,}8f\sigma_F \qquad \text{(psi)}$$
$$(\tau_{br} = 2{,}76 + 0{,}8f\sigma_F) \qquad (\text{MN/m}^2))$$

still with the upper bound at $\tau_{br} = 0{,}3\sigma_c$, but now also $f\sigma_F \leq 200$ psi (1.38 MN/m^2).

It should be noted that (c) and (d) are advanced independent of the concrete strength and that the movement of the straight line is experimentally warranted.

An explanation of the movement of the straight line was first given by Hermansen and Cowan [74.5], who proposed, in general,

(e)
$$\tau_{br} = c + 0{,}8f\sigma_F$$

The quantity c appearing here is called the apparent cohesion, and (e) is called the modified shear-friction theory. The contribution from the concrete is thus c, and Hermansen and Cowan also propose that it can be put at 4 MN/m^2 for uncracked test specimens of the type shown in fig. 5.6 and for shear failure in brackets, regardless of the concrete strength.

If we insert (2-6) in (5-51), we can write this in the form

(f) $$\tau = \nu c + \tan\varphi f \sigma_F$$

and (e) is thus largely identical with (5-51).

The difference between (e) and (d) is insignificant apart from the fact that (d) is proposed for calculation of cracked cross-sections, while (e) is proposed for uncracked cross-sections. As will be seen from examples 5.1 and 5.2, a straight line is correct within a very big range for cracked cross-sections, but is only correct in a small range for uncracked cross-sections.

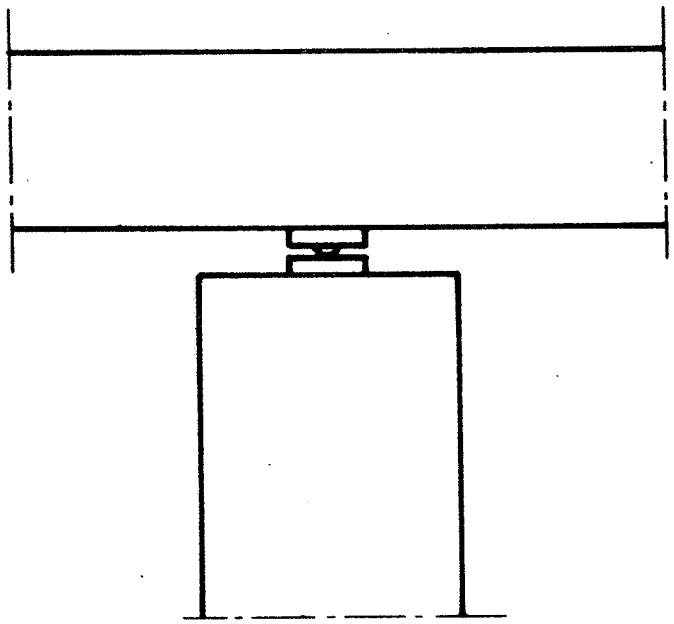

Fig. 6.1 Concentrated load on column from a continuous beam.

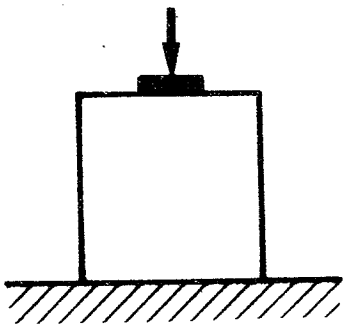

Fig. 6.2 Concentrated load on unreinforced concrete.

6. CONCENTRATED LOADS ON PLAIN CONCRETE

6.1 Introduction

In connection with the transmission of loads to a part of a structure, we often find that these have to transmitted through a limited area, whereby we get the phenomenon: concentrated loads. An example is shown in fig. 6.1.

Here we will restrict ourselves to the case in which a plane concrete prism is supported on one surface and subjected to a concentrated load acting on the opposite surface, see fig. 6.2. The aim here is to find a procedure for calculating the ultimate load for such concrete bodies. The problem will be dealt with by considering the concrete partly as a linear elastic material and partly as a rigid-plastic material, and as the results arrived at on these bases cannot be used for determination of the carrying capacity, some empirical formulae will be proposed.

6.2 Linear-Elastic Solutions

The theory of elasticity can be used for determining the carrying capacity of a body of a material that is linear-elastic all the way up to failure. If this is not the case, the theory of elasticity will still give safe values for the carrying capacity.

It is well known that tensile stresses oc perpendicular to the direction of the concentrated load some way below this load. If these tensile stresses can cause failure, i.e. if (2-10) is satisfied, it will be natural to try to use the theory of elasticity for determination of the carrying capacity

because concrete often exhibits almost linear-elastic behaviour up to uniaxial tensile failure, cf. section 2.4.

In a plane stress field we can introduce Airy's stress function $\psi(x,y)$, where x and y are the position coordinates in a right-angled coordinate system.

Neglecting the mass forces, we introduce this stress function such that

$$\sigma_x = \frac{\partial^2 \psi}{\partial y^2} \qquad \sigma_y = \frac{\partial^2 \psi}{\partial x^2} \qquad \tau_{xy} = \frac{\partial^2 \psi}{\partial x \partial y} \tag{6-1}$$

A unique solution to a problem with a plane stress field is found by satisfying the biharmonic equation

$$\frac{\partial^4 \psi}{\partial x^4} + 2 \frac{\partial^4 \psi}{\partial x^2 \partial y^2} + \frac{\partial^4 \psi}{\partial y^4} = 0 \tag{6-2}$$

and the boundary conditions relating to the problem.

Plane deformation fields can be solved in the same way by determining the stress perpendicular to the plane deformation field from

$$\sigma_z = \nu(\sigma_x + \sigma_y) \tag{6-3}$$

where ν is Poisson's ratio.

The biharmonic equation (6-2) with related boundary conditions can only be solved exactly in a few cases, see, for example, Timoshenko and Goodier [70.2]. We must therefore often make do with approximate methods, e.g. series development.

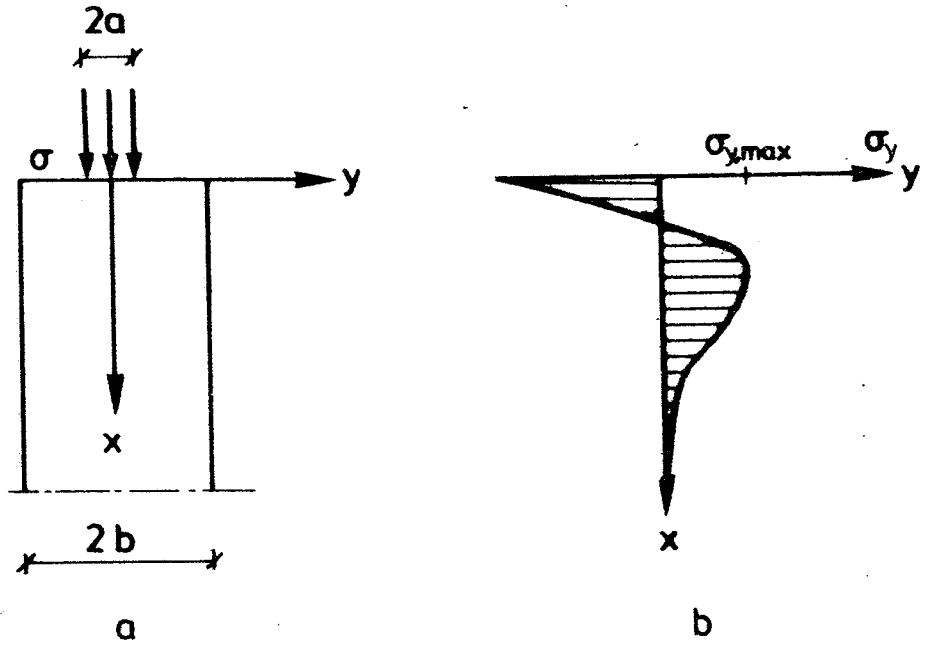

Fig. 6.3 a. Concentrated load on semi-infinite bar.
b. Transverse stress along the x-axis.

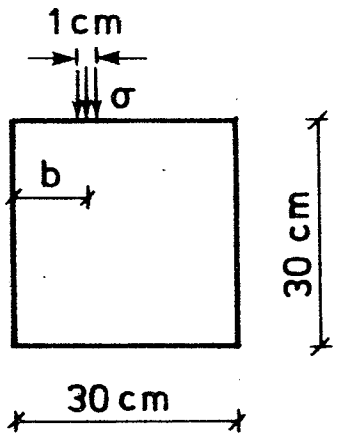

Fig. 6.4 Test by Rathkjen [73.2].

For a semi-infinite diaphragm loaded on three free sides, Iyengar [60.2], [62.1] and [62.2] has indicated a solution by means of Fourier-series. The expressions are extremely complicated and will normally require computer treatment in order to be used.

For some loading cases Iyengar has prepared tables [60.2] and plotted curves [60.2], [62.1] and [62.2].

The loading case which research workers have found of particular interest is the case of a centrally acting load as shown in fig. 6.3. The figure also shows the theoretical course of the stress σ_y along the x-axis. For this stress Guyon [53.1] has given an approximate formula which is frequently used and which results in almost the same values as Iyengar's solution.

An evaluation of the carrying capacity can now be carried out in accordance with the theory of elasticity by putting $\sigma_{y,max}$ equal to the tensile strength σ_t of the concrete. Here, we will consider a test series of Rathkjen [73.2], in which 30 cm cubes were loaded on one side over their entire width through a steel rail with a width of 1 cm. The cube was supported over the entire opposite side. In the test series, the concrete strength was varied, together with the distance of the steel block from the edge of the cube, see fig. 6.4.

For such a load, the transverse stress σ_y along the vertical line centrally under the load has the same form as shown in fig. 6.3b.

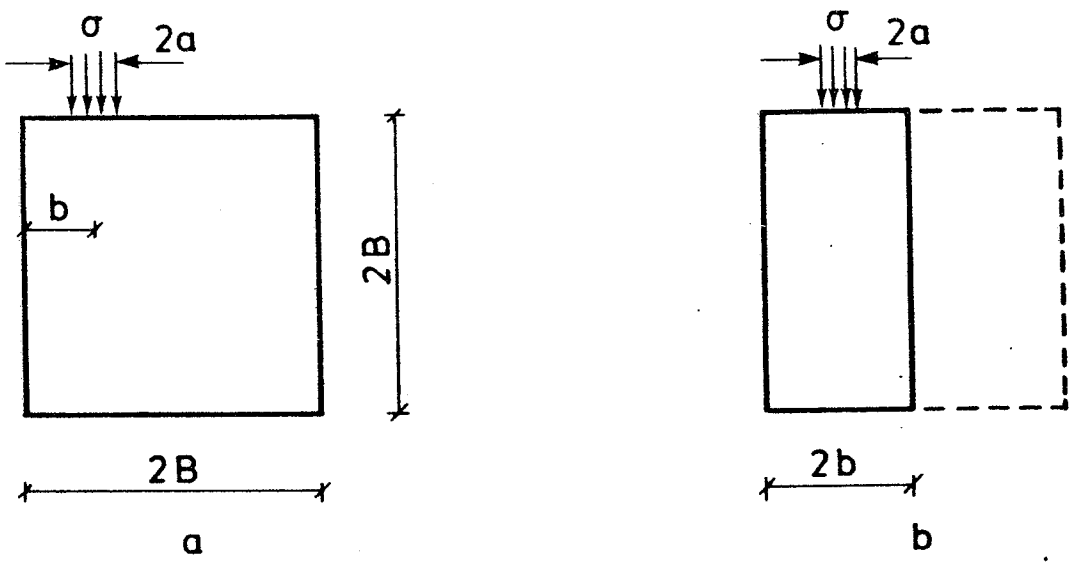

Fig. 6.5 Notations used in table 6.1.

$\frac{a}{b}$	$\frac{1}{30}$	$\frac{1}{20}$	$\frac{1}{10}$	$\frac{1}{5}$	$\frac{1}{3}$
Iyengar	0,015	0,022	0,042	0,072	0,100
STRUDL	0,014	0,019	0,037	0,068	0,093

Table 6.1 Value of $\frac{\sigma_{y,max}}{\sigma}$, determined by the element method for $\frac{a}{B} = \frac{1}{30}$, cf. fig. 6.5.

Determination of this by means of Iyengar's formulae is not directly possible because the length of the test specimen is limited. The stresses needed in order to investigate whether the theory of elasticity can be used for determination of the carrying capacity are therefore determined by means of calculations in accordance with the element method.

The element calculations are carried out by means of the computer programme ICES STRUDL-II, which has been developed at the Massachusetts Institute of Technology [71.3]. The calculations are carried out as a plane stress field with a rectangular element called type "PSR" in ICES STRUDL-II. In the calculations the body was divided into 575 elements with maximum density at the concentrated load.

Table 6.1 shows $\frac{\sigma_{y,max}}{\sigma}$ as obtained in the element calculations. The notation used is shown in fig. 6.5.

The geometrical conditions chosen are equivalent to those used by Rathkjen in his tests. In these tests, the failure load P_{br} for the concentrated load is determined.

We now define the failure stress σ_f as

$$\sigma_f = \frac{P_{br}}{f} = \frac{P_{br}}{2a\,l} \tag{6-4}$$

where f is the surface of the concentrated load. 2a and l are its extent, in this case, 1 x 30 cm.

$\frac{a}{b}$	$\frac{1}{30}$	$\frac{1}{20}$	$\frac{1}{10}$	$\frac{1}{5}$	$\frac{1}{3}$
$\frac{\sigma_t}{\sigma_f}$	0,043		0,055	0,088	0,096
	0,045	0,040	0,063	0,059	0,081
	0,025	0,031	0,042	0,048	0,058
	0,030	0,028	0,035	0,047	0,060
	0,027	0,029	0,045	0,059	0,069
Middle	0,034	0,032	0,048	0,060	0,073

Tabel 6.2: Test results from [73.2]. σ_t is put at the measured split tensile strength.

$\frac{a}{b}$	$\frac{1}{30}$	$\frac{1}{20}$	$\frac{1}{10}$	$\frac{1}{5}$	$\frac{1}{3}$
$\frac{\sigma_t}{\sigma_f}$	0,031		0,038	0,060	0,065
	0,031	0,028	0,043	0,046	0,056
	0,024	0,027	0,033	0,043	0,055
	0,022	0,024	0,032	0,040	0,050
	0,031	0,029	0,039	0,056	0,074
Middle	0,028	0,027	0,037	0,049	0,060

Tabel 6.3: Test results from [73.2]. σ_t is determined by means of (6-5).

In order to investigate whether the above can be used for determination of the carrying capacity we must thus compare

$$\frac{\sigma_{y,max}}{\sigma} \quad \text{with} \quad \frac{\sigma_t}{\sigma_f}$$

where σ_t is the tensile strength of the concrete used.

Table 6.2 shows the results obtained for $\frac{\sigma_t}{\sigma_f}$ from the tests, where σ_t is put equal to the measured split tensile strength. The same is done in table 6.3, except that σ_t is found by the commonly used empirical formula

$$\sigma_t = 1{,}5\sqrt{\sigma_c} \qquad [kp/cm^2] \tag{6-5}$$

A comparison of the average values in tables 6.2 and 6.3 with the values in table 6.1 shows that the procedure cannot be used for determination of the carrying capacity. We also see that, for small loading widths, i.e. small values of a/b, the procedure gives far too optimistic estimates of the carrying capacity.

This is apparently at variance with the fact that the theory of elasticity gives safe values for the carrying capacity. And an investigation of the stress field under the local loading surface in the area in which the transverse stresses are compressive stresses shows, in fact, that the criterion for sliding failure (2-7) is satisfied at considerably smaller loads than the criterion for separation failure.

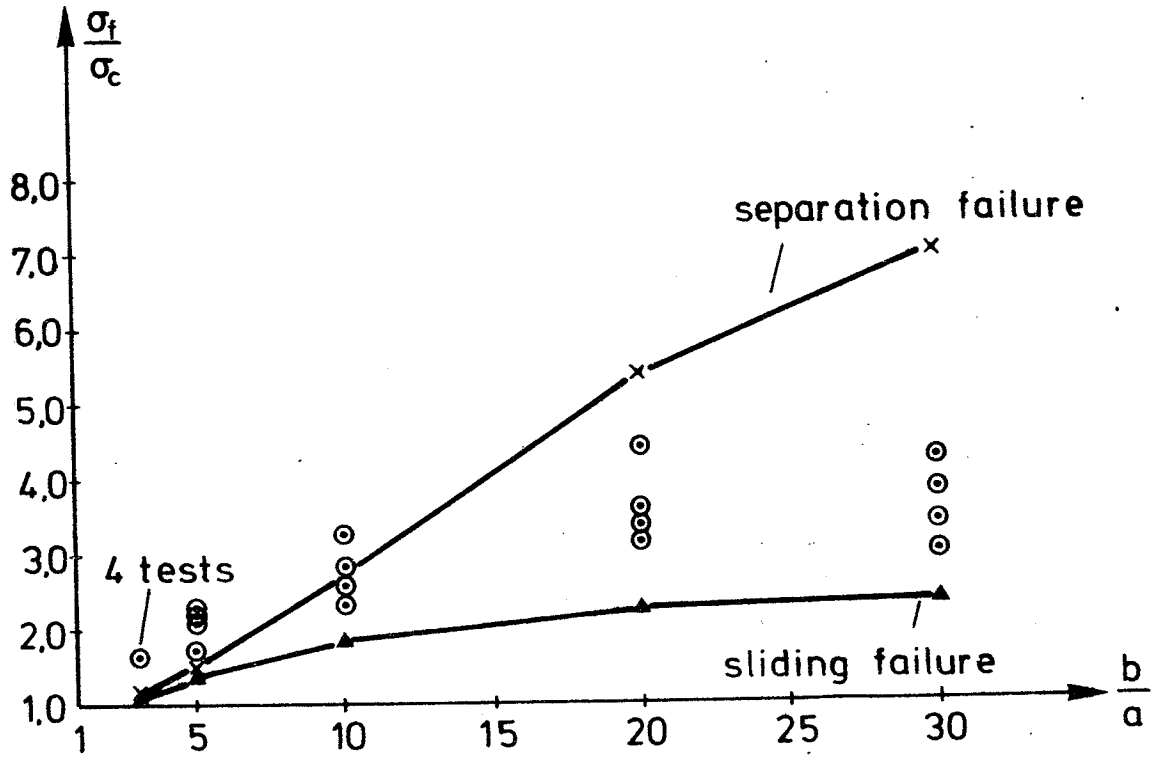

Fig. 6.6 Test results from [73.2] and result from element analysis.

The element calculations are carried out on the assumption of a plane stress field. The other extreme case is plane strain field, which, with good approximation, we have under the loading surface. In this case, the last principal stress is found analogously with (6-3), viz, from

$$\sigma_3 = \nu(\sigma_1 + \sigma_c) \tag{6-6}$$

As we thus find that σ_3 lies between the two other stresses, it is of no significance to the failure load whether we assume plane stress or plain strain.

Fig. 6.6 shows $\frac{\sigma_f}{\sigma_c}$ as a function of $\frac{b}{a}$ from Rathkjen's tests. The sliding failure load found by means of the element method is also included. This load is found for the same $\frac{b}{a}$ values as those with which tests have been carried out. Straight lines are drawn between the values. The figure also shows the "separation failure load", i.e. the load at which $\sigma_{y,max}$ is equal to the tensile strength. In order to be able to include this relationship, the tensile strength is estimated as $\frac{1}{10}$ of the compressive strength σ_c.

It will be seen from the figure that, for the values investigated, the criterion for sliding failure is always satisfied for lower loads than the criterion for separation failure. Under concentrated loading, failure thus often commences as sliding failure.

It will also be seen that the theory of elasticity gives safe values for the carrying capacity when it is used as here.

All in all, it must, however, be ascertained

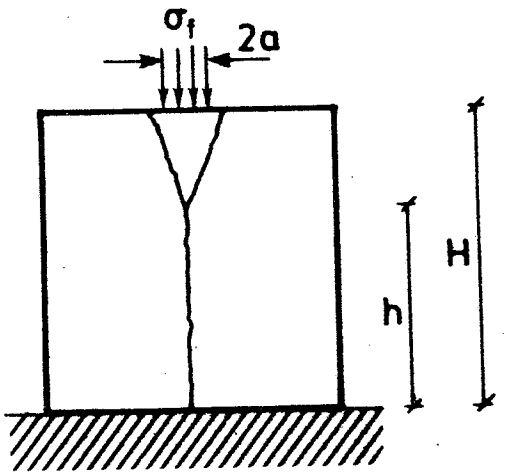

Fig. 6.7 Failure mechanism.

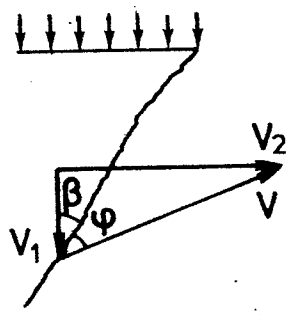

Fig. 6.8 Movements in the failure mechanism, fig. 6.7.

that the theory of elasticity does not provide the means of determining the carrying capacity very accurately.

Similar considerations have been made by Jensen and Nielsen [75.2] in the split test. Here, too, it is found that failure often commences with sliding failure near the loading strips, so that the split test cannot be said to be a particularly suitable tool for determining the tensile strength of concrete.

6.3 Plastic Solutions

In this section we will investigate the possibility of calculating the carrying capacity when concrete is considered as a rigid- plastic material. As in the foregoing chapters, we will concentrate on upper-bound solutions, using failure patterns that largely correspond to observed failure patterns.

In contrast to the elastic solutions, we will here consider both plane and 3-dimensional failure problems.

6.3.1 Plane Failure Mechanisms

Let us first consider a plane failure mechanisms, as shown in fig. 6.7, which corresponds to the type of failure frequently observed and known as split failure.

The wedge formed directly under the concentrated load moves downwards, and the remaining two parts of the prism move out sideways. We thereby get sliding failure along the sides of the wedge and separation failure along the vertical line.

If we assume that the vertical angle of the wedge is 2β, and that the relative movement V along the sides of the wedge forms the angle φ (= the angle of friction) with this, we get the relationship between the movements shown in fig. 6.8. In the figure, V_1 is the vertical movement of the wedge and $2V_2$ is the total horizontal movement in the vertical line of discontinuity. This relationship between the movements is found directly from the figure:

$$V_1 = V \cos(\beta + \varphi)$$

(6-7)

$$V_2 = V \sin(\beta + \varphi)$$

Let us first consider the case in which the tensile strength of the concrete is 0, i.e. there is no contribution to the internal work along the vertical line.

The external work is

(6-8) $$A_y = \sigma_f \, 2a \, V \cos(\beta + \varphi)$$

The internal work is found by means of (3-39) and as $\alpha = \varphi$, we find:

(6-9) $$A_i = \frac{1-\sin\varphi}{2} \sigma_c \frac{2a}{\sin\beta} V$$

From this we find the upper bound:

(6-10) $$\sigma_f = \frac{1-\sin\varphi}{2\cos(\beta+\varphi)\sin\beta} \sigma_c$$

We find that (6-10) has minimum for $\beta = \frac{\pi}{4} - \frac{\varphi}{2}$. and that minimum is $\sigma_f = \sigma_c$.

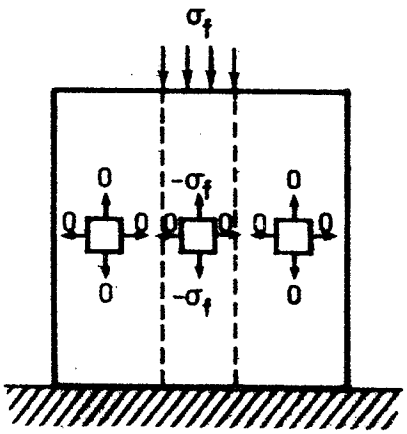

Fig. 6.9 Permissible stress distribution.

This carrying capacity is, moreover, an exact solution, since a permissible stress distribution that gives the same carrying capacity can easily be constructed, see fig. 6.9.

To find a carrying capacity that is greater than the uniaxial compression strength, it is thus necessary to include the tensile strength. In this case, the external work is still determined from (6-8). The internal work is found from (3-39), in that we have $\alpha = \varphi$ along the sides of the wedge and $\alpha = \frac{\pi}{2}$ along the vertical line of discontinuity.

$$A_i = \sigma_t (H - a\cot\beta)\, 2V \sin(\beta+\varphi) + \frac{1-\sin\varphi}{2}\,\sigma_c\,\frac{2a}{\sin\beta}\,V \tag{6-11}$$

From (6-8) and (6-11) we find

$$\sigma_f = \frac{\frac{1}{2}(1-\sin\varphi)\sigma_c + \sin(\beta+\varphi)\left(\frac{H}{a}\sin\beta - \cos\beta\right)\sigma_t}{\sin\beta\,\cos(\beta+\varphi)} \tag{6-12}$$

(6-12) can be shown to have minimum for

$$\cot\beta = \tan\varphi + \frac{1}{\cos\varphi}\sqrt{1 + \frac{\frac{H}{a}\cos\varphi}{\frac{\sigma_c}{\sigma_t}\left(\frac{1-\sin\varphi}{2}\right) - \sin\varphi}} \tag{6-13}$$

after which (6-12) can be written as

$$\sigma_f = \sigma_t\left(\frac{H}{a}\tan(2\beta+\varphi) - 1\right) \tag{6-14}$$

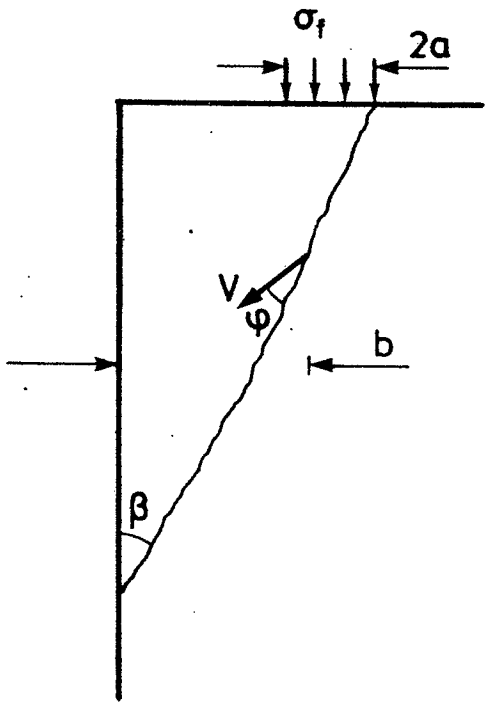

Fig. 6.10 Failure mechanism.

Formulae (6-12) to (6-14) have been found by Chen and Drucker [69.2] , who also mention that, as done here, V must form the angle φ with the diagonal line of discontinuity to get minimum.

The above formulae are independent of the distance from the load to the edge of the prism. However, if this distance is sufficiently small, another failure mechanism applies, see fig. 6.10. This spalling, too, is known from tests.

With the notation from fig. 6.10, we find

(6-15) $$A_y = \sigma_f \, 2a \, V \cos(\beta+\varphi)$$

(6-16) $$A_i = \frac{1-\sin\varphi}{2} \, \sigma_c \, \frac{b+a}{\sin\beta} \, V$$

which gives the upper bound:

(6-17) $$\sigma_f = \frac{(1-\sin\varphi)(b+a)}{4 \sin\beta \cos(\beta+\varphi) a} \, \sigma_c$$

The minimum is found for $\beta = \frac{\pi}{4} - \frac{\varphi}{2}$ to be

(6-18) $$\sigma_f = \frac{b+a}{2a} \, \sigma_c$$

It will be seen that, logically enough, (6-18) gives a force corresponding to a load on σ_c over the whole of the area that is broken off.

In fig. 6.11 (6-14) and (6-18) are compared with Rathkjen's test. For the purposes of (6-14), the tensile strength is put at $\frac{1}{10}$ of the compression strength, σ_c , and φ is put at 37°.

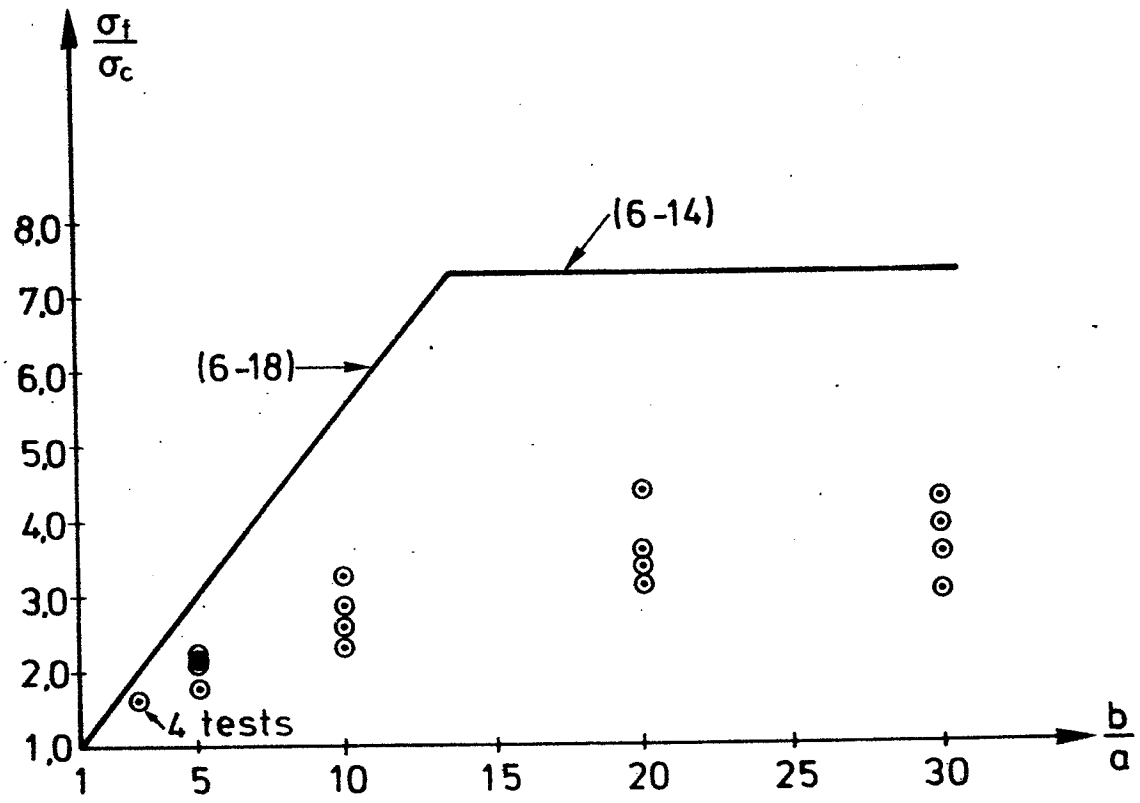

Fig. 6.11 Test results compared with plastic calculations.

It will be seen from the figure that the carrying capacity cannot be be directly determined on the basis of the theory of plasticity. For the failure pattern in fig. 6.7 it can easily be seen that the carrying capacity cannot be calculated in this way because the vertical failure surface is assumed to be fully active, even though separation failure is usually only slightly plastic.

We can now consider introducing efficiency factors ν , as was done in chapter 5. However, it can be seen that this gives a factor that is dependent on the distance from b. In the failure pattern in fig. 6.10, ν must, for example be unity when b = a, after which it decreases with increasing $\frac{b}{a}$. For the failure pattern in fig. 6.7 we can presumably make do with an efficiency factor for the separation failure. This, too, proves to be possibly dependent on $\frac{b}{a}$. Influence from the height H must also be expected, especially in the case of small heights.

Thus, if we want to use the plastic calculation outlined for determining the carrying capacity, we must reckon on having to use different efficiency factors depending on different parameters. However, for the simple, plane problem under consideration, the possibility cannot be excluded that the procedure may be usable.

6.3.2 3-Dimensional Failure Mechanisms

We will now consider a prismatic concrete body with a square top. The prism is centrally loaded over a square area with the load σ, see fig. 6.12.

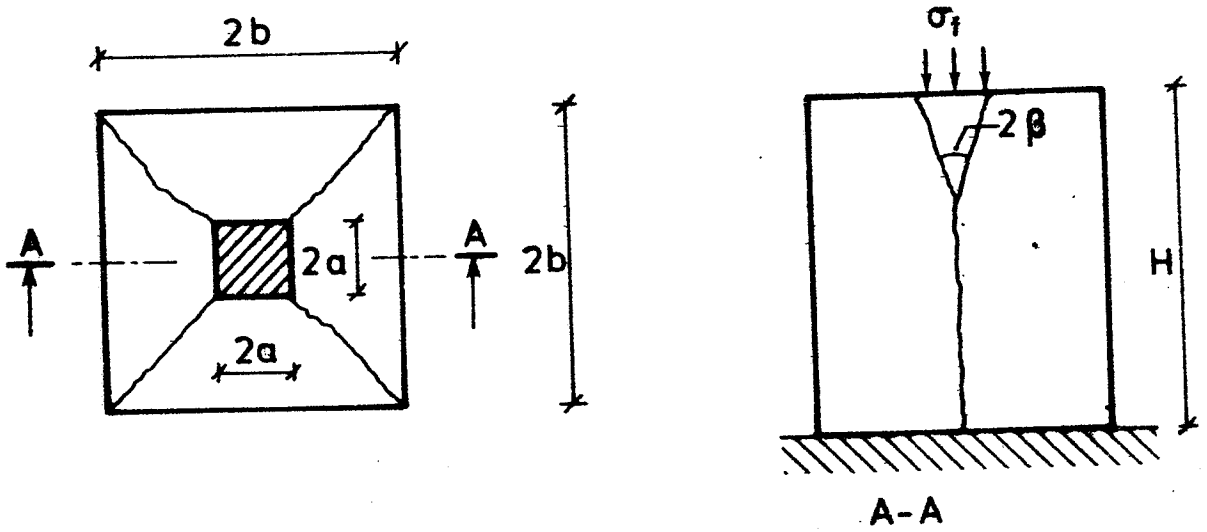

Fig. 6.12 Loaded prism with 3-dimensional failure mechanism.

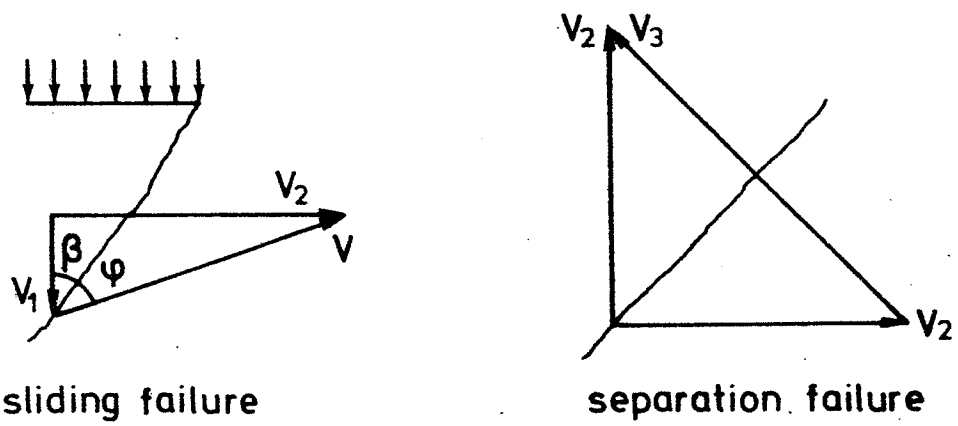

Fig. 6.13 Movements in the failure mechanism, fig. 6.12.

The failure mechanism we will use is a pyramid, which is pressed down in the splitting prism, see fig. 6.12. There is thus sliding failure along the four sides of the pyramid, while the other failure surfaces arise from separation failure. The relationship between the movements can be seen from fig. 6.13. It is here assumed that V forms the angle with the sides of the pyramid.

We get:

$$V_1 = V \cos(\beta+\varphi)$$

(6-19)
$$V_2 = V \sin(\beta+\varphi)$$

$$V_3 = \sqrt{2}\, V \sin(\beta+\varphi)$$

The area with sliding failure is found to be

(6-20)
$$F_1 = 4\,\frac{a^2}{\sin\beta}$$

The area with separation failure is

(6-21)
$$F_2 = 4\,[\sqrt{2}\, b H - \frac{\sqrt{2}}{2}\, a^2 \cot\beta]$$

The external work is

(6-22)
$$A_y = \sigma_f\, 4a^2\, V \cos(\beta+\varphi)$$

and the internal work,

(6-23)
$$A_i = (\frac{1-\sin\varphi}{2}\, \sigma_c F_1 + \sigma_t F_2 \sqrt{2} \sin(\beta+\varphi))V$$

From $A_y = A_i$, and by insertion of (6-20) and (6-21), we find the upper bound

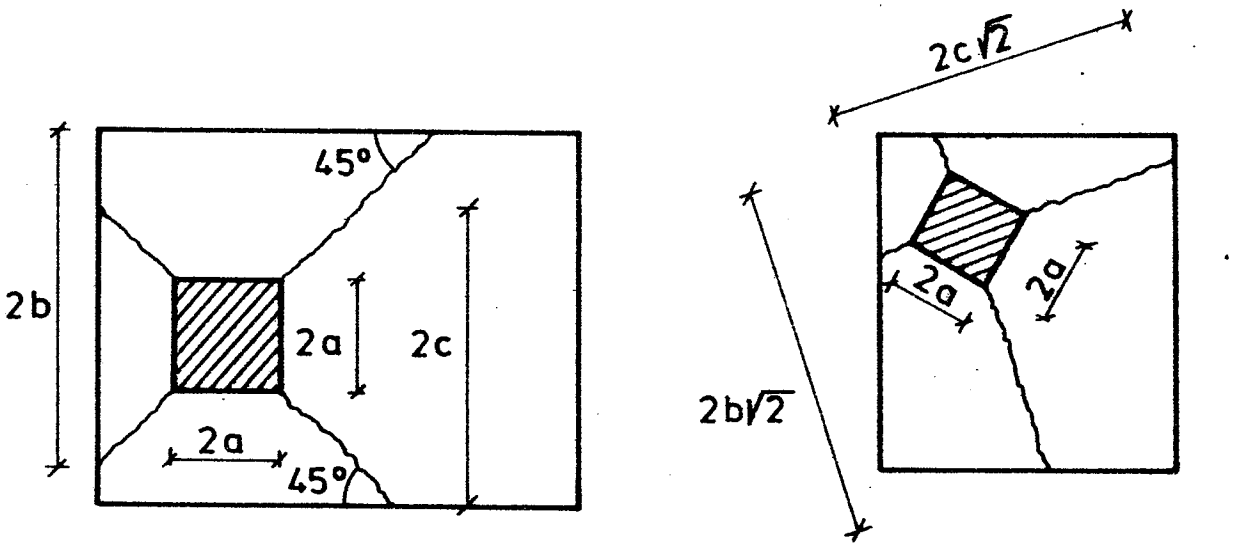

Fig. 6.14 Failure mechanisms under excentric loading.

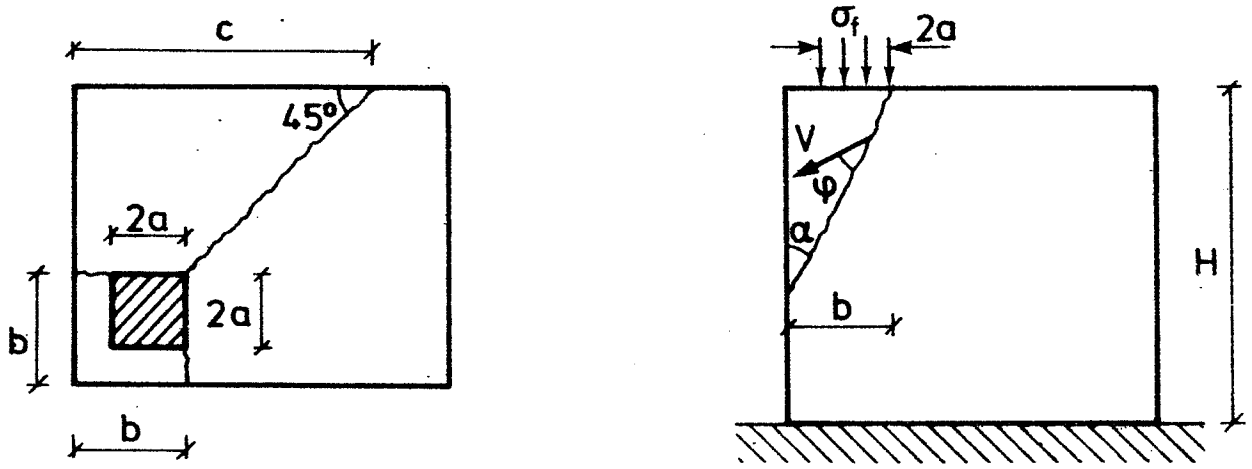

Fig. 6.15 Failure mechanisms.

$$(6\text{-}24)\qquad \sigma_f = \frac{\frac{1}{2}(1-\sin\varphi)\sigma_c + \sin(\beta+\varphi)\left(\frac{2Hb}{a^2}\sin\beta-\cos\beta\right)\sigma_t}{\sin\beta\,\cos(\beta+\varphi)}$$

This equation is completely analogous with (6-12), such that the minimum is found for

$$(6\text{-}25)\qquad \cot\beta = \tan\varphi + \frac{1}{\cos\varphi}\sqrt{1 + \frac{\frac{2Hb}{a^2}\cos\varphi}{\frac{\sigma_c}{\sigma_t}\left(\frac{1-\sin\varphi}{2}\right)-\sin\varphi}}$$

The minimum is thus

$$(6\text{-}26)\qquad \sigma_f = \sigma_t\left(\frac{2Hb}{a^2}\tan(2\beta+\varphi)-1\right)$$

Like the corresponding plane solution, this solution has been found by Chen and Drucker [69.2].

The same type of failure mechanism can be used in the case of other, non-symmetrically placed loads, as shown in fig. 6.14. With the notation used in fig. 6.14, the factor $\frac{2HB}{a^2}$ in (6-25) and (6-26) must be altered to $\frac{H(c+b)}{a^2}$.

Fig. 6.15 shows a failure pattern in which a skew pyramid spalls off through sliding failure, while the rest of the body splits through separation failure.

For this failure pattern it can be shown that, with the notation from fig. 6.15, the equations corresponding to (6-24), (6-25) and (6-26) are

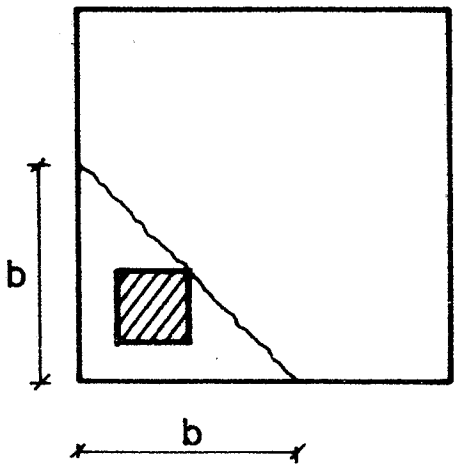

Fig. 6.16 Failure mechanism.

$$(6\text{-}27)\quad \sigma_f = \frac{b^2}{4a^2} \cdot \frac{\frac{1}{2}(1-\sin\varphi)\sigma_c + \sin(\beta+\varphi)\left(\frac{2Hc}{b^2}\sin\beta - \cos\beta\right)\sigma_t}{\sin\beta\cos(\beta+\varphi)}$$

$$(6\text{-}28)\quad \cot\beta = \tan\varphi + \frac{1}{\cos\varphi}\sqrt{1 + \frac{\frac{2Hc}{b^2}\cos\varphi}{\frac{\sigma_c}{\sigma_t}\left(\frac{1-\sin\varphi}{2}\right) - \sin\varphi}}$$

$$(6\text{-}29)\quad \sigma_f = \frac{b^2}{4a^2}\,\sigma_t\left(\frac{2Hc}{b^2}\tan(2\beta+\varphi) - 1\right)$$

It will be seen that, as is reasonable, the ultimate load $P_{br} = \sigma_f\, 4a^2$ is independent of the size of the loaded area, provided this area lies on the skew pyramid that spall off.

Yet another geometrically admissible failure pattern must be mentioned, and that is a corner that has broken off through sliding failure, fig. 6.16, analogously with the plane case in fig. 6.10. As in the case of fig. 6.10, the ultimate load corresponds to a load of σ_c over the area that is broken off. The ultimate load is thus

$$(6\text{-}30)\quad P_{br} = \tfrac{1}{2}b^2\,\sigma_c$$

A comparison of the formulae with tests, e.g. by Au and Baird [60.2], shows, as in the plane case, that the theory gives too high a carrying capacity because all failure surfaces are assumed to be fully active.

Efficiency factors might, perhaps, be introduced, but it must be borne in mind that it is hardly possible to take care of all loading cases with the failure mechanisms calculated.

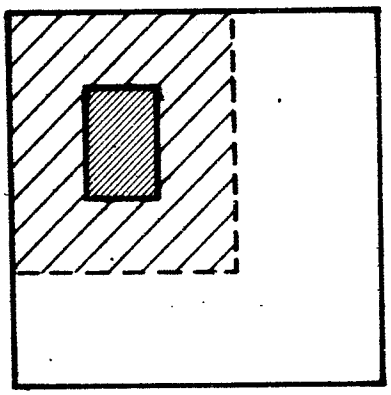

Fig. 6.17 Design F under eccentric loading.

here, so it may be necessary to find other failure mechanisms and, possibly, to supplement these with empirical formulae.

6.4 Empirical Solutions

Empirical formulae for the determination of carrying capacity go as far back as 1876, when the great German scientist Bauschinger [1876.1] performed tests on sandstone prisms. On the basis of tests on centrally loaded prisms, Bauschinger proposed the formulae

$$\sigma_f = \sigma_F \sqrt[3]{\frac{F}{f}} \tag{6-31}$$

Here, σ_F is the failure stress when the entire area F of the prism is loaded. σ_f is the ultimate load distributed over the loaded area f. In the case of cubes, σ_F is thus equal to the cube strength.

For non-central loads, Bauschinger states that the formula can be used if an area corresponding to central loading is included, see fig. 6.17.

For concrete the formula has been confirmed by Graf [21.1] , and it has been used in the Danish code of practice for structural concrete since 1930. In the guide to the current code, σ_c is used instead of σ_F, and $\sigma_f < 2\sigma_c$ is prescribed.

Tests show that for high values of $\frac{F}{f}$ (6-31) gives too small values of σ_f, a fact that made Wästlund 34.1 recommend

$$\sigma_f = 0{,}765\ \sigma_T \sqrt{\frac{F}{f}} \qquad \text{for } \frac{F}{f} > 5 \tag{6-32}$$

Many different formulae have been proposed for determination of σ_f. A study of some

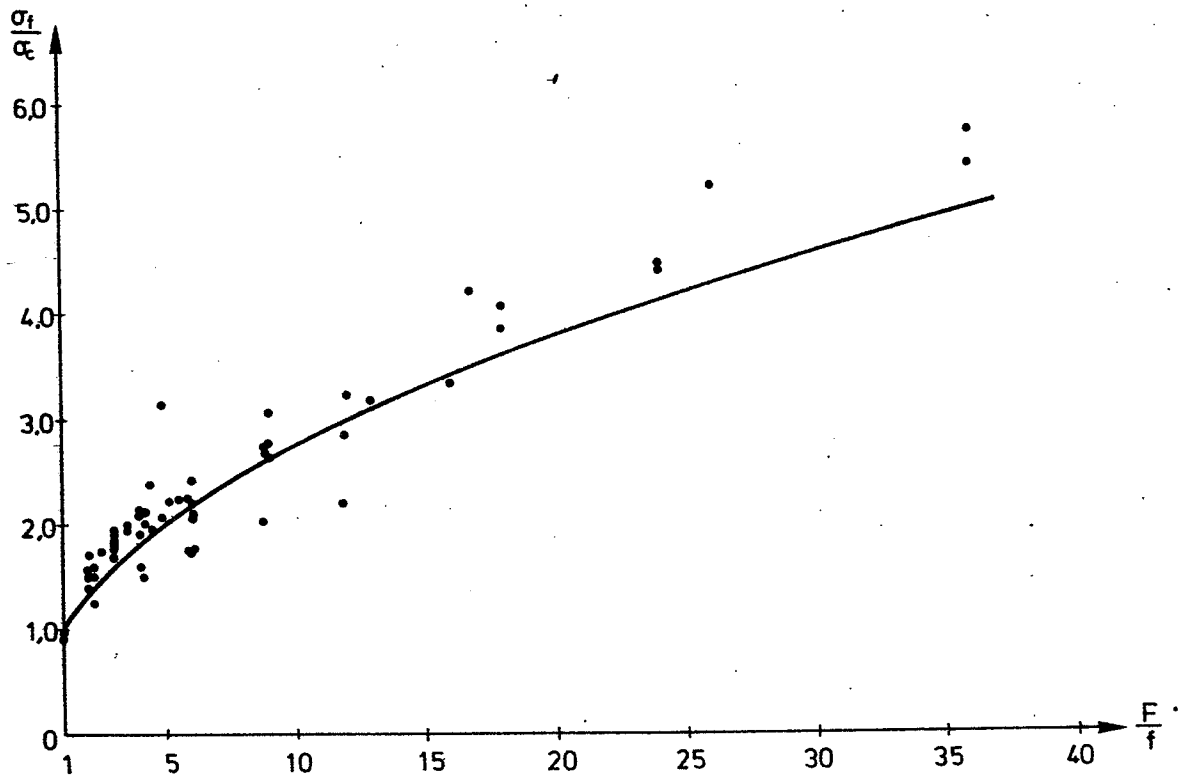

Fig. 6.18 Tests by Hawkins [68.2] and (6-33).

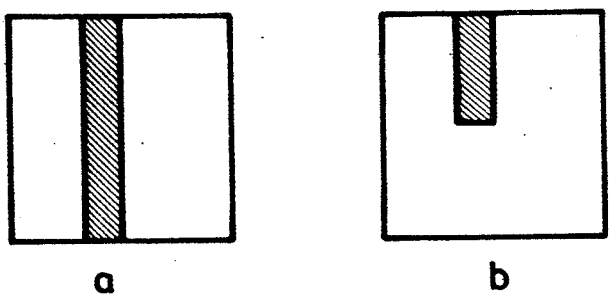

Fig. 6.19 Load locations with same $\frac{F}{f}$.

of these is to be found in Jensen [73.3] , where the author himself proposes the formula:

$$\frac{\sigma_f}{\sigma_c} = 0{,}2 + 0{,}8\sqrt{\frac{F}{f}} \qquad \frac{F}{f} \leq 180 \tag{6-33}$$

This formula is arrived at by means of a regressive analysis of many tests with widely varying shape and placing of the area f. In all cases, the test specimens were cubes or had a height of 1½ times the side length and a square base. In the case of non-central loading, F is also determined here as shown in fig. 6.17.

In (6-33) we have a single formula that is intended to cover the influence of many factors on the carrying capacity. In fig. 6.18 the formula is compared with 64 tests carried out by Hawkins [68.2]. These tests were not included in the formulation of (6-33). It will be seen that the formula gives reasonable results, but it will also be seen that there is a big scatter on the test results.

This is mainly due to two factors, which are not taken into account by (6-33). One is that the formula predicts the same $\frac{\sigma_f}{\sigma_c}$ in the two cases shown in fig. 6.19. Tests show that $\frac{\sigma_f}{\sigma_c}$ is bigger in the loading case in fig. 6.19b. The second factor is that $\frac{\sigma_f}{\sigma_c}$ increases more for weak concrete than for strong concrete.

Despite these drawbacks, it must, however, be said that (6-33) gives a usable forecast for the carrying capacity. If (6-33) is

Fig. 6.20 Location of load with $\frac{F}{f} = 1$.

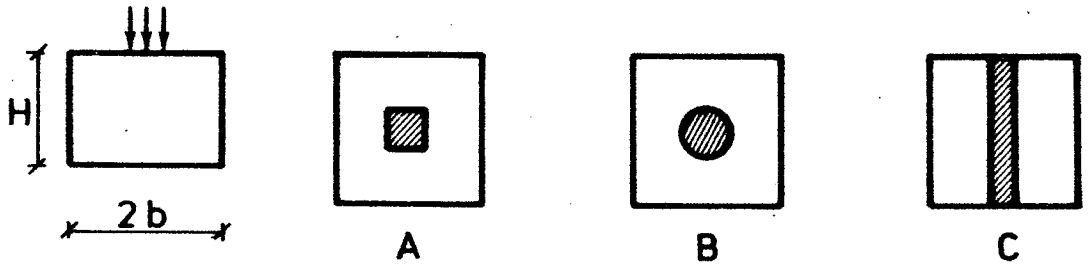

Fig. 6.21 Locations of loads. Type designations from table 6.4.

Lit.	Type	$\frac{F}{f}$	$\frac{H}{2b}$	Results
[53.2]	B	29,2	1, ½, ¼	÷
[60.2]	A	2 - 16	1, ½	+
[65.4]	A C	1 - 44,4 1 - 25	2 - ½ 2 - 0,6	+ +
[73.3]	A	4, 8,15, 16	1,5 - 0,35	÷

÷ : $\frac{\sigma_f}{\sigma_c}$ decrease with decreasing H/2b

\+ : $\frac{\sigma_f}{\sigma_c}$ increase with decreasing H/2b

Table 6.4 Main results of tests on influence of height.

used, account must be taken of the fact that an increase in the carrying capacity in excess of σ_c is conditional upon the existence of a tensile strength in the concrete beneath the load. Furthermore, as mentioned earlier, it must be borne in mind that, in very strong concrete, $\frac{\sigma_f}{\sigma_c}$ does not increase as much as predicted by (6-33), whereas, in weak concrete a bigger increment is obtained. The formula is directly applicable for the concrete strengths normally used ($\sigma_c \sim 15\text{-}40$ MN/m^2).

The bound, $\sigma_f \leq 2\sigma_c$, which is recommended in th guide to DS 411, the Danish Code of Practice for the Structural Use of Concrete, 1973, is, however, very conservative. As a cautious upper bound, $\sigma_f \leq 5\sigma_c$ is proposed, corresponding to $\frac{F}{f} = 36$ in (6-33).

6.4.1 The Influence of the Height

In both (6-33) and in the other empirical formulae mentioned, the height of the loaded body is not taken into account. (6-33) is primarily formulated for cubic test specimens and it can also be used for taller specimens.

For a test cube loaded completely on two opposite sides ($\frac{F}{f} = 1$), (6-33) gives $\sigma_f = \sigma_c$. However, such a test corresponds to finding the cube strength, which is about 1.25 σ_c. That (6-33), however, gives $\sigma_f = \sigma_c$ is due to the fact that the curve in the regressive analysis is forced through this point, see [73.3]. Among other things, this means that $\sigma_f = \sigma_c$ is achieved when the load lies at an edge, as shown in fig. 6.20.

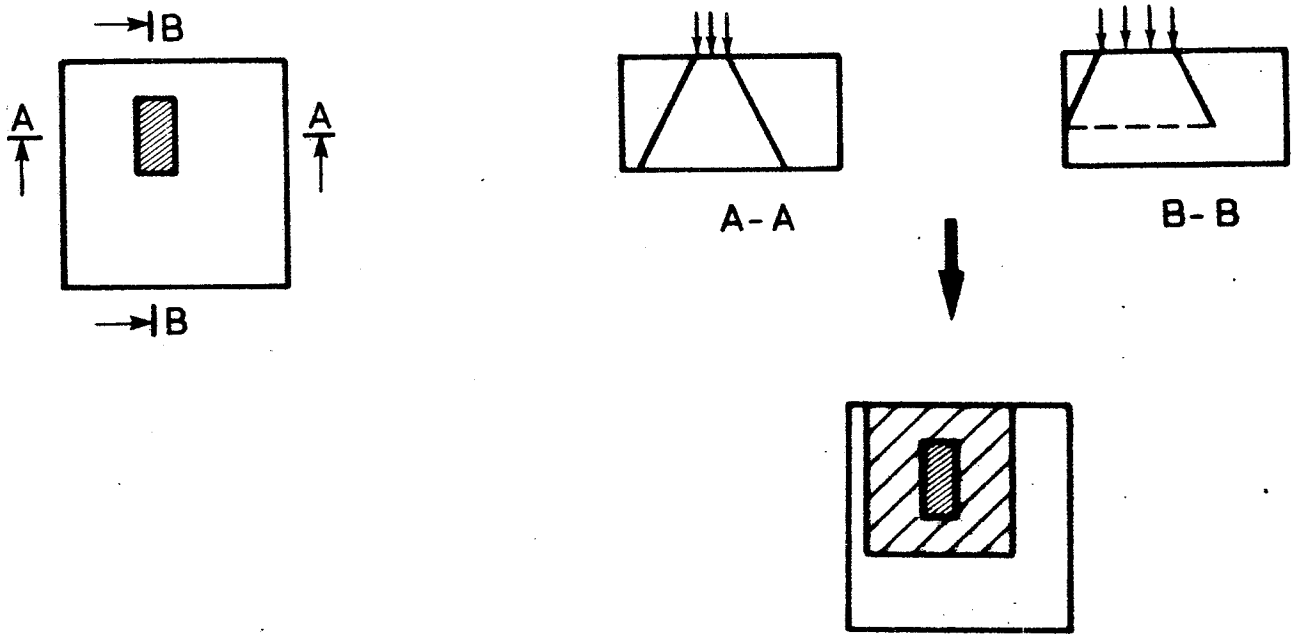

Fig. 6.22 Example of determination of F.

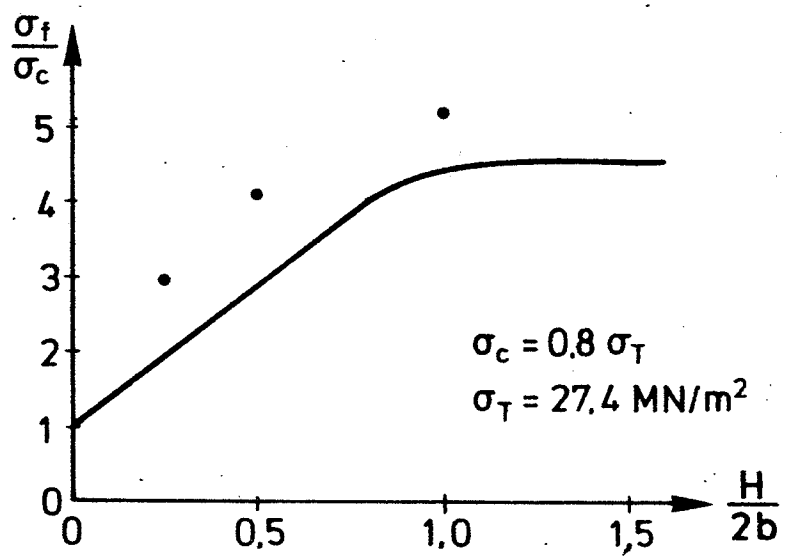

Fig. 6.23 Influence of height. Tests by Meyerhof [53.2].

In the case of very big heights the problem may arise of not being able to achieve $\sigma_f = \sigma_c$ for $\frac{F}{f} = 1$, see example 6.1.

For heights smaller than that corresponding to cubic test specimens, test results are available that show both that σ_f increases and that σ_c decreases with decreasing height. Fig. 6.21 and table 6.4 show the main results of 4 test series. A study of the 4 references in table 6.4 does not provide a means of judging between the credibility of the various test series.

It must thus be ascertained that there is great uncertainty regarding the significance of small heights of the loaded body. If rules were laid down that took account of the height and that were not at variance with the test results in [53.2] and [73.4], such rules should give reliable values for the carrying capacity in the case of small heights.

In the guide to the Danish Code of Practice for the Structural Use of Concrete, (6-31) is proposed, where σ_F is put at σ_c. A procedure is also proposed for determination of F. This procedure is synonymous with finding the centrally loaded area obtained by dispersing the load at a slope of 1:2. Some examples are shown in fig. 6.22. In table 6.4, account is not taken of the height in the determination of F in the column $\frac{F}{f}$.

In fig. 6.23, the rule is used together with (6-33) and compared with the tests from [53.2]. The tests were of type B, cf. fig. 6.21, and 2b = 6 in. The results lie above

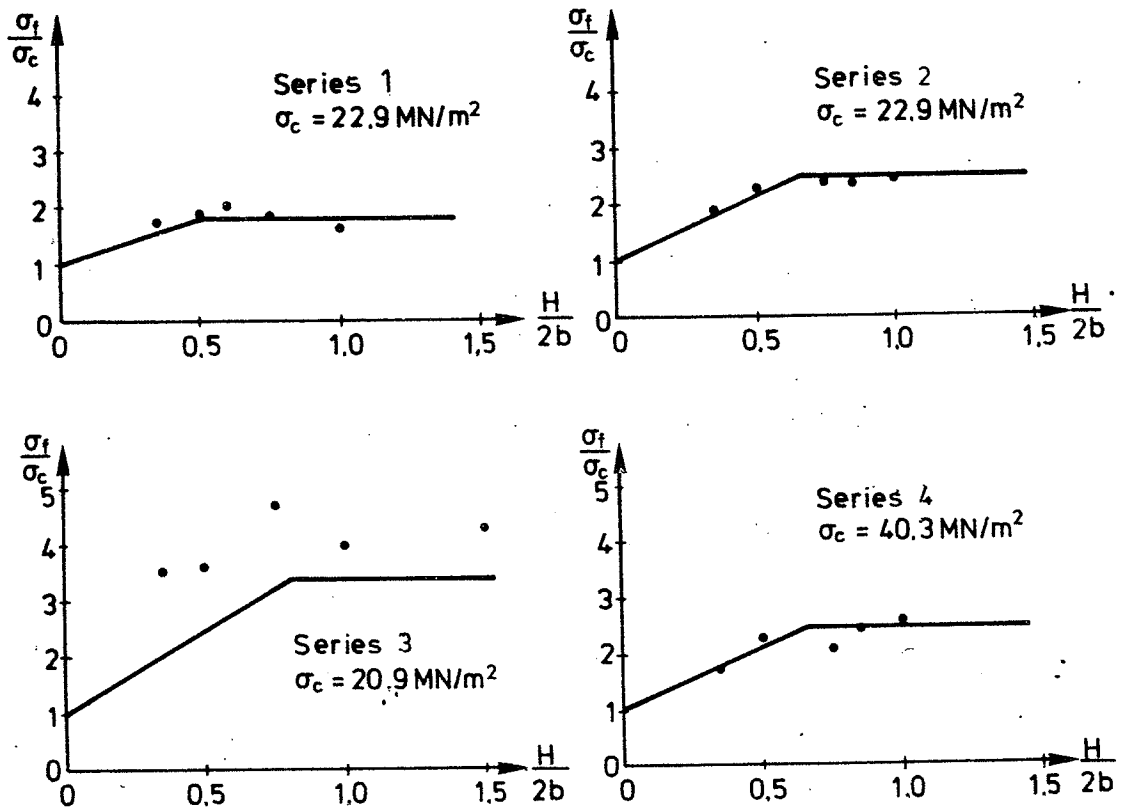

Fig. 6.24 Influence of height. Tests by Houborg [73.3].

the values obtained from the formulae, but for decreasing $\frac{H}{2b}$, the strength decreases in a way that fits the rules contained in the Code.

In fig. 6.24 a corresponding comparison is carried out with 4 series from [73.4]. The tests were all of type A, cf. fig. 6.21, and 2b = 200 mm. In series 1, f = 10 x 10 cm, in series 2 and 4, f = 7 x 7 cm, and in series 3, f = 5 x 5 cm. It will be seen that, combined with the Code's rules for determination of F, (6-33) gives excellent values.

6.5 Conclusion

From the above study it can be concluded that the theory of elasticity cannot be used for determination of the carrying capacity in the case of concentrated loading. The theory for rigid- plastic materials can, perhaps, be used in some cases, but in this event it will be necessary to introduce an efficiency factor $\nu \leq 1$, in the same way as in chapter 5.

Today, we have no choice but to use empirical formulae for determination of carrying capacity. In this connection, a particularly useful formula is (6-33). The area F used in the formula is determined as the centrally loaded area,, which can be found by dispersing the load by means of lines with a slope of 1:2 drawn down from the edges of f to the sides or bottom of the loaded body.

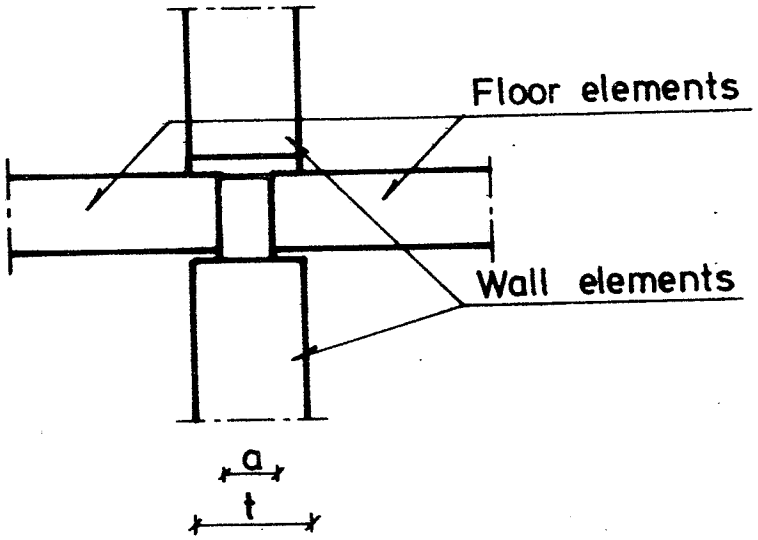

Fig. 6.25 Floor-wall connection.

Example 6.1 Floor-Wall Connection

Fig. 6.25 shows a floor-wall connection in a prefabricated concrete building. At the bottom there is a wall component, which supports two floor components, between which joint concrete is cast. Another wall component is placed on top, and the joint betweer this and the subjacent components and floor-floor joint is grouted with mortar.

We cannot normally reckon on the joint concrete ensuring contact between the floor components and the subjacent wall component. The floor components are therefore not supported at all points, so the transmission of vertical compressive stresses should be assumed to take place only through the joint concrete. This results in a concentrated load on the bottom wall component.

The floor components may be cut straight at the ends, e.g. the so-called Spirol-slab, where the width a is well defined, or they may be the well-known components with keyed ends, where the width a varies along the floor-wall connection. In the following, we will let a denote the average width of the joint concrete.

Tests have shown that a carrying capacity with $\sigma_f = \sigma_c$ cannot be achieved with a = t. The uniaxial compression strength appears to lie at about 75 per cent of the cylinder strength.

In order to calculate the carrying capacity of a floor-wall connection by means of (6-33), we must thus use $0.75\ \sigma_c$ instead of σ_c. In addition we have:

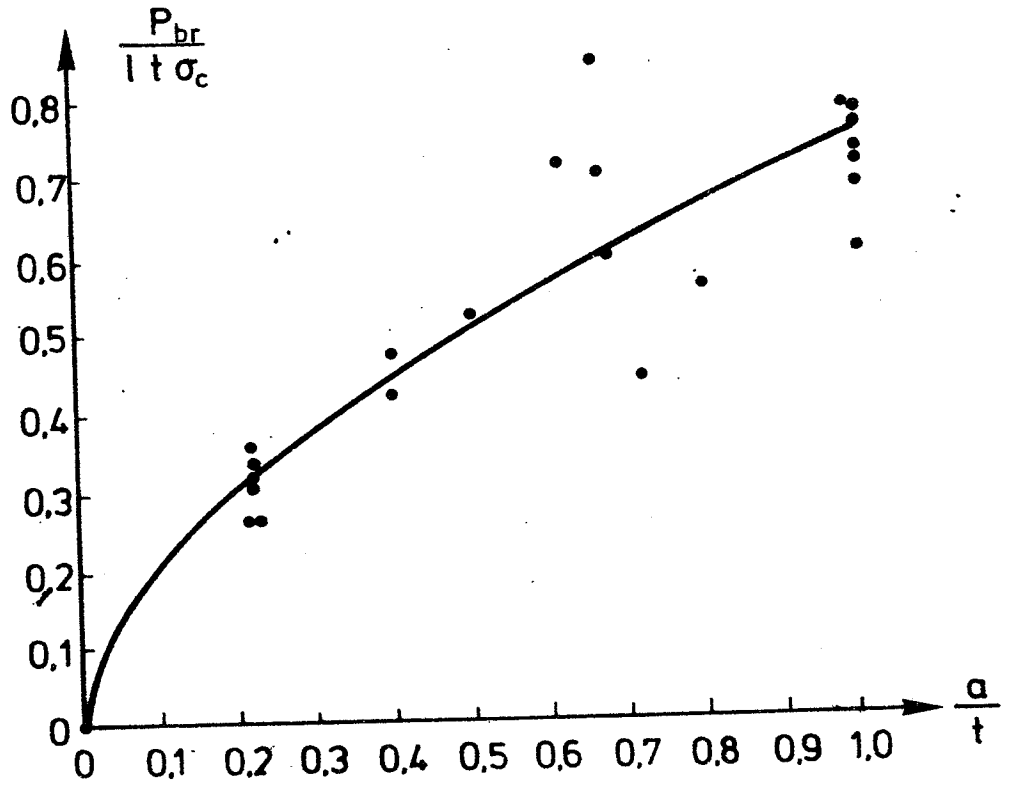

Fig. 6.26 (c) compared with tests from [76.1].

(a) $$\frac{F}{f} = \frac{t}{a}$$

(b) $$\sigma_f = \frac{P_{br}}{la}$$

where l is the length of a floor-wall connection.

Inserting these expressions in (6-33) and rewriting the formula, we find the carrying capacity to be:

(c) $$\boxed{\frac{P_{br}}{t\,l\,\sigma_c} = 0{,}15\,\frac{a}{t} + 0{,}6\sqrt{\frac{a}{t}}}$$

Several tests have been performed to determine the carrying capacity of a floor-wall connection. Buhelt et al. [76.1] have plotted the results, and these are reproduced in fig. 6.26, where (c) is also included. σ_c is the cylinder compression strength measured for the concrete in the wall component. It will be seen that there is good agreement between (c) and the tests.

$\frac{a}{t} = 1.0$ is achieved by ensuring support for the floor components in the casting of the joint concrete. In a single case, however, a continuous floor component is used.

It will thus be seen that (c) is a usable formula for determination of the carrying capacity of the floor-wall connection. It should be noted, incidentally, that the averag width a used in the case of keyed components is only used to facilitate the formulation o

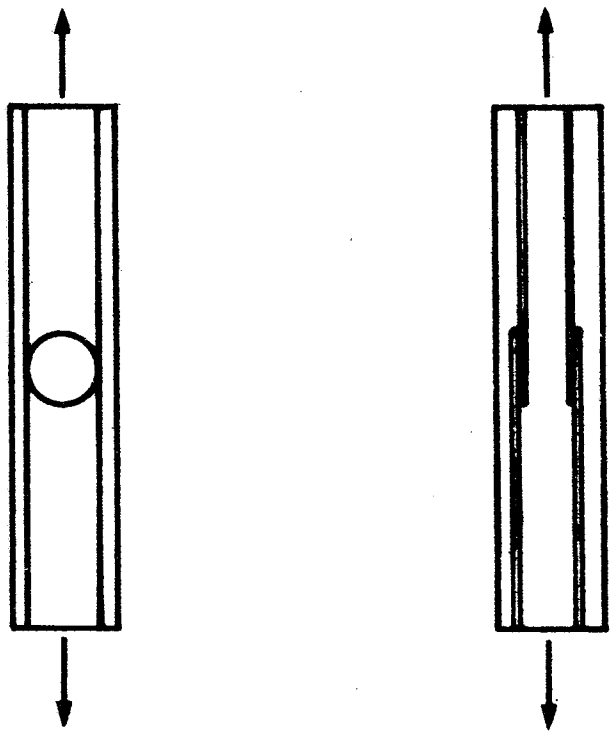

Fig. 6.27 Tension in stirrup connection.

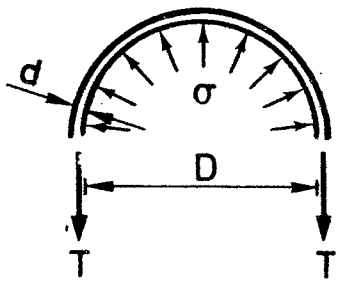

Fig. 6.28 Forces in stirrup.

(c) and the plotting of fig. 6.26. $\frac{F}{f}$ remains the same, whether use is made of the average width a or the correct shape of the area f.

Example 6.2 Stirrup Connection

We will now consider the reinforced concrete body shown in fig. 6.27, which is subjected to tensile forces via the reinforcing stirrups At the middle of the body, the tensile stresses must be transmitted from one set of stirrups, through the concrete, to the other set of stirrups.

The specimen can fail in two ways, either through failure of the reinforcement or through failure (split failure) of the concrete between the two sets of stirrups. Here, we will investigate whether (6-33) can be used to predict the load at which split failure of the concrete between the stirrups will occur. The calculations will be compared with tests by Leonhardt et al. [73.5].

We will limit the investigation to the case in which there is a circular opening between the stirrups. Fig. 6.28 shows a stirrup with the tensile forces T indicated by arrows. The concrete is assumed to act with a constant pressure σ against the stirrups. The relationship between σ and T is found to be

(a) $$\sigma = \frac{2T}{d\,D}$$

In order to avoid split failure in the concrete, the following must apply:

(b) $$T_{br} < \frac{\sigma_f\, d\, D}{2}$$

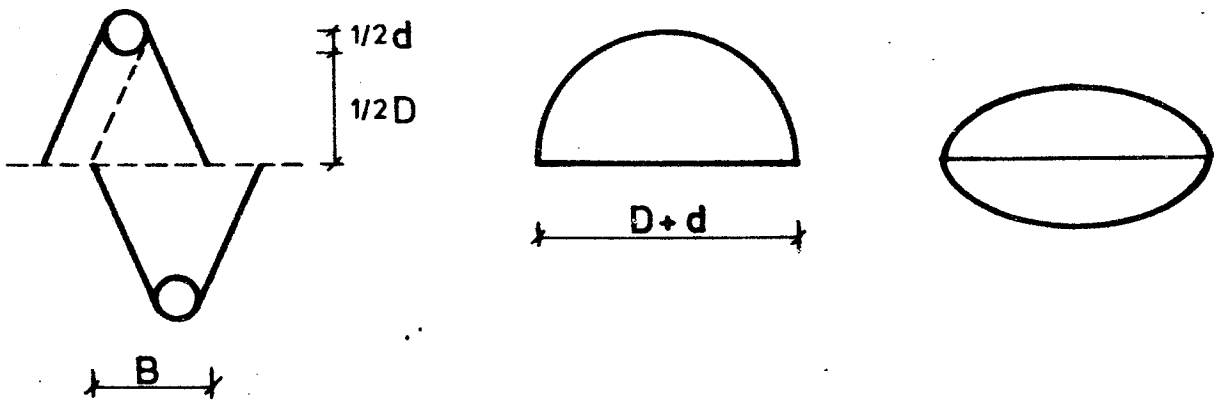

Fig. 6.29 Determination of F. Case 1.

where σ_f is the yield stress under the concentrated loading in question.

The tests with which we will compare the calculations here all resulted in split failure. We must thus find σ from (a) for the force at which failure occurred, and compare this with σ_f, which is determined from (6-33).

In (6-33) we know that

(c) $$f = d\,D$$

which corresponds to a projection of σ on the diameter of the opening between the stirrups.

The determination of F is slightly more difficult, but we will apply the rule on dispersing lines with the slope 1:2, after which we can divide the treatment up into three cases:

1. F is limited by the opposite stirrup.

This means that the area found by dispersing the load with lines with the slope 1:2 meets the area obtained from the opposite stirrup, as shown in fig. 6.29.

Fig. 6.29a shows a section at the middle of the stirrup connection with the dispersing lines 1:2. The overlap between the two areas is characterized by the length B, which is found as follows:

(d) $$B = \frac{1}{2}(D + d)$$

Such lines must be drawn from the edge of the reinforcement, all the way round. F is thereby the area obtained by introducing dispersing lines from a semi-circle (fig. 6.29b) with

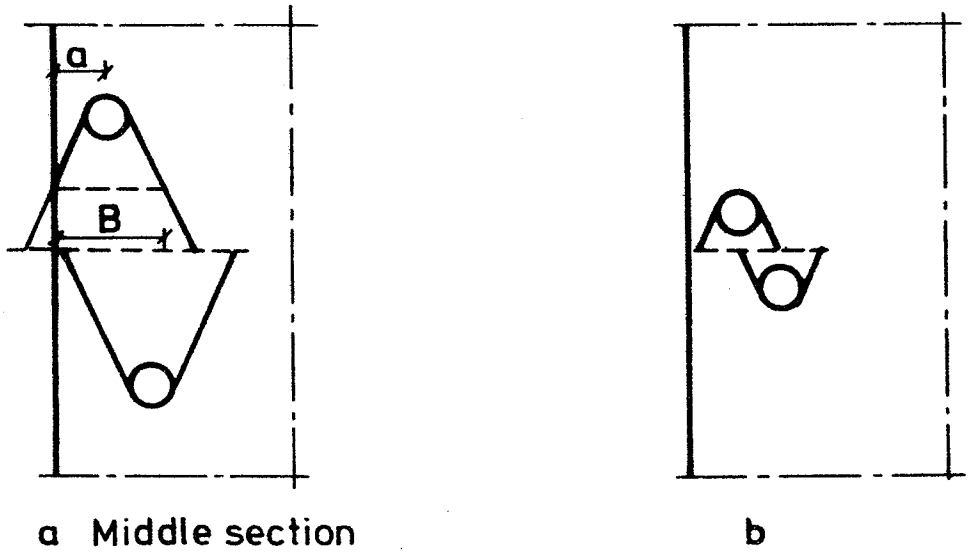

Fig. 6.30 Determination of F. Case 2.

Nr	D mm	d mm	$\sigma_{f,theory}$ N/mm^2	$\sigma_{f,test}$ N/mm^2	$\frac{\sigma_{f,test}}{\sigma_{f,theory}}$
A3	120	12	54,4	46,6	0,86
A4	120	12	54,4	49,4	0,91
B1	121	12	53,1	54,0	1,02
B2	90	12	51,9	63,2	1,22

Table 6.5 Comparison of (f) with tests from [73.5].

diameter D + d. Fig. 6.29c shows F, which has the same area as the semi-circle in fig. 6.29b.

(e) $$F = \frac{\pi}{8} (D + d)^2$$

For the concentrated load we now obtain:

(f) $$\frac{\sigma_f}{\sigma_c} = 0,2 + 0,4(D + d)\sqrt{\frac{\pi}{2d\,D}}$$

In table 6.5, (f) is compared with 4 tests from [73.5], where the two sets of stirrups are placed in such a way that F can be determined in the manner prescribed here. In the tests the cube strength of the concrete was measured. The cylinder strength is put at 80 per cent of the cube strength. The test numbers used refer to the numbers in [73.5].

It will be seen that there is reasonably good agreement .

2. F is limited by the free side.

This case occurs when the stirrups are placed so close to the surface that the dispersing line intersects the free side, as shown in fig. 6.30a. The figure is a section through the middle of the stirrup connection, and the piece obtained is characterized by the the length

(g) $$B = 2a$$

where a is the distance to the centre of the outermost stirrup.

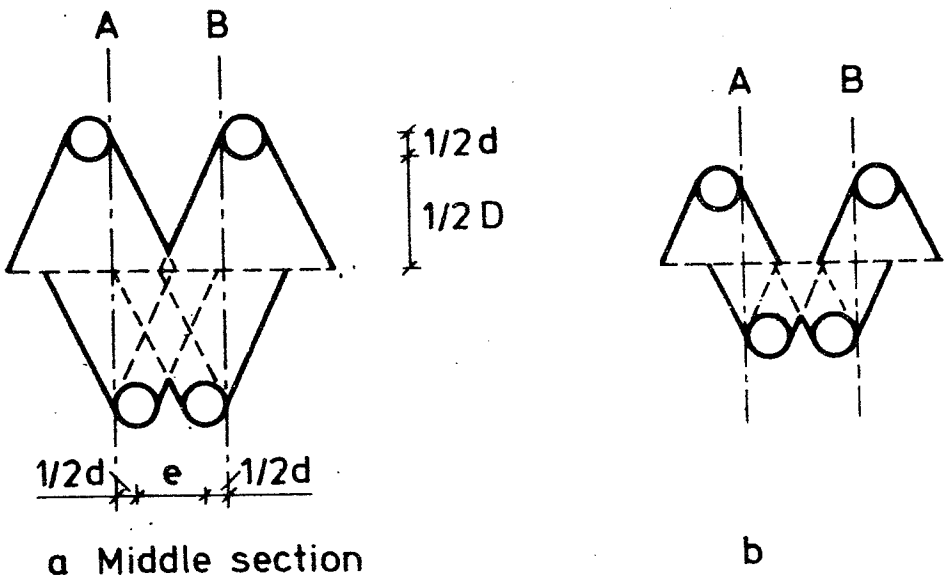

Fig. 6.31 Determination of F. Case 3.

If we move away from the middle of the stirrup connection, the distance between the stirrups becomes less than D, and at some point the dispersing lines will no longer intersect the free side before they meet the corresponding lines from the opposite stirrup, see fig. 6.30b. In this way, F becomes the area of a semi-circle with diameter D + d, but minus a segment with the camber $\frac{1}{2}(d + d) - B$.

Only one of the tests in [73.5] corresponded to this case. The test in question was C3, and it gave $\sigma_{f,test} = 41.9$ N/mm^2 and $\sigma_{f,theory} = 48.7$ N/mm^2; in other words, there is also reasonable agreement here.

3. F is limited by opposite stirrups and a nearby set of stirrups.

We will now consider the case in which two sets of stirrups are placed so close together that F is limited by the dispersing lines from one stirrup meeting the dispersing lines from an adjacent stirrup before they meet those from the opposite stirrup. Fig. 6.31a shows a section for such a case.

Here, we have two concentrated loads acting together. Determination of f and F is therefore not so simple as in the foregoing cases. One approach might, for example, be to put f at 2dD and let F be the whole of the common area formed by the dispersing lines with a slope of 1:2 from all 4 stirrups.

The contribution to F can be divided into two parts. The contribution on the left of the line AA and on the right of the line BB, see fig. 6.31, together constitute a contribution analogous to that in case 1.

Nr	D mm	d mm	e mm	$\sigma_{f,theory}$ N/mm^2	$\sigma_{f,test}$ N/mm^2	$\frac{\sigma_{f,test}}{\sigma_{f,theory}}$
C1	170	12	43	612	466	0,76
C2	120	12	37	526	357	0,68
A1	121	12	36	524	430	0,82
A2	121	12	39	530	482	0,91

Tabel 6.6: Comparison of theory with tests from [73. 5]. Case 3.

This consequently gives the area of a semi-circle with diameter D + d.

The contribution between the lines AA and BB is analogous to case B, in that we get

(h) $$B = e + d$$

The contribution is thus a semi-circle with diameter D + d minus the area of a segment with the camber $\frac{1}{2}(D + d) - (e + d)$.

In table 6.6, the theoretical results are com pared with the test results from [73.5], and it will be seen that slightly too high values are generally found with the method used here

The calculations carried out here indicate that the tensile strength of the stirrup connections can, in some cases, be determined on the basis of (6-33) and the rule on dispersin lines with a slope of 1:2. However, it must be emphasized that the test material is limited and that the method requires further substantiation.

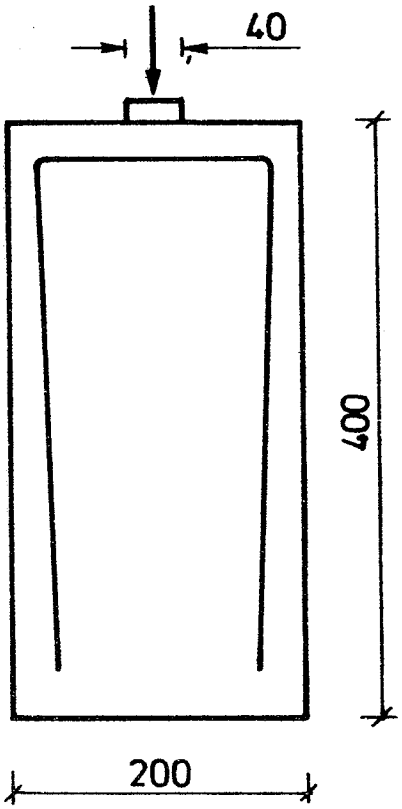

Fig. 7.1 Test specimen from [75.4].

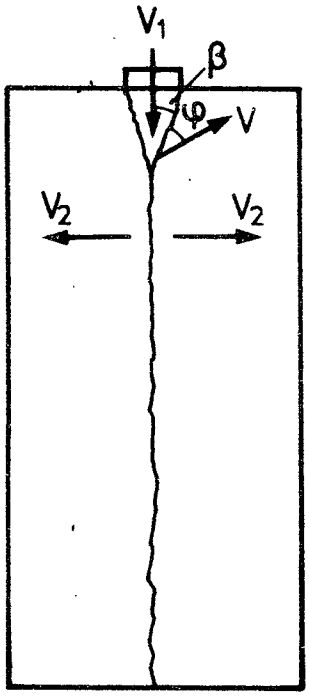

Fig. 7.2 Failure mechanism.

7. CONCENTRATED LOADS ON REINFORCED CONCRETE PRISMS

7.1 Introduction

In this chapter we will consider a problem that is related to the one dealt with in chapter 6. In the present case, however, we are only dealing with a linear load, i.e. a plane problem. We consider a concrete prism with reinforcement perpendicular to the direction of the load, and it is the effect of this reinforcement that we are interested in.

The considerations made and calculations performed will be compared with tests carried out at the Building Research Institute [75.4]. The tests were carried out on 20 x 20 x 40 cm prisms with varying concrete strength. The reinforcement consisted of stirrups designed as shown in fig. 7.1. The number of stirrups used and the depth of cover were varied. Stirrups of both deformed steel and round bars were used.

In the tests, $\frac{F}{f} = 5.0$.

7.2 Favourable Location of Reinforcement

We consider the same failure mechanism as in the case of plain prisms, fig. 7.2. The relationship between the movements in the failure mechanism is shown in fig. 7.2 and is found, as in section 6.3.1, to be:

$$V_1 = V \cos(\beta+\varphi) \tag{7-1}$$

$$V_2 = V \sin(\beta+\varphi) \tag{7-2}$$

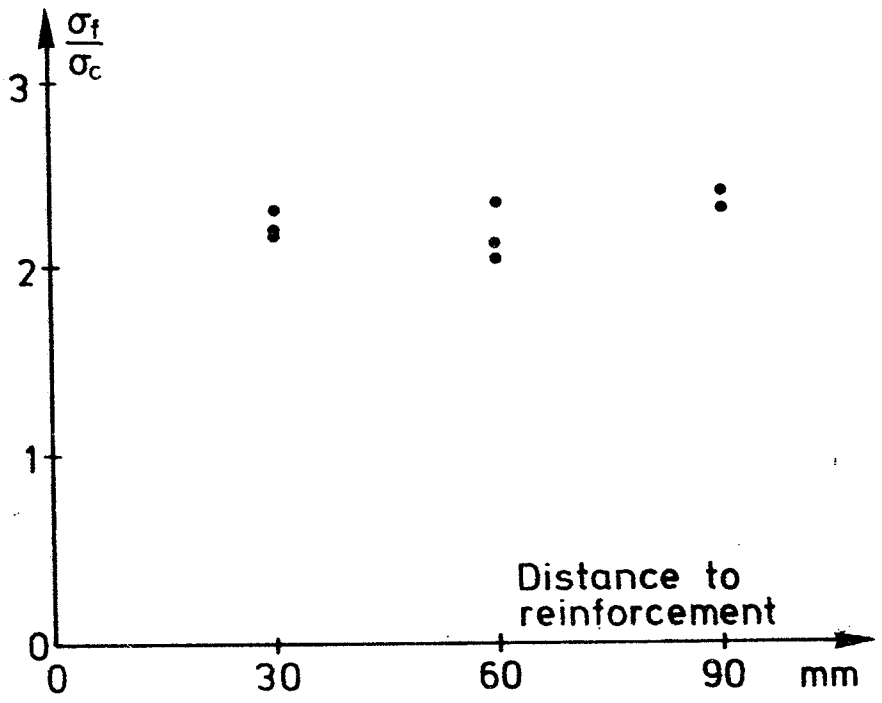

Fig. 7.3 Ultimate carrying capacity. Transverse reinforcement 3R10. Tests from [75.4].

The transverse reinforcement is placed perpendicular to V_1. If it is placed so far down that it lies in the zone with separation failure, its contribution to the equation of work will be

$$W_{IR} = F\,\sigma_F\,2V_2 = F\,\sigma_F\,2\,V\sin(\beta+\varphi) \tag{7-3}$$

where F is the cross-sectional area of the reinforcement, and σ_F is its yield stress.

We make the usual assumption that the reinforcement can only resist forces in its longitudinal direction. However, this means that reinforcement that is place against the load that it passes between the two faces of sliding failure will also make a contribution to the internal work, given by (7-3). The fact is that the movement in the longitudinal direction of the reinforcement is the horizontal projection of V, which is equal to V_2.

The depth at which the reinforcement is placed thus has no effect on the ultimate carrying capacity. This conclusion must naturally be subject to certain reservations since the transverse reinforcement deep down is inactive. What we are talking about here is reinforcement close to the local load. The interesting point, however, is that reinforcement placed in the zone in which, according to the theory of elasticity, there is transverse compression, see fig. 6.3, is just as effective as reinforcement placed in the zone with transverse tension.

Some test results are shown in fig. 7.3 to illustrate this. In the tests the transverse reinforcement consisted of 3 nos. R10. The

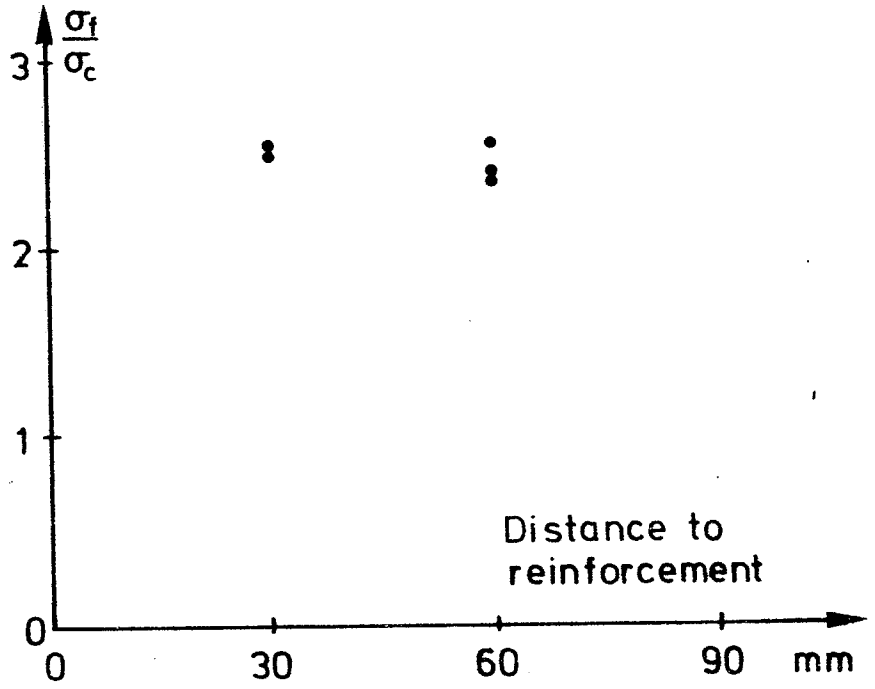

Fig. 7.4 Ultimate carrying capacity. Transverse reinforcement 4R10. Tests from [75.4].

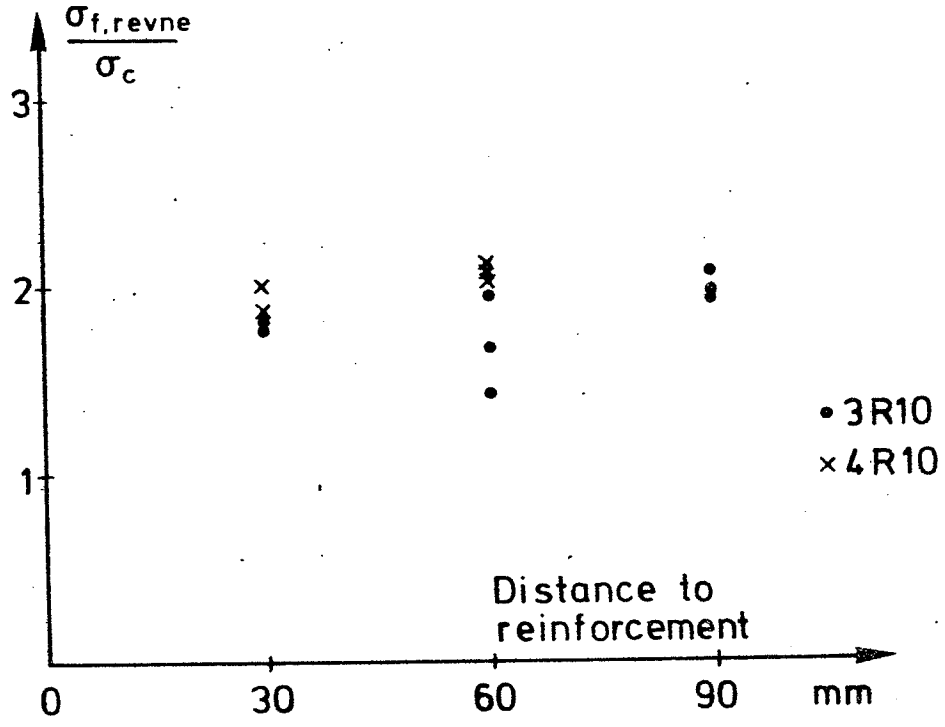

Fig. 7.5 Cracking load. Tests from [75.4].

concrete used for the tests came from the same batch, with σ_c = 31.8 MN/m^2. The cover was measured from centre of the reinforcement to the surface of the prism.

It will be seen that the ultimate carrying capacity is largely the same for the three thickness of cover.

An elastic calculation in accordance with Iyengar's method shows that maximum tension occurs at a depth of 70 mm in the prism, and that the transition between tension and compression occurs at a depth of 28 mm. Tests with the transverse reinforcement placed right in the compression zone according to the theory of elasticity are thus lacking. However, the tests show that reinforcement placed where, according to the theory of elasticity, there are no transverse stresses (28 mm 30 mm), is just as effective as reinforcement placed in the zone with big transverse tensile stresses.

Tests with 4 nos. R10 with the distance from the surface of the prism to the centre of the reinforcement at 30 and 60 mm show the same picture, as will be seen from fig. 7.4. In the tests with the distance 30 mm, σ_c = 28.3 MN/m^2, while in the others, σ_c = 31.9 MN/m^2.

In the tests in [75.4],the cracking load was also observed. The first crack that could be observed was always a part of the separation crack directly under the load.

After occurrence of the non-plastic separation failure, the load can still be increased on account of the plastic sliding failure and the reinforcement.

The effect of the location of the reinforcement on the cracking load is shown in fig. 7.5. According to the theory of elasticity maximum tension occurs at a depth of 70 mm, but the tests do not indicate that reinforcement placed elsewhere in the tensile zone has less effect on the cracking load. Even reinforcement placed where the theory of elasticity predicts no transverse stresses gives the same cracking load.

On the basis of the above it can thus be concluded that the depth of the cover over the transverse reinforcement has no effect on the carrying capacity or the cracking load. However, this conclusion is based on tests that do not include tests with transverse reinforcement very close to the local load, i.e. within the zone in which the theory of elasticity predicts transverse compression. Reinforcement placed there will presumably be just as effective as regards the ultimate carrying capacity, whereas the possibility of the cracking load being lower cannot be excluded.

7.3 Determination of Carrying Capacity

We will here calculate the carrying capacity on the basis of the failure mechanism in fig. 7.2, and we will assume that the vertical separation failure does not contribute to the carrying capacity. This assumption is synonymous with an assumption that separation failure occurs before total failure. This failure, on the other hand, is assumed to be rigid-plastic.

The equation of work is written up, and the contribution from the reinforcement, regardless of where this is placed, is given by (7-3). The contribution from the sliding failure in the concrete is

$$W_{IC} = \frac{1-\sin\varphi}{2} \sigma_c \frac{2a\,l}{\sin\beta} V \tag{7-4}$$

where a is half the loading width and l is the loading length normal to the plane of the paper. The external work is

$$W_E = 2a\,l\,\sigma_f \cos(\beta+\varphi) V \tag{7-5}$$

$W_E = W_{IR} + W_{IC}$ gives the upper bound

$$\sigma_f = \frac{2F\sigma_F \sin(\beta+\varphi)\sin\beta + (1-\sin\varphi)a\,l\,\sigma_c}{2a\,l\cos(\beta+\varphi)\sin\beta} \tag{7-6}$$

We can now introduce a degree of reinforcement as

$$\Phi = \frac{\sigma_F F}{2a\,l\,\sigma_c} \tag{7-7}$$

after which (7-6) can be written as

$$\frac{\sigma_f}{\sigma_c} = \frac{4\Phi \sin(\beta+\varphi)\sin\beta + (1-\sin\varphi)}{2\cos(\beta+\varphi)\sin\beta} \tag{7-8}$$

The minimum for (7-8) is found for

$$\tan\beta = \frac{-\sin\varphi + \sqrt{1 + \frac{4\Phi\cos\varphi}{1-\sin\varphi}}}{\frac{4\Phi}{1-\sin\varphi} + \cos\varphi} \tag{7-9}$$

If we put $\Phi = 0$, (7-8) naturally gives the same result as (6-10), where the tensile strength is put at zero in an unreinforced prism.

The first derivation of (7-8) and (7-9) is given in [75.4].

If we put $\varphi = 37^{o}$ and rewrite (7-8), we find the carrying capacity to be

$$\frac{\sigma_f}{\sigma_c} = \frac{0,4 + 2\Phi(0,8 - \cos(2\beta+\varphi))}{\sin(2\beta+\varphi) - 0,6} \tag{7-10}$$

where we have

$$\tan\beta = \frac{-0,6 + \sqrt{1 + 8\Phi}}{10\Phi + 0,8} \tag{7-11}$$

If the degree of reinforcement Φ is very small, the reinforcement will be torn apart the moment the cracking load is reached. We thus have an under-reinforced cross section, using designations analogous to those of DS411. The carrying capacity of this cross section can be determined from the formula for the unreinforced concrete prism (6-33). This formula is thus a lower bound for the validity of (7-10).

In an over-reinforced cross section, local crushing of the concrete under the load will occur, and (7-10) cannot be used.

Fig. 7.6 depicts (7-10), together with the test results from [75.4]. The results shown are the average of 3 tests and, in a few cases, the average of 2 tests. The horizontal, broken line represents the carrying

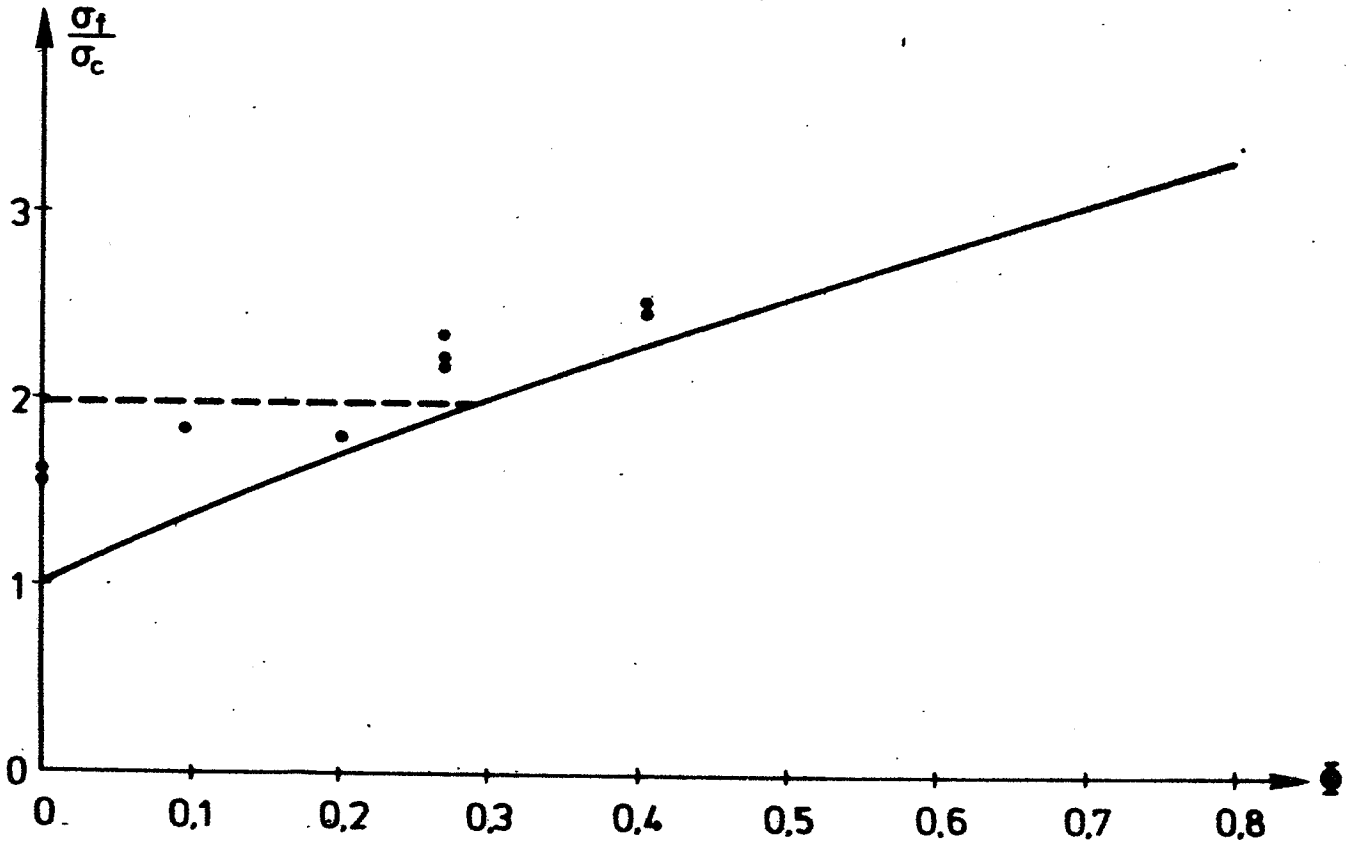

Fig. 7.6 Comparsion of (7-10) with tests from [75.4].

capacity of an unreinforced prism determined by means of (6-33), with $\frac{F}{f} = 5$.

The test material is otherwise very limited, so very few conclusions can be drawn on the basis of the figure. However, the results seem to show that the carrying capacity is constant at small Φ, and that this value is only slightly bigger than the carrying capacity of the unreinforced prism.

With higher values of Φ, the carrying capacity increases with increasing Φ. In all cases, (7-10) gives a lower carrying capacity than the tests.

With the exception of $\Phi = 0.202$, all the tests on reinforced prisms showed distinctly plastic properties, with big deformations prior to failure. For $\Phi = 0.202$, the cracking load and the failure load coincided, and failure occurred suddenly and without warning in the same way as for an unreinforced concrete prism.

In addition to the results shown in the figure, three further tests were performed in which failure took the form of pull-out failure. Whereas the tests shown in fig. 7.6 were made on prisms reinforced with round bars (R7 and R10), two of the tests for pull-out failure were carried out on prisms reinforced with deformed bars. The third was with R10,but with so many bars (6 nos. $\sim \Phi = 0.54$) that the pull-out strength was inadequate.

7.4 Conclusion

We can see from the foregoing that transverse reinforcement under a local load increases the carrying capacity. From fig. 7.6 we also see that the increment is modest.

Transverse reinforcement offers the further advantage that, with a suitable volume of reinforcement, warning of failure is given and that the failure is distinctly plastic. However, a small degree of reinforcement does not alter the form of failure in relation to the sudden and unheralded failure of an unreinforced test specimen.

Just as long as the transverse reinforcement is placed in the proximity of the concentrated load, the ultimate carrying capacity and, to some extent, the cracking load will be independent of the distance of the reinforcement from the load.

A limited test material indicates that a safe value for the carrying capacity can be found as the maximum of (6-33) and (7-10). In this connection, it can be seen from fig. 7.6 that (7-10) can be linearized since we can neglect the curve for small Φ. The carrying capacity is then determined as

$$\frac{\sigma_f}{\sigma_c} = \max \begin{cases} 0,2 + 0,8\sqrt{\frac{F}{f}} \\ 2,6\Phi + 1,2 \end{cases} \tag{7-12}$$

An upper bound for the validity of (7-12) and (7-10) is not known. However, it should be noted that, in addition to the difficul-

ties of finding an upper bound in the case of over-reinforced cross sections, problems may arise with the anchorage of the transverse reinforcement.

8. REFERENCES

In addition to the chronological list of references, a classification of part of the literature according to subject is given on page 119.

Chronological List

[1773.1] Coulomb, C.A.: Essai sur une application des regles de maximis et minimis a quelques a problemes de statique, relatifs a l'architechture. Memoire présantés a l'Academie des Sciences. Paris 1773.

[1876.1] Bauschinger, J.: Mittheilungen aus dem Mechanisch-Technischen Laboratorium der Königl. Polytechn. Schule in München. 6. Heft, 1876.

[1882.1] Mohr, O.: Über die Darstellung des Spannungszustandes und Deformationszustandes eines Körperelementes und über die Anvendung derselben in der Festigkeitslehre. Zivilingenieur, vol. 28, 1882.

[20.1] Prandtl, L.: Über die härte plasticher Körper. Nachrichten Kgl. Ges. d. Wiss. Math. - phys. Klasse, Göttingen, Heft 1, 1920.

[21.1] Graf, O.: Versuche mit Beton- und Eisenbetonquadern zu brückengelenken und auflagern. Forschungsarbeiten auf Gebiete des Ingenieurwesens, Heft 232, Berlin 1921.

[28.1] Richart, F.E., A. Brandtzæg & R.L. Brown: A Study of the Failure of Concrete under Combined Compressive Stresses. University of Illinois, Eng. Exp. Stat. Bull., No. 185, 1928.

[28.2] Von Mises, R.: Mechanik der plastischen Formänderung von Kristallen. Z. angew. Math. Mech., vol. 8, 1928.

[29.1] Richart, F.E., A. Brandtzæg & R.L. Brown: The Failure of Plain and Spirally Reinforced Concrete in Compression. University of Illinois, Eng. Exp. Stat. Bull., No. 190, 1920.

[30.1] Johansen, K.W.: Styrkeforhold i støbeskel i beton. Bygningsstatiske Meddelelser, 1930.

[34.1] Wästlund, G.: Untersuchungen über die Festigkeit vor Beton. Avhandling, Stockholm, 1934.

[38.1] Gvozdev, A.A.: The Determination of the Value of the Collapse Load for Statically Indeterminate Systems Undergoing Plastic Deformations. Proceedings of the Conference on Plastic Deformations, Dec. 1936. Akademiia Nauk SSSR. Moscow-Leningrad, 1938. Translated by Haythornthwaites in Inst. J. Mech. Sci., Vol. 1, 1960.

[51.1] Drucker, D.C.: A More Fundemental Approach to Plastic Stress-Strain Relations. Proceedings. 1'st US. Nat. Congr. Appl. Mech., 1951.

[51.2] Hill, R.: On the State of Stress in Plastic-Rigid Body at the Yield. Phil. Mag., Ser. 7, Vol. 42, 1951.

[52.1] Wright, P.J.F.: The Effect of the Method of Test on the Flexural Strength of Concrete. Magazine of Concrete Research, October 1952.

[52.2] Prager, W.: The General Theory of Limit Design. Proceedings 8th Int. Congr. Theor. and Appl. Mech. University of Istanbul, Vol. II, 1952.

[52.3] Drucker, D.C., W. Prager & H.J. Greenberg: Extended Limit Design Theorems for Continuous Media. Quarterly of Applied Mathematics, Vol. 9, 1952.

[52.4] Drucker, D.C. & W. Prager: Soil Mechanics and Plastic Analysis or Limit Design. Quarterly of Applied Mathematics, Vol. 10, 1952.

[53.1] Guyon, Y.: Prestressed Concrete. Contractors Record and Municipal Engineering, London, 1953.

[53.2] Meyerhof, G.G.: The Bearing Capacity of Concrete and Rock. Magazine of Concrete Research, April, 1953.

[55.1] Nielsen, J.: Brudteori for beton. Bygningsstatiske Meddelelser, Vol. 26, No. 1, 1955.

[55.2] Nylander, H. & S. Sahlin: Undersökning av kontinuerliga betongbalkar vid långtgående betonstukning. Beton, Vol. 4, No. 3, 1955.

[58.1] Johansen, K.W.: Brudbetingelser for sten og beton. Bygningsstatiske Meddelelser, Vol. 29, No. 2, 1958.

[58.2] Lundgren, H. & J. Brinch Hansen: Geoteknik. Teknisk Forlag, København 1958.

[59.1] Prager, W.: An Introduction to Plasticity. Addison-Wesley Publishing Company, Massachusetts, U.S.A., 1959.

[60.1] Anderson, A.R.: Composite Designs. Progressive Architecture, Sept. 1960.

[60.2] Iyengar, K.T. Sundara Raja: Der Spannungszustand in einem elastischen Halbstreifen und seine technischen Anvendung, Diss. Technischen Hochschule, Hannover, 1960.

[60.3] Au, T. & D.L. Baird: Bearing Capacity of Concrete Blocks. Journal of the American Concrete Institute, March, 1960.

[61.1] Zelger, C. & H. Rüsch: Der Einfluss von Fugen auf die Festigkeit von Fertigteilschalen. Beton- und Stahlbetonbau, Vol. 56, Heft 10, 1961.

[62.1] Iyengar, K.T. Sundara Raja: Über den Spannungszustand in einem elastischen Halbstreifen. Österreichisches Ingenieur Arkiv, Vol. 16, 1962.

[62.2] Iyengar, K.T. Sundara Raja: Two-Dimensional Theories of Anchorage Zone Stresses in Post-Tensioned Prestressed Beams. Journal of the American Concrete Institute, Oct. 1962.

[64.1] Lange-Hansen, P.: Grundlaget for teorien for idealt plastiske konstruktioner. Ingeniøren, Nr. 2, 1964.

[65.1] Muguruma, H. & S. Okamoto: Study on Bearing Capacity of Concrete. Proceedings of the Eight Japan Congress on Testing Materials, Japan, 1965.

[65.2] Sandbye, P.: A Plastic Theory for Plain Concrete. Bygningsstatiske Meddelelser, Vol. 36, No. 2, 1965.

[66.1] Hughes, B.P. & G.P. Chapman: The Deformation of Concrete and Microconcrete in Compression and Tension with Particular Reference to Aggregate Size. Magazine of Concrete Research, Vol. 18, No. 54, March 1966.

[66.2] Birkeland, P.W. & H.W. Birkeland: Connections in Precast Concrete Construction. Journal of the American Concrete Institute, March 1966.

[67.1] Sandbye, P.: Fænomenologiske brudteorier. Danmarks Ingeniørakademi, Bygningsafdelingen, København, 1967.

[67.2] Nielsen, M.P.: Om forskydningsarmering af jernbetonbjælker. Bygningsstatiske Meddelelser, Vol. 38, No. 2, 1967.

[68.1] Mast, R.F.: Auxiliary Reinforcement in Concrete Constructions. Journal of the Structural Division, ASCE, Vol. 94, No. ST6, 1968.

[68.2] Hawkins, N.M.: The Bearing Strength of Concrete Loaded through Rigid Plates. Magazine of Concrete Research, Vol. 20, No. 62, March 1968.

[68.3] Prager, W. & P.G. Hodge: Theory of Perfectly Plastic Solids. Dover Publications, New York, 1968.

[69.1] Sørensen, H.C. & M.P. Nielsen: Om forskydningsarmering i jernbetonbjælker. Diskussionsindlæg. Bygningsstatiske Meddelelser, Vol. 40, No. 1, 1969.

[69.2] Chen, W.F. & D.C. Drucker: Bearing Capacity of Concrete Blocks or Rock. Journal of the Eng. Mech. Div., ASCE, Vol. 95, No. EM4, 1969.

[69.3] Chen, W.F.: Soil Mechanics and Theorems of Limit Analysis. Journal of the Soil Mech. and Found. Div., ASCE, Vol. 95, No. SM2, 1969.

[69.4] Nielsen, M.P.: On the Strength of Reinforced Concrete Discs. Acta Polytechnica Scandinavica, Ci 70, Copenhagen 1971.

[69.5] Hofbeck, J.A., I.O. Ibrahim & A.M. Mattock: Shear Transfer in Reinforced Concrete. Journal of the American Concrete Institute, Feb. 1969.

[69.6] Newman, K. & J.B. Newman: Failure Theories and Design Criteria for Plain Concrete. Paper No. 83. International Conference on Structure, Solid Mechanics and Engineering Design in Civil Engineering Materials, Southampton University, 1969.

[70.1] Harremoës, Krebs Ovesen & Moust Jacobsen: Lærebog i geoteknik 2, 2. udgave. Polyteknisk Forlag, 1970.

[70.2] Timoshenko, S.P. & J.N. Goodier: Theory of Elasticity. 3rd Edition. International Student Edition, McGraw-Hill Book Company, Kogakusha Company, Tokyo, 1970.

[70.3] Jensen, Å.P.: On Failure in Concrete. Acta Polytechnica Scandinavica, Ci66, Copenhagen, 1970.

[71.1] Pommeret, M.: La resistance aux efforts tangents des joints verticaux entre grand panneaux prefabriques coplanaires. Service d'Etude des Structures. Bulletin Interne d'Information No. 3, France, June 1971.

[71.2] Birkeland, P.W.: A Proposed Industry-Standard Beam Connection. Journal of the Prestressed Concrete Institute, Vol. 16, No. 1, 1971.

[71.3] ICES-STRUDL II, Engineering User's Manual, Vol. 1 and 2, Department of Civil Engineering, Massachusetts Institute of Technology, Cambridge, Massachusetts, 1971.

[72.1] Endebrock, E.G. & L.A. Traina: Static Concrete Constitutive Relations Based on Cubical Specimens. Technical Report No. AFWL-TR-72-59, Vol. 1 and Vol. 1, Dec. 1972.

[72.2] Liu, T.C.Y., A.H. Nielson & F.O. Slate: Biaxial Stress-Strain Relations for Concrete. Journal of the Structural Division, ASCE, Vol. 98, No. ST5, 1972.

[72.3] Mattock, A.H. & N.H. Hawkins: Shear Transfer in Reinforced Concrete. Journal of the Prestressed Concrete Institute, Vol. 17, No. 2, 1972.

[72.4] Nielsen, M.P. & N.A. Harder: Træk af mekanikkens historiske udvikling. Mekanik. Bind 0.0. Danmarks Ingeniørakademi, Bygningsafdelingen, Ålborg, 1972.

[73.1] Kupfer, H.: Das Verhalten des Betons under mehrachsiger Kurzzeitbelastung under besonderer Berucksichtigung der zweiachsigen Beanspruchung. Deutscher Ausschuss für Stahlbeton. Heft 229, Berlin 1973.

[73.2] Rathkjen, A.: The Test Report is being prepared at Ålborg Universitetscenter, Instituttet for Bygningsteknik. Some of the results are published in [73.3].

[73.3] Jensen, B.C.: Koncentrerede belastninger på uarmerede betonprismer. Bygningsstatiske Meddelelser, Vol. 44, No. 4, 1973.

[73.4] Hauborg, J.: Koncentrerede belastninger på betonprismer med variabel højde. A project made by a student at the Institute of Building design, Technical University of Denmark, under the direction of E. Borchersen and B.C. Jensen.

[73.5] Leonhardt, F., R. Walther & H. Dieterle: Versuche zur Ermittlung der Tragfähigkeit von Zugschlaufenstössen. Deutscher Ausschuss für Stahlbeton, Heft 226, Berlin 1973.

[74.1] Rajendran, S. & C.T. Morley: A General Yield Criterion for Reinforced Concrete Slab Elements. Magazine of Concrete Research, Vol. 26, No. 89, Dec. 1974.

[74.2] Houborg, J. & A.B. Sørensen: Støbeskel. A project made by a student at the Structural Research Laboratory, Technical University of Denmark, under the direction of E. Skettrup and T. Brøndum-Nielsen.

[74.3] Hansen, K., M. Kavyrchine, G. Melhorn, S.Ø. Olesen, D. Pume & H. Schwing: Design of Vertical Keyed Shear Joints in Large Panel Buildings. Building Research and Practice, July/August, 1974.

[74.4] Mattock, A.H.: Shear Transfer in Concrete Having Reinforcement at an Angle to the Shear Plan. Shear in Reinforced Concrete, SP-42, American Concrete Institute, Detroit, 1974.

[74.5] Hermansen, B.R. & J. Cowan: Modified Shear-Friction Theory from Bracket Design. Journal of the American Concrete Institute, Feb. 1974.

[74.6] Jensen, B.C.: Plasticitetsteori for Coulomb-materialer. Instituttet for Husbygning, Danmarks tekniske Højskole, Internt notat nr. 7, 1974.

[75.1] Nielsen, M.P. & M.W. Bræstrup: Plastic Shear Strength of Reinforced Concrete Beams. Bygningsstatiske Meddelelser, Vol. 46, No. 3, 1975.

[75.2] Jensen, B.C. & M.P. Nielsen: Om spalteforsøget og koncentrerede kræfter på uarmerede betonprismer. Nordisk Betong, No. 3, 1975.

[75.3] Jensen, B.C.: On the Ultimate Load of Vertical, Keyed Shear Joints in Large Panel Buildings. II. International Symposium on Bearing Walls, Warsaw, 1975. Published by the Institute of Building Design, Technical University of Denmark, as Report No. 108, 1975.

[75.4] Munch-Petersen, C.: Bæreevneformler for koncentrerede belastninger på betonprismer med ilagt spaltearmering. A project made by a student at the Institute of Building Design, Technical University of Denmark, under the direction of E. Borchersen and B.C. Jensen.

[75.5] Jensen, B.C.: Lines of Discontinuity for Displacements in the Theory of Plasticity of Plain and Reinforced Concrete. Magazine of Concrete Research, Vol. 27, No. 92, Sept. 1975.

[76.1] Buhelt, M., K. Hansen, K.F. Hansen, A. Odgaard, S.Ø. Olesen & J.E. Staalby: Skivebygningers stabilitet 2. beregningsmetoder. The report is being prepared at the Danish Building Research Institute.

Subject list

FORTEGNELSE OVER RAPPORTER, UDGIVET AF
INSTITUTTET FOR HUSBYGNING, DANMARKS TEKNISKE HØJSKOLE

Nr.	Forfatter	Titel	
101	Hilbert, Niels-Ole	Pilotforsøg med vacuumpakning i tørblandet cementmørtel, 1972	udgået
102	Jensen, Bjarne Chr.	12 forsøg med momentpåvirket bøjlesamling i bjælker, 1973	udgået
103	Jensen, Bjarne Chr.	Forsøg med stribeformede belastninger på beton, 1973	
104	Hilbert, Niels-Ole	Undersøgelse af Kelementdæk, 1973	udgået
105	Jessen, Richard	Die Weissenhof Siedlung, 1974	
106	Jensen, Bjarne Chr.	Rigid Jointed Concrete Frame, 1974	
107	Jensen, Bjarne Chr.	Koncentrerede belastninger på uarmerede betonprismer, 1974	
108	Jensen, Bjarne Chr.	On the Ultimate Load of Vertical, Keyed Shear Joints in Large Panel Buildings, 1975	
109	Jensen, Bjarne Chr.	Lines of Discontinuity for Displacements in the Theory of Plasticity of Plain and Reinforced Concrete, 1975	
110	Larsen, Henning	Recent Danish Facade Joint Design, 1975	
111	Jensen, Bjarne Chr.	Nogle plasticitetsteoretiske beregninger af beton og jernbeton, 1976	
112	Borchersen, Egil & Rasmussen, Lauritz	Bæreevneforsøg med sandwichvægelementer med mineraluldskerne og krydsfinérsflanger, 1976	
113	Larsen, Henning	Projektering - beslutninger og bindinger, 1976	
114	-	O-ENERGIHUSET - EN MODEL I 1:1,1976 Særtryk af Arkitektur DK 1-76	
115	Haagentoft, Jens	Momentstive rammehjørner. Efterspændte boltede samlinger udsat for lukkende momentpåvirkning, 1976	

LIST OF REPORTS' PUBLISHED BY THE INSTITUTE OF BUILDING DESIGN, TECHNICAL UNIVERSITY OF DENMARK, BUILDING 118, DK-2800 LYNGBY

FORTEGNELSE OVER RAPPORTER, UDGIVET AF
INSTITUTTET FOR HUSBYGNING, DANMARKS TEKNISKE HØJSKOLE

Nr.	Forfatter	Titel
116	Hilbert, Niels-Ole & Holtse, Cyrill	Fugttransport fra Fugemørtel til Betonelementer 1976
117	Hilbert, N.-O.	Hulrumsdiagrammer for tørblandinger af betonmaterialer, 1976
118	Rasmussen, Lauritz	Mineraluldbaserede sandwichelementers luftlydisolation, 1976
119	Haagentoft, Jens H.	Momentstive rammehjørner. Efterspændte boltede samlinger udsat for åbnende momentpåvirkning, 1977.
120	Lewicki, Bohdan	Housing in Poland and other CMEA contries and its financing, 1977
121	Lewicki, Bohdan	Structural Joints in large panel Buildings, 1977
122	Rasmussen, Lauritz	Brandforsøg med 2 mineraluldbaserede sandwichdækelementer, 1977
123	Jensen, Bjarne Chr.	Some Applications of Plastic Analysis to Plain and Reinforced Concrete, 1977